EFFECT IN THE WATER BALANCE OF THE TEESTA RIVER BASIN DUE TO DIFFERENT CLIMATE CHANGES AND UPSTREAM DEVELOPMENT

IMRAN KHAN

Student No: 0413162003 P

DEPARTMENT OF WATER RESOURCES ENGINEERING

BANGLADESH UNIVERSITY OF ENGINEERING AND TECHNOLOGY

DHAKA, BANGLADESH

MARCH, 2018

EFFECT IN THE WATER BALANCE OF THE TEESTA RIVER BASIN DUE TO DIFFERENT CLIMATE CHANGES AND UPSTREAM DEVELOPMENT

IMRAN KHAN

Student No: 0413162003 P

A thesis Submitted to The Department of Water Resources Engineering of Bangladesh University of Engineering and Technology in partial fulfillment of the requirement for the degree of

MASTER OF SCIENCE IN WATER RESOURCES ENGINEERING

Department of Water Resources Engineering

Bangladesh University of Engineering and Technology

Dhaka, Bangladesh

March, 2018

CERTIFICATION OF APPROVAL

The thesis titled "Effect in the Water Balance of the Teesta River Basin due to Different Climate Changes and Upstream Development", submitted by Imran Khan, Roll No. 0413162003 P, Session April/2013, has been accepted as satisfactory in partial fulfillment of the requirement for the degree of **Master of Science in Water Resources Engineering** on 21 March, 2018.

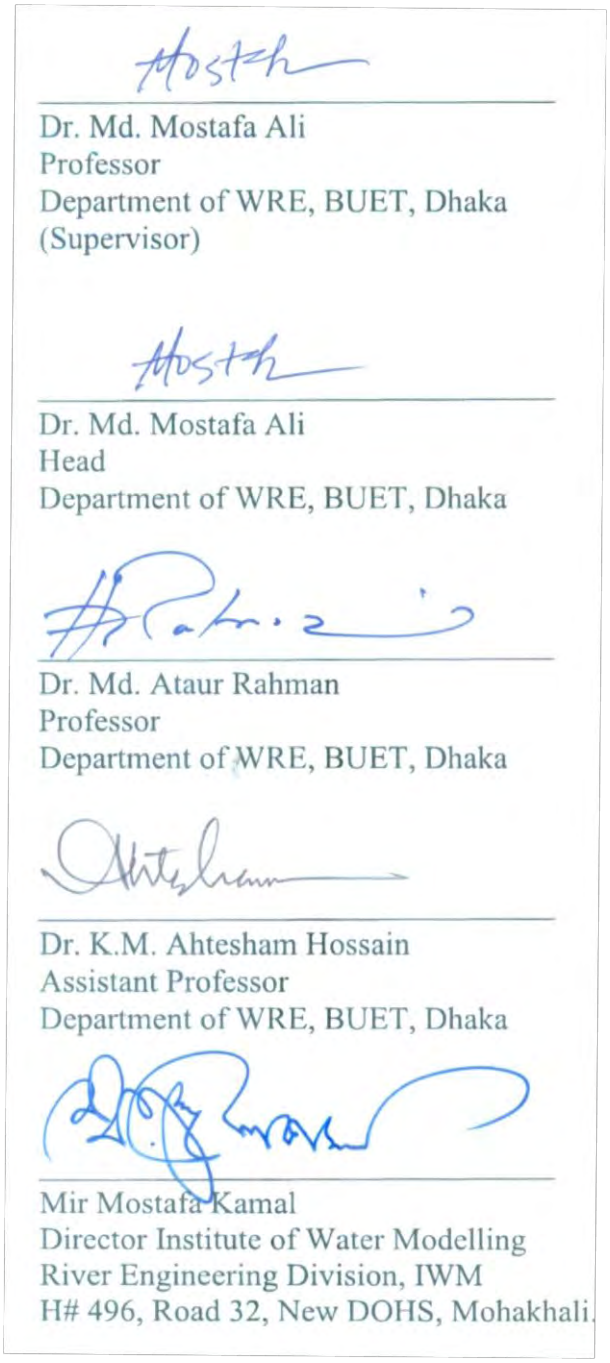

Dr. Md. Mostafa Ali
Professor
Department of WRE, BUET, Dhaka
(Supervisor)

Chairman

Dr. Md. Mostafa Ali
Head
Department of WRE, BUET, Dhaka

Member
(Ex-Officio)

Dr. Md. Ataur Rahman
Professor
Department of WRE, BUET, Dhaka

Member

Dr. K.M. Ahtesham Hossain
Assistant Professor
Department of WRE, BUET, Dhaka

Member

Mir Mostafa Kamal
Director Institute of Water Modelling
River Engineering Division, IWM
H# 496, Road 32, New DOHS, Mohakhali.

Member
(External)

DECLARATION

It is hereby declared that this thesis work or any part of it has not been submitted elsewhere for the award of any degree or diploma.

_____

Imran Khan
Signature of the Candidate

Table of Contents

List of Figures

List of Tables

ACKNOWLEDGEMENT

First of all, the author would like to express his gratefulness to the almighty Allah the creator of universe. Without the rahmat of Allah the author couldn't have finished the degree.

The author acknowledges his deepest gratitude to his supervisor Dr. Md. Mostafa Ali, Professor and Head, Department of Water Resources Engineering, BUET for providing an interesting idea for the thesis and encouraging to work with it. His cordial supervision, valuable suggestion and expertise contributed greatly to this thesis.

The author is also grateful to Dr. Md. Ataur Rahman, Professor, Department of Water Resources Engineering, BUET, Dr. K.M. Ahtesham Hossain, Assistant Professor, Department of Water Resources Engineering, BUET and Mr. Mir Mostafa Kamal, Director, River Engineering Division, IWM, who were the members of the board of Examiners. Their valuable comments on this thesis are duly acknowledged.

The author would like to thank his parents for their encouragement and inspiration. The author is grateful for their guidance and blessings. Without their help and support he wouldn't have finished his M.Sc. The author is grateful for their limitless sacrifice and love.

The author is truly grateful to his wife for her continuous support and inspiration. He appreciates and admires her patience and encouragement throughout his study.

The author would like to express his sincere gratitude and appreciation to his all colleagues and friends for their help, support and inspiration.

Imran Khan
March 2018

ABSTARCT

The Teesta River is one of the most important trans-boundary river of Bangladesh with only the Ganges and Brahmaputra have a higher annual runoff than the Teesta. Bangladesh has long argued that India's construction of the Gazaldoba Barrage upstream of Dalia has significantly reduced the availability of water in the dry season. Furthermore, the release of water during the monsoon season causes flooding and bank erosion in downstream. The availability of water for irrigation, particularly in the lean or dry season, has been at the crux of the longstanding dispute between the two countries.

The analysis of secondary flow data shows that annual maximum and annual mean flow at the Dalia point is on the decline. The annual minimum flow and minimum water level at Dalia shows very low water availability during lean period. The maximum water level shows an increasing trend meaning increasing intensity of floods. But increasing maximum water level with decreasing flow means that the Teesta Basin is experiencing siltation or aggradation. And with the impending threat of climate change, the water balance of the Teesta Basin is going to become a more important factor in an already water stressed region.

With this issues in mind, a semi-distributed hydrological model of the Teesta basin has been developed using Soil Water Assessment Tool (SWAT). The model was calibrated and validated for the stream flow measured at Dalia, upstream of the Teesta barrage for 1999 up to 2013. Potential change in the water balance due to climate change and upstream development in the Teesta River Basin has been assessed with this developed SWAT hydrological model. The climate change scenarios have been developed based on the projection of couple of GCM models (HAD GEM2 ES and CSIRO MK 3.6.0) for all the RCP scenarios of IPCC AR-5, during the 2050s and 2080s. While the upstream control scenarios were prepared by withdrawing the stream flow at three different points (Gozoldoba, Teetsa III and Rammam III) and analyzing the impact of it further downstream.

The downscaled GCM model data of temperature and precipitation for all the RCPs were analyzed at different points in and around the Teesta to find the driest, wettest, warmest and coolest scenario of the Teesta basin in 2080s. For the wettest scenario the precipitation had increased by 11.71% while it decreased by 1.76% for the driest scenario. The increase

in temperature for the coolest and the warmest scenario is found to be 2.24°C and 5.34°C. These scenarios were used as the input data for SWAT model to assess the changes in water balance due to climate change.

The developed hydrological model of 1998-2013 timeframe also served as the base model output to be compared against climate change model results. Comparing the water balance of the climate change model with the base model, it was clearly evident that the monsoon season will become more wetter and the dry season become more drier due to climate change for all the climate change scenarios. The monsoon may see as much as 80% increase in surface runoff (wettest scenario) while the dry season might see a 70% decrease in surface runoff (driest scenario). The base flow is expected to decrease in the month of April, May and June while increase in temperature means the evapotranspiration is expected to increase all throughout the year. The outputs of water yield shows it might increase by more than 50% in the monsoon season and reduce by 30% for the dry seasons.

The flow comparison at the Dalia point, upstream of Teesta Barrage for different climate change scenarios shows similar kind of trend to that of the water balance comparison. The general trend emerging from the flow analysis is that the Dalia point will experience a more severe shortage of water during the lean season even without further upstream controls.

The impact of upstream development (control structures) by analyzing different flow diversion scenarios shows that Gozoldoba has a severe impact on water availability at Dalia. Being hydroelectric structures, the Teesta III and Rammam III stores the water during monsoon reducing the peak flow but releases the storage during lean season hence increases the lean season flow. A regression analysis was carried out to develop an equation to find the percent flow reduction at Dalia point due to different flow control scenarios. The equation can be used to assess the impact on Bangladesh side of the Teesta River flow due of upstream development (control structures) of the basin.

CHAPTER ONE
INTRODUCTION

1.1 Background

South Asia is one of the most densely populated regions of the world, and also one of the most water scarce. With access to only 8.3 percent of the world's water resources, the region supports more than 21 percent of the world's population (Prasai & Mandakini, 2013). Despite registering impressive growth over the past decade, countries in the region continue to struggle with high rates of poverty and low levels of human development. By 2005 estimates, close to 595 million people in South Asia lived on less than $1.25 a day (World Bank, 2008). In recent decades, population expansion, urbanization, and changes in production and consumption patterns in the region have increased the demand for water, food, and energy. Simultaneously, variations in rainfall patterns and weather systems due to climate change have made the region highly susceptible to floods, droughts, and natural disasters.

The Himalayas, known as the "water tower" of Asia or the "third pole," supply the three major trans-boundary river systems of the Indus, the Ganges, and the Brahmaputra, which collectively support an estimated 700 million people (Prasai & Mandakini, 2013). In addition, the annual southwest monsoons supply 70–90 percent of annual rainfall in the region (Jaitley, 2009). The majority of countries in South Asia rely on trans-boundary water flows to meet their domestic water needs. Bangladesh, for example, draws an estimated 91.3 percent of its water from trans-boundary river systems such as the Brahmaputra and the Ganges (Prasai & Mandakini, 2013). Similarly, Pakistan relies on the Indus river system to meet its agricultural and industrial needs, and has a high water dependency ratio of 75.6 percent (Chellaney, 2011).

Meanwhile, water availability per capita in South Asia has declined by a staggering 70 percent since 1950 (Jaitley, 2009). In addition, climate change studies of South Asia increasingly suggest that the effects of glacial melt and erratic monsoon patterns will significantly reduce the availability of water in river basins in the region. As the demand for water for agriculture, industry, and hydropower generation in these countries grows, water is increasingly a driver of tension and potential conflict in the region.

Water governance policies in South Asia tend to be state centric, technocratic, exclusionary, nationalistic, and very often do not adequately recognize human, ecological, and social costs and their implications (Prasai & Mandakini, 2013). Governments in South Asia have traditionally endowed themselves with the exclusive right to articulate public interests on water resources, and have continued to show a deep resistance to parting from that tradition. In recent years, the situation has been exacerbated by collusion among politicians and domestic and foreign investors involved in water related infrastructure projects (Prasai & Mandakini, 2013). Water is a contested resource that attracts multiple and unmediated economic, ecological, and political claims on its usage, distribution, conservation, and management. As a result, the use of water resources within and among South Asian countries has always been contentious, and has often been politically contested by excluded stakeholders.

With water issues now part of the larger ecological concerns surrounding climate change, there is an opening for greater cooperation on trans-boundary water governance. In that respect, the demand for more inclusive and democratic deliberations on water governance is not just a moral appeal, but an engineering, ecological and economic necessity.

The Teesta River is one of the most important trans-boundary river of Bangladesh with only the Ganges and Brahmaputra have a higher annual runoff than the Teesta. It is a tributary of the Brahmaputra River and falls under the Brahmaputra sub-basin in the Eastern Himalayan region.

Bangladesh has long argued that India's construction of the Gozaldoba Barrage upstream of Dalia (Teesta Barrage) has significantly reduced the availability of water in the dry season. Water diversion at Gozoldoba and Dalia are used mainly for surface water irrigation and high rate flow diversion at Gozoldoba creates water scarcity for the Bangladesh part of the Teesta River. Furthermore, the release of water during the monsoon season causes flooding and bank erosion downstream. The availability of water for irrigation, particularly in the lean or dry season, has been at the crux of the longstanding dispute between the two countries.

And with the impending threat of climate change, the water balance of the Teesta Basin is going to become a more important factor in an already water stressed region. In recent

years, Sikkim has experienced a number of sudden and devastating glacial lake outburst floods (GLOFs) (Prasai & Mandakini, 2013). Several potentially dangerous small and medium sized glacial lakes have been identified in the upper catchment of the Sikkim region (CISMHE, 2006). These lakes are evidence of increasing glacial melt and retreat in the upper reaches of the basin due to climate change. It is predicted that the Himalayan river catchments will experience more extreme weather events such as cloudbursts and heavy rainfall, increasing the rate of soil erosion, landslides, and flash floods (IPCC, 2013). The general pattern of hydrological impact of climate change in the Brahmaputra river basin can be extrapolated to the Teesta to predict a future in which accelerated melting of the glaciers feeding the rivers will lead initially to more frequent and intense flooding, but subsequently, as the glaciers retreat ever further, to decreases and eventually drastic reductions in the Teesta's flow (Immerzeel et al., 2010).

With those things in mind, a study was carried out to assess the water availability, water balance and potential changes in the water balance due to climate change in one of South Asia's most contentious sub basins, the Teesta River Basin. This study captures the salient findings of that analysis.

1.2 Teesta River Basin

The river Teesta is one of the main Himalayan rivers and originates from the glaciers of Sikkim in North at an elevation of about 5,280 m (CISMHE, 2006). The glacial lake is located at the tip of the Teesta Khangse glacier, which descends from Pauhunri peak. The river rises in mountainous terrain in extreme north as Chhombo Chhu, which flows eastward and then southward to be joined by Zemu Chhu, upstream of Lachen village near Zema. The river takes a gentle turn in southeast direction and meets Lachung Chhu at Chungthang where it takes the form of a mighty Himalayan river. After the confluence of Teesta River and Lachung Chhu at Chungthang, the river gradually widens and takes a strong westward turn upstream of Tong and after flowing down to Singhik, the river drops from 1,550 m to 750 m (CISMHE, 2006). At Singhik, the river receives one of its major tributaries, Rangyong Chhu on its right bank, which originates from the Talung glacier, a part of the Khangchendzonga mountain range. From Singhik, the river flows southwards to Dikchu with a 200 m drop through a very deep valley for about 30 km (CISMHE, 2006). From Dikchu onwards, the river takes many sharp and wide curves and flows down to Singtam with a further drop of about 200m. Rangpo Chhu, which

drains the Chhangu lake area in East Sikkim joins Teesta river on its left bank at Rangpo. Downstream of Rangpo, Teesta River widens and is joined by Rangit river at Melli Bazar on Sikkim-West Bengal border. From Melli Bazar downstream, the river leaves the hilly terrain and enters the plains of West Bengal at Sevoke near Siliguri. A map showing the route of the river has been shown in **Figure 1.1**.

The Teesta drains nearly 95 percent of the mountainous state of Sikkim (CISMHE, 2006). Teesta and most of its tributaries are flashy mountain rivers and carry boulders and considerable quantity of sediment. Throughout its course in Sikkim, the river is turbulent, flowing with high velocity through deep, narrow valleys. Within a distance of 100 kilometers, the elevation of the Teesta basin varies from 8,598 meters to 213 meters (CISMHE, 2006). It has been argued that the rapid descent of the river from high elevations makes it ideally suited for hydropower development. Notably, the Sikkim stretches of the Teesta are prone to earthquakes, landslides, and frequent floods. As it travels towards the plains, the Teesta is joined by a number of tributaries, including the Lachung Chhu, the Dik Chhu, the Chakung Chhu, the Rani Khola, and the Rangpo on the left bank, and the Zemu, the Rangyong, the Rongli, and the Rangit on the right bank (Prasai & Mandakini, 2013).

The Teesta is the fourth largest trans-boundary river in Bangladesh, flowing through the five northern districts of Gaibandha, Kurigram, Lalmonirhat, Nilphamari, and Rangpur (Rangpur Division), comprising 9,667 square kilometers, 35 upazilas, and 5,427 villages, with an estimated population in 2011 of 9.15 million (Bangladesh Bureau of Statistics, 2012). According to one estimate, 21 million people in Bangladesh are directly or indirectly dependent on the river for their livelihoods (Bangladesh Bureau of Statistics, 2012). In total, the Teesta flood plain covers nearly 14 percent of the total cultivated area of Bangladesh and provides livelihood opportunities directly to approximately 7.3 percent of the population, or 9.15 million people, in five districts of Rangpur Division (Bangladesh Bureau of Statistics, 2012). The population density in the river basin is high and is growing at a fast pace. The population mostly resides in rural areas (around 78%) but is urbanizing at a rapid rate. Poverty is high in both the Indian and Bangladeshi part of the basin (Strategic Foresight Group, 2013).

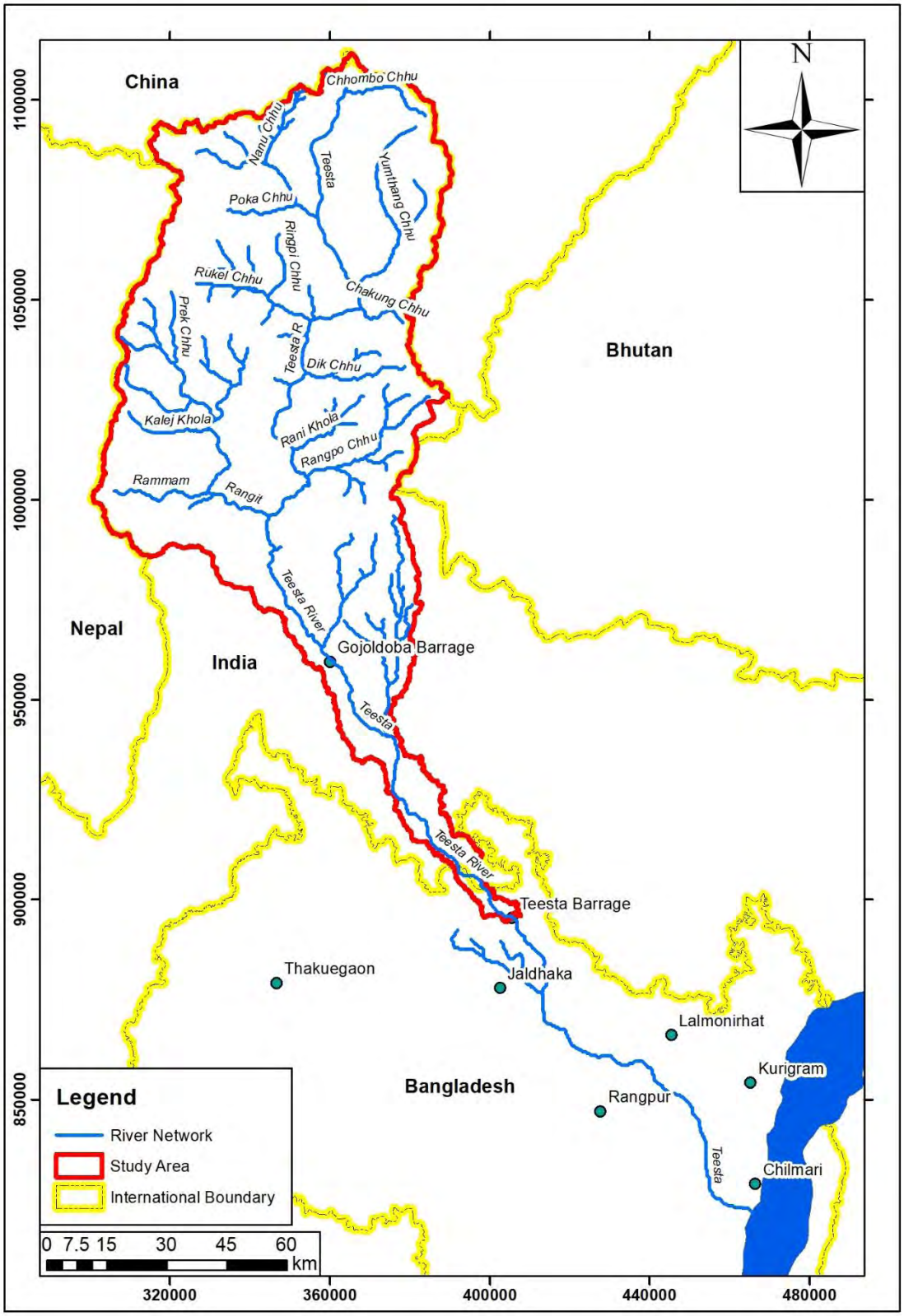

Figure 1.1: River Network in the Teesta Basin

The Teesta is a perennial, rain- and snow-fed river (Prasai & Mandakini, 2013). The discharge of water through the Teesta varies significantly between dry and wet spells. Historically, the Teesta River has had an average maximum flow of 280,000 cusec and a minimum of 10,000 cusec at Dalia, upstream of the Teesta Barrage in Bangladesh

(Khalid, 2013). Presently, the dry flow of the river is highly controlled for hydro and for irrigation projects both in India and in Bangladesh (Haque et al., 2014). Excessive control over the Teesta flow has made this mighty river sluggish, and this flow has come down to about 1000 cusec and even 500 cusec during droughts (Khalid, 2013) in Bangladesh.

After traveling a distance of approximately 414 kilometers through India and Bangladesh, the Teesta merges with the Brahmaputra (Jamuna) at an elevation of 23 meters at Teestamukh Ghat (Kamarjani Bahadurabad) in Rangpur District in Bangladesh. It then traverses 151 kilometers in Sikkim, 142 kilometers along the Sikkim West Bengal boundary and through West Bengal, and 121 kilometers in Bangladesh (CISMHE, 2006).

The trans-boundary basin of the Teesta River encompasses 12,159 square kilometers, of which 10,155 are in India and 2,004 are in Bangladesh. Approximately 8,051 square kilometers of the river basin lie in hilly parts of Sikkim (6,930 square kilometers) and West Bengal (1,121 square kilometers). Approximately 4,108 square kilometers of the basin lie in the plains of West Bengal (2,104 square kilometers) and Bangladesh (2,004 square kilometers) (Prasai & Mandakini, 2013). The Teesta River has an average annual runoff of 60 billion cubic meters (BCM) (90% of the river's flow occurs during the monsoon or wet season i.e. between June and September (Strategic Foresight Group, 2013). The importance of the flow and seasonal variation of this river is felt during the lean season (October to April/May) when the average flow is about 500 million cubic meters (MCM) per month (Strategic Foresight Group, 2013).

Historically, the Teesta was part of the Ganges river system, flowing south from Jalpaiguri in West Bengal in three separate channels: the Karatoya, the Purnabhaba, and the Atrai. It is speculated that the three channels led to the name "Trisrota" ("possessed of three streams") and subsequently to "Teesta." Following a flood in 1787, the Teesta changed its course southeast to join the Brahmaputra (Prasai & Mandakini, 2013).

1.3 Objectives of the Study

The main objective of this research is to compute the water distribution and availability in the Teesta River Basin and the possible change of the water balance due to future climate change scenarios and upstream developments. The specific objectives of the studies are:

i. Assessment of existing water availability of Teesta River at Dalia point.
ii. To develop a hydrological model of the Teesta basin using SWAT.
iii. Selection of future climate change scenarios and different upstream controls scenarios
iv. Simulation of impact of climate changes and upstream control to investigate its effect on the water availability and water balance of the Teesta River basin.

1.4 Outputs

The most important output of this research is a hydrologically calibrated and validated model of the Teesta River basin incorporating all the complex dynamics and features of this unique basin. Furthermore, the impact of climate change for different scenarios from selected GCM models have been assessed along with the baseline mode. This helps to better understand the changes in water balance of the Teesta Basin due to the impacts of climate change. As well as analyzing the probable impact of upstream developments on the Teesta River basin can be visualized from this study. So the possible outcomes of the research work can be summarized as follows

- Baseline hydrological information of the Teesta River Basin
- Probable impact of climate changes and upstream developments in the Teesta River Basin

1.5 Organization of the Thesis

Considering literature review, location of the study area, theories related to the hydrological modeling, data analysis, model calibration, results and discussions the report has been organized under five chapters which are described below:

Chapter 1 describes the background, highlights the objectives of the study and contains organization of the thesis.

Chapter 2 describes the salient features of the study area, the existing and planned hydraulic structures in the vicinity of the study area. It also provides an insight on the problems of the Teesta River Basin and finally summarizes the relevant studies related to changes in water balance due climate change in Bangladesh and globally. It also

reviews the past studies carried out to develop a hydrological model of the Teesta River Basin. It also describes the theories regarding this research work. It also describes the equations developed for hydrological modeling and contains a short description about the mathematical modeling tools used in the study.

Chapter 3 describes the methodology of this study briefly. The data collection and model development processes has been explained thoroughly in this chapter.

Chapter 4 discusses the study analysis and outputs it detail. Data analysis, climate change scenario development, model outputs for different scenarios have been included in this chapter.

Chapter 5 provides the overall conclusions of the study and also some recommendations for further study.

CHAPTER TWO
LITERATURE REVIEW AND THEORY

2.1 Hydrometeorology of Teesta River Basin

The Teesta is a perennial, rain and snow fed river. A number of glaciers and glacial lakes in the upper reaches of the basin in Sikkim supply the headwaters of the Teesta. The largest glacier in the basin is the Zemu glacier, covering an area of 107.3 square kilometers, and the largest glacial lake is the Khangchung Chho, with coverage of approximately 1.6 square kilometers (Parsai, 2013). It is estimated that there are over 300 glacial lakes dotting the Teesta Basin in the Sikkim Himalayas (CISMHE, 2006). In addition to glacial melt water, the Teesta is also fed by a number of tributaries as it journeys towards the plains. The tributaries of the Teesta are considered "flashy" mountain rivers that travel at high velocities with large quantities of debris and sediment.

The maximum discharge of the Teesta river at Kaunia station is 8,500 cumec with the minimum flow is 5.50 cumec (Mondal & Islam, 2017). The water level at Dalia station varies from 52.97 mPWD to 48mPWD (Mondal & Islam, 2017). Mean daily maximum temperature in the sub-basin varies from about 26.8º C in September to 20.7º C in the month of January (CISMHE, 2006). Mean daily Relative Humidity varies from 63.8 percent to 88.7 percent over the basin (CISMHE, 2006). The mean daily Relative Humidity is 68.3 percent in January, 66.2 percent in April, 88.7 in July and 68.0 in October (CISMHE, 2006). The mean monthly wind speed varies from as low as 43.2 km/day from July to September to high of 98.4 km/day in the month of April (CISMHE, 2006).

The upper catchment of the Teesta Basin in Sikkim is prone to sudden variations in rainfall and temperature due to the high altitude and mountainous topography. The average annual rainfall in Sikkim is 2,534 millimeters, with the maximum rainfall occurring in the month of July and the minimum 32mm in December (CISMHE, 2006). The climate in the basin ranges from extremely cold and alpine conditions in the north to humid and sub-tropical conditions in the south, west, and east. Notably, the Sikkim region is geologically fragile and prone to frequent powerful earthquakes and landslides.

2.2 Existing and Proposed Hydraulic Structures in the Teesta Basin:

In India, the most significant development activity on the Teesta is the construction of a series of cascade dams for hydropower generation in the state of Sikkim. Approximately 30 major hydropower projects have been planned on the river, with a planned capacity of over 5,000 megawatts of electricity (Parsai, 2013). The rapid construction of mega power projects in Sikkim and large parts of India's northeast comes in the wake of the liberalization of India's power sector in 2003 and a significant drive by the Indian government to meet the country's energy needs through hydropower generation. Some of the major hydropower projects in Sikkim include Teesta Stage II (330 megawatts), Teesta Stage III (1200 megawatts), Teesta Stage IV (520 megawatts), Teesta Stage V (510 megawatts), Teesta Stage VI (500 megawatts), and Panan HEP (300 megawatts) (Parsai, 2013). The image of Teesta V Dam in Sikkim is shown in **Figure 2.1**. The map of all the major existing and proposed structures in the Teesta River Basin is shown in **Figure 2.2**. The structures in that figure is marked with different notations the details of which are given in **Table 2.1**.

Figure 2.1: Teesta V Dam in Sikkim (510 MW project)

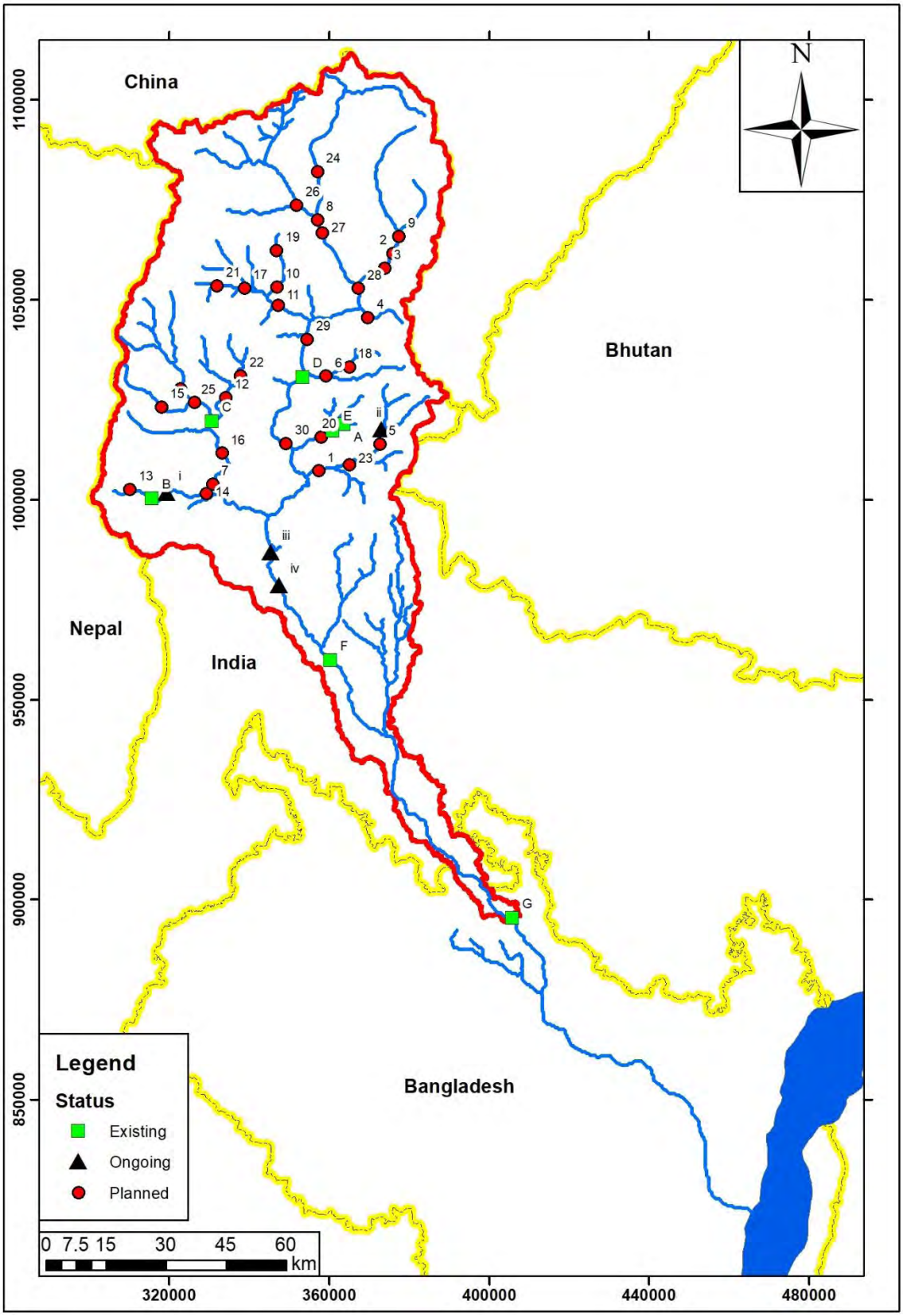

Figure 2.2: Map of all the existing and proposed structures in the Teesta River Basin (*Reproduced from Prasai & Mandakini, 2013*)

Table 2.1: List of Control Structures in the Teesta River Basin

Structure No	Structure Name	Status	Power Capacity (MW) / Diversion	River Name	Main/Tributary
1	Bhasme	Proposed	32	Rangpoo Chhu	Tributary
2	Bimkyong	Proposed	99	Lachung Chhu	Tributary
3	Bop	Proposed	99	Lachung Chhu	Tributary
4	Chhakung Chhu	Proposed	50	Chhakung Chu	Tributary
5	Chuzachen	Proposed	99	Rangpoo Chhu	Tributary
6	Dik Chhu	Proposed	90	Dik Chhu	Tributary
7	Jorethang Loop	Proposed	96	Rangit	Tributary
8	Lachen	Proposed	210	Teesta	Main
9	Lachung	Proposed	99	Lachung Chhu	Tributary
10	Lingza	Proposed	160	Ringpi Chhu	Tributary
11	Panan	Proposed	200	Rangyong	Tributary
12	Ralang	Proposed	40	Rangit	Tributary
13	Rammam I	Proposed	36	Rammam	Tributary
14	Rammam IV	Proposed	30	Rammam	Tributary
15	Rangit II	Proposed	60	Rimbi Khola	Tributary
16	Rangit IV	Proposed	90	Rangit	Tributary
17	Rangyong	Proposed	90	Rukel Chhu	Tributary
18	RateyChu-BakchaChu	Proposed	40	Dik Chhu	Tributary
19	Ringpi	Proposed	160	Ringpi Chhu	Tributary
20	Rongni	Proposed	95	Rani Khola	Tributary
21	Rukel	Proposed	90	Rukel Chhu	Tributary
22	Sada Mangder	Proposed	71	Kayam Chhu	Tributary
23	Suntaley Tar	Proposed	30	Rangpoo Chhu	Tributary
24	Talem	Proposed	75	Teesta	Main
25	Tashiding	Proposed	60	Prek Chhu	Tributary
26	Teesta I	Proposed	300	Teesta	Main
27	Teesta II	Proposed	480	Teesta	Main
28	Teesta III	Proposed	1200	Teesta	Main
29	Teesta IV	Proposed	495	Teesta	Main
30	Teesta VI	Proposed	500	Teesta	Main
31	Ting Ting	Proposed	70	Prek Chhu	Tributary
i	Rammam III	Ongoing	120	Rammam	Tributary
ii	Rolep	Ongoing	32	Rangpoo Chhu	Tributary
iii	Teesta Low Dam III	Ongoing	132	Teesta	Main
iv	Teesta Low Dam IV	Ongoing	160	Teesta	Main
A	Lower Lagyap	Existing	12	Taksom Chhu	Tributary
B	Rammam II	Existing	50	Rammam	Tributary
C	Rangit III	Existing	60	Rathong Chhu	Tributary
D	Teesta V	Existing	510	Teesta	Main
E	Upper Rongnichu	Existing	8	Rani Khola	Tributary
F	Gojoldoba Barrage	Existing	Diversion	Teesta	Main
G	Teesta Barrage	Existing	Diversion	Teesta	Main

These projects are “run of the river” hydroelectric projects, which involve the construction of large dams to divert river water through tunnels and a powerhouse before the river water is deposited downstream. The large scale construction of dams in the region has been controversial, with local communities, civil society groups, academics, and environmentalists raising concerns about the ecological, environmental, and sociocultural impact of run of the river projects in the region. Groups and communities in the state of West Bengal have also raised concerns about the downstream impacts of these projects on agriculture, navigation, fishing, and other livelihoods.

In West Bengal, the Teesta Barrage Project (TBP) is one of the largest irrigation projects in eastern India, intended on completion to irrigate 922,000 hectares in six districts of north Bengal and provide 67.50 megawatts of hydropower (Irrigation and Waterways Department, Government of West Bengal). The three phase project seeks to utilize Teesta River waters for “irrigation, hydropower generation, navigation, and flood control” through a network of barrages and canals on the river (Irrigation and Waterways Department, Government of West Bengal). Though it was initiated in 1976, only certain stages of the project have been completed to date, including construction of the Teesta Barrage at Galzaldoba in Jalpaiguri District of West Bengal, and barrages on the Mahananda and Dauk rivers (Parsai, 2013). In addition to the ambitious TBP, NHPC Limited (formerly the National Hydroelectric Power Corporation) is in the process of developing two “low dams” in Darjeeling District of West Bengal — Teesta Low Dam III (132 megawatts) and Teesta Low Dam IV (160 megawatts) (CISMHE, 2006).

The Government of India’s controversial Inter Linking of Rivers Project also involves utilization of the Teesta River. Under the plan, water from India’s Himalayan and peninsular rivers would be diverted through a series of inter basin canals and dams, to water scarce and drought prone areas of Southern India. The project is intended to eventually irrigate 30 million hectares and generate 20,000 to 25,000 megawatts of power (National Council for Applied Economic Research, 2008). The project has been criticized by groups in both India and Bangladesh. Officials in Bangladesh fear that it will increase flooding in the country and reduce the availability of water in the dry season. They have also argued that the project violates the 1996 Helsinki Rules on Water Resources and the subsequent 2004 Berlin Rules on Water Resources governing equitable sharing of river waters between co riparians (Condon, E., and P. Hillman, et al 2009). Notably, in February 2012, the Supreme Court of India ordered the setting up of a special committee

to expedite implementation of the project (Parsai, 2012).

In Bangladesh, the Teesta is critical to meeting the agricultural and irrigation needs of northern parts of the country that are water scarce and drought prone. Initiated in the 1970s, the Teesta Barrage Irrigation Project (TBIP) aims to increase agricultural production, food security, and employment opportunities in the country's northern districts. The two phase project covers 12 upazilas and has a total planned command area of 750,000 hectares and an irrigable area of 540,000 hectares. Phase I of the project, with a command area of 154,250 hectares and a net irrigable area of 111,406 hectares, was completed in 1998. It covers the districts of Nilphamari, Dinajpur, and Rangpur (Rangpur Division), and consists of a barrage at Dalia in Lalmonirhat District, a canal head regulator, flood embankments, irrigation canal networks, and drainage channels..

Bangladesh has long argued that India's construction of the Gazaldoba Barrage upstream of Dalia has significantly reduced the availability of water in the dry season. Afroz & Rahman (2013) calculated that the flow reduced up to 88% in Bangladesh due to construction of Gozoldoba Barrage. Furthermore, the release of water during the monsoon season causes flooding and bank erosion downstream. The availability of water for irrigation, particularly in the lean or dry season, has been at the crux of the longstanding dispute between the two countries. The plan image and photos of the Teesta Barrage Dalia and Gozoldoba are shown in **Figure 2.3** and **Figure 2.4** respectively.

Figure 2.3: Teesta Barrage in Dalia

Figure 2.4: Teesta Barrage in Gozoldoba

2.3 Basin Governance and the State of Bilateral Negotiations

India and Bangladesh share as many as 54 trans-boundary rivers, including the three major river systems of the Ganges, the Brahmaputra, and the Meghna. The majority of these rivers originate in the Himalayas and travel through India and Bangladesh to the Bay of Bengal. As the upper riparian, India has traditionally staked a prior claim to rivers flowing through its territory, and in so doing, has controlled the quantity of water flowing into Bangladesh. Due to its unique topography, lower riparian Bangladesh is prone to seasonal variations in river flows, and scarcity of water in the dry season. Consequently, Bangladesh relies heavily on trans-boundary river flows from India. Given this scenario, water sharing has frequently been a source of tension between the two South Asian neighbors.

The two countries have a long history of water disputes, notably over the sharing of Ganges river waters. India's diversion of the Ganges from Farrakka Barrage to the Bhagirathi Hoogli river system was for decades a major source of discord between the two countries. While the Ganges Water Treaty of 1996 signaled a shift in bilateral

relations, in recent years, disagreements over India's construction of the Tipaimukh dam in the Indian state of Manipur upstream of the Bangladesh border, over India's Inter Linking of Rivers Project, and over the sharing of other transboundary rivers such as the Teesta, the Feni, the Manu, the Muhuri, the Dharla, and the Dudhkumar, have continued to flare up (Chellaney, 2011).

Negotiations between India and Bangladesh on the Teesta can be traced back to the 1950s and 1960s, when authorities in India and the former East Pakistan began discussing proposed projects on the river. While the negotiations proved inconclusive, both sides agreed to share technical data and information. Following the independence of Bangladesh in 1971, the Indo Bangladesh Joint River Commission was set up to anchor talks on the sharing of river waters. In 1983, India and Bangladesh agreed to an ad hoc arrangement to share 75 percent of the Teesta waters, with India using 39 percent and Bangladesh 36 percent, and the remaining 25 percent to be allocated following further study.

As the upper riparian country, India controls the flow of water into Bangladesh from the Teesta barrage at Gazaldoba, constructed to provide water to northern parts of West Bengal. Bangladesh has also constructed a barrage downstream, at Dalia in Lalmonirhat District, which supplies water for agriculture and irrigation to drought prone areas of northern Bangladesh. It is argued by Bangladesh that the construction of the Gazaldoba Barrage and the diversion of water has drastically reduced water availability at the Dalia Barrage, particularly in the dry season (Prasai & Mandakini, 2013). Afroz & Rahman (2013) calculated that the flow reduced up to 88% in Bangladesh due to construction of Gozoldoba Barrage.

1997, a Joint Committee of Experts was formed to examine the sharing of the river. Although a series of meetings were held between 1997 and 2004, little progress was made. Subsequently, a Joint Technical Group (JTG) was formed in 2004 to develop draft terms of reference for a joint scientific assessment of the Teesta, and an interim agreement on sharing of lean season flows between the two countries (Prasai & Mandakini, 2013). In 2005, in its fourth meeting, the JTG recorded its inability to come up with a solution. In the same year, the Joint River Commission, in its 36th meeting, recognized that "the lean season flows in the Teesta will not meet the needs of both the countries and hence any sharing formula for the lean season flows should be based on

shared sacrifices" (Parsai, 2013). In 2010, the prime ministers of India and Bangladesh issued a joint communiqué calling for the Teesta issue to be resolved expeditiously. The two countries prepared a draft agreement on the Teesta and a statement of principles for sharing river waters in the lean season. These documents were to form the basis of an interim agreement on the Teesta between India and Bangladesh (Parsai, 2013).

In September 2011, during Indian Prime Minister's visit to Dhaka, the two countries were poised to sign a new agreement on the Teesta. However, the agreement fell through when West Bengal Chief Minister protested the proposed allocation of 50 percent of the river's water to Bangladesh. As water falls under the jurisdiction of the states in India's federal system, the Indian government could not proceed without further consultations with the West Bengal government. Notably, during the Indian prime minister's visit, India and Bangladesh signed a broad framework agreement on bilateral cooperation emphasizing, among other issues, the need to explore the possibility of "common basin management of common rivers". However, India's failure to sign the Teesta agreement in 2011 has continued to be a sore point between both countries, and has slowed bilateral discussions on other issues, including transit facilities for India through Bangladesh and discussions on the sharing of other transboundary rivers such as the Feni, the Manu, the Muhuri, the Khowai, the Gumti, the Dharla, and the Dudhkumar (Ahmed, 2012).

To date, bilateral discussions between India and Bangladesh on the Teesta have proven intractable. Despite several meetings of the Joint River Commission, the Joint Committee of Experts, and the Joint Technical Group, little progress has been made on critical issues such as lean season flow. Discussions between the two countries have largely been technical in nature, with little discussion of social and ecological issues or stakeholder concerns. Spaces for civil society engagement or public participation have also been extremely limited (Prasai & Mandakini, 2013). West Bengal Chief Minister's refusal to endorse the proposed Teesta agreement on the grounds that her government had not been adequately consulted demonstrates the exclusive nature of the discourse even at the national level. Notably, in May 2012, then External Affairs Minister announced that the Government of India was working "to develop a political consensus in India" on the Teesta, and was in the process of consulting the state government of West Bengal (Ahmed, 2012). More recently, in March 2013, on an official visit to Bangladesh, President of India assured Bangladesh of its commitment to "a fair, reasonable solution" on the Teesta, and that consultations with stakeholders in India, including the government

of West Bengal, would be concluded at the earliest. While progress on these consultations is unclear, the government's statement reflects the growing recognition that broader stakeholder concerns and interests regarding the Teesta have largely been neglected in mainstream bilateral discussions.

2.4 Climate Change Modeling for Hydrological Impact Assessment

Warming of the climate system in recent decades is unequivocal because of the observational evidences which confirm the increases in global average air and ocean temperatures (Bates et.al., 2008). These changes in global climate can affect a number of components of the hydrological cycle and hydrological systems (e.g. precipitation, snowmelt, evaporation, soil moisture, runoff etc). Such changes in hydrologic system will affect nearly every aspect of human well-being, from agricultural productivity and energy use to flood control, municipal and industrial water supply, fishery and wildlife management. So it is obvious to understand how a change in global climate could affect regional water supplies. Literature review of current studies indicates that climate change modeling for hydrological impact studies generally done in three steps (Islam, 2011):

Step 1: Runoff simulation under present climatic conditions for climate normal period (a 30 years period, usually 1961-1990 or 1971-2000 or 1981-2010) using a hydrologic model calibrated and validated with historical data;

Step 2:Generation of climate change scenarios for different future periods (usually three 30 years period of 21st century, namely, 2010-2039, 2040-2069, and 2070-2099);

Step 3: Runoff simulation under changed climatic conditions for future periods based on the generated climate change scenarios.

The effect of climate change on surface water resources in future is usually demonstrated by comparing the runoff generated from step 3 and step 1. Runoff simulation under present and changed climate (Step 1 and 3) is usually conducted by hydrologic models. Scientific literatures on hydrological impacts of climate change contain a large number of reports detailing the application of various hydrologic models in global, regional, or basin scale.

2.5 Approaches of Climate Change Scenario Generation

There are different approaches to generate climate change scenarios for hydrological impact studies. They can be broadly classified as synthetic approach, analogue approach and climate model based approach (**Figure 2.5**) and will be discussed in the following paragraphs:

2.5.1 Synthetic Approach

In the synthetic approach the future climatic variables (mostly precipitation and temperature) are changed incrementally by arbitrary amounts. These changes can be made in annual, seasonal or monthly scales. Climate change scenario generation in this method consists of three steps:

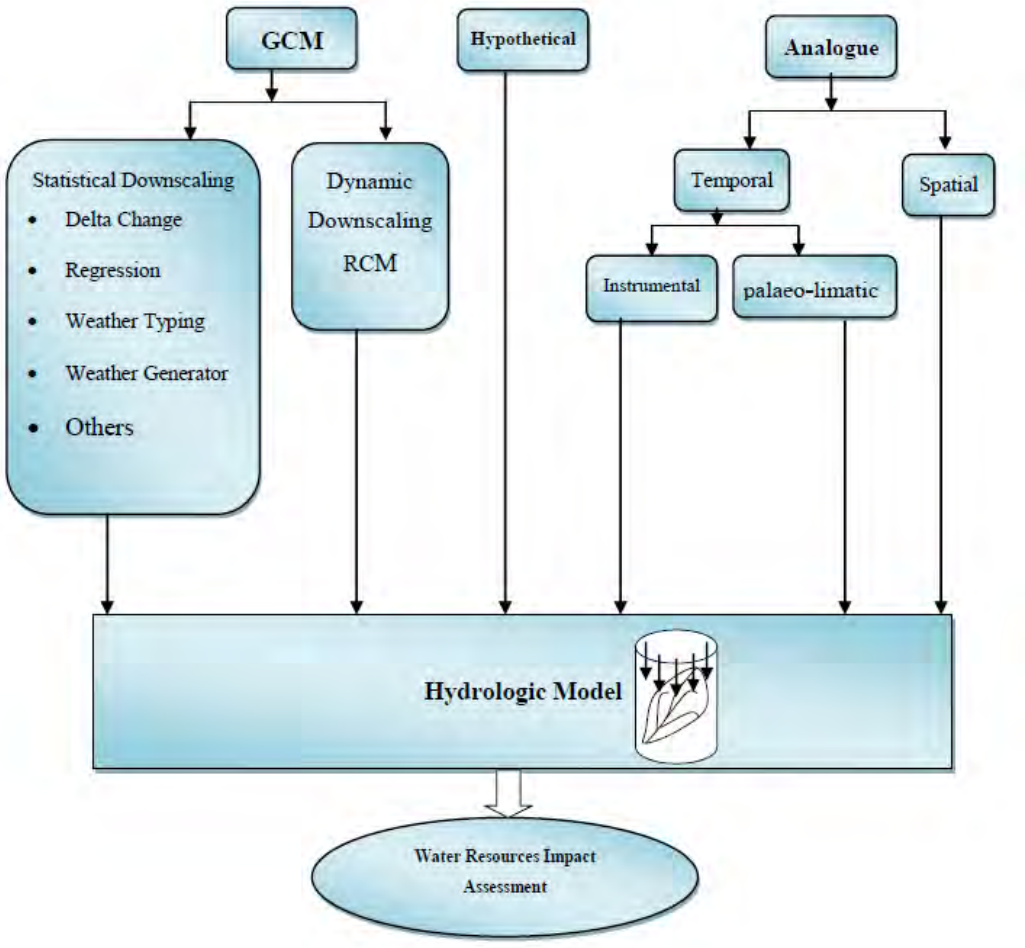

Figure 2.5: Different approaches of climate change modeling for water resources impact assessment (Source: Islam, 2011)

Step 1: Estimation of average annual or monthly changes in climate data. Typically temperature and precipitation changes are estimated by,

$$\Delta T = +1°, +2°, \text{ and } +4°$$
$$\Delta P = 0, \pm 10\%, \pm 20\%$$

Step 2: Perturbation of historical time series of climatic data. Typically temperature and precipitation for climate change scenario are perturbed as,

$$T_2 = T_1 + \Delta T \quad (2.1)$$
$$P_2 = P_1 + \Delta P \quad (2.2)$$

where T_1, T_2 and P_1, P_2 are the historic and future temperature and precipitation respectively.

Step 3: Drive a calibrated hydrological model based on perturbed precipitation and temperature to simulate hydrological characteristics (runoff, soil moisture, evapotranspiration etc.).

Many climate change studies on water resources impact assessment are based on this approach (e.g. Nemec and Schaake, 1982; Schaake and Liu, 1989; Nash and Gleick, 1990; Whetton et.al., 1993; Xu and Halldin, 1997; Xu, 2000; Guo et.al., 2002; Davies, 2004; Jiang et.al., 2007). A summary of those studies is shown is **Table 2.2**

Table 2.2: Examples of Hydrological Impact Studies Based on Synthetic Climate Change Scenarios *(Source: Islam, 2011)*

Authors	Location	Predictand	Perturbation
Nemec and Schaake(1982)	Leaf River Basin, USA Pease River Basin, USA Nzoia River Basin, western Kenya.	T P	±1, +3 °C ± 10%, ± 25%
Schaake and Liu (1989)	Southeast, USA	ET P	+10% +10%
Nash and Gleick (1990)	Colorado River Basin	T P	+2, +4 °C 0, ± 10%, ± 20%
Whetton et.al.(1993)*	Perth, Australia	ET P	+20% to 40% -20% to 40%
Chiew et. al. (1995)	Australia	T P	0, +2, +4 °C 0, ± 10%, ± 20%, ± 30%, ± 40%
Xu and Halldin (1997)	NOPEX Area ,Europe	T P	+2, +4 °C ± 10%, ± 20%

Authors	Location	Predictand	Perturbation
Fowler (1999)*	Auckland, New Zealand	ET P	-20% to 40% -20% to 40%
Xu (2000)	Central Sweden	T P	+1, +2, +4 °C 0,± 10%, ± 20%
Davies (2004)*	North-Central Sweden	T P	-5 to +15 °C -10% to 40%
Jiang et.al. (2007)	Dongjiang Basin, South China	T P	+1, +2, +4 °C 0, ±10%, ± 20%
Guo et.al. (2002)	China	T P	±1, ±2, ±3 ° C 0%, ±25%,

* Response surfaces plotting; Abbreviations: T–Temperature, P– Precipitation, ET– Potential Evapotranspiration

2.5.2 Analogue Approach of Climate Change Modeling

In analogue approach, climate change scenarios are constructed by identifying recorded climate regimes which may resemble the future climate in a given region (IPCC, 2001). In this approach the fundamental assumption is that, climate will respond in the same way to a unit change in forcing despite its source or the boundary conditions in place at the time. Analogue approach can be spatial or temporal. In spatial analogue approach attempts are made to identify regions which have a climate that is similar to that projected for the study region in the future. In temporal analogues for a given location a past climate is analyzed to resemble the projected future climate for that location (Islam, 2011)

Many climate change studies on water resources are found in literature were based on analogue approach (e.g. Palutikof, 1987; Krasovskaia and Gottschalk, 1992; Knox,1993; Zorita and Storch, 1999; Cohen and Kulkarni, 2001; Bouraoui et.al., 2004; Yao et.al., 2009; Orlowsky et.al., 2010). Most of them used temporal analogue approach based on historical measurement of precipitation, temperature and river flows.

2.5.3 Climate change modeling based on general circulation models

Development of General Circulation Models (GCMs) is one of the most prominent climate change research advancements starting from the early 1990s onwards, and they are the most advanced tools currently available for simulating the response of the global climate system to changing atmospheric composition (e.g. increase in atmospheric CO_2 on the mean global climate) (IPCC, 2001; Shackley et.al., 1998). GCMs are numerical

atmospheric model coupled with three dimensional dynamic ocean models, together with complex land surface schemes and sea ice models, and can provide considerable potential for the study of climate change and variability (Fowler et.al., 2009; Shackley et.al., 1998). GCMs used to solve equations describing the movement of energy and momentum, along with the conservation of mass at discrete points on the entire surface of the Earth, at a fixed time interval, and for separate layers in the atmosphere defined by a regular grid (Wilby, 2009).

Initially atmospheric General Circulation Models (GCMs) were run to equilibrium under current ($1xCO_2$) and doubled ($2xCO_2$) emissions forcing to estimate their potential effect on global climate. After being coupled with Oceanic Circulation Models, these GCMs are forced with transient greenhouse emissions to allow for the estimation of the rate at which climate changes might occur. **Table 2.3** shows different GCMs available, their institution and resolutions.

Table 2.3: Spatial Resolution of selected GCMs in IPCC TAR and AR5 *(Source: IPCC, 2013)*

Sl	Model	**Institution**	**Resolution Lat x Long**	**Reference**
1	BCC-CSM 1.1	Beijing Climate Center, China Meteorological Administration	2.8125 x 2.8125	Wu, T., 2012
2	BCC-CSM 1.1(m)	Beijing Climate Center, China Meteorological Administration	2.8125 x 2.8125	Wu, T., 2012
3	CSIRO-Mk3.6.0	Commonwealth Scientific and Industrial Research Organisation and the Queensland Climate Change Centre of Excellence	1.875 x 1.875	Collier, M.A.et.al., 2011
4	FIO-ESM	The First Institute of Oceanography	2.812 x 2.812	Song, Z., Qiao, F., Song, Y.
5	GFDL-CM3	Geophysical Fluid Dynamics Laboratory	2.0 x 2.5	Donner, L.J.et.al., 2011
6	GFDL-ESM2G	Geophysical Fluid Dynamics Laboratory	2.0 x 2.5	Dunne, J.P.et.al., 2012
7	GFDL-ESM2M	Geophysical Fluid Dynamics Laboratory	2.0 x 2.5	Dunne, J.P.et.al., 2012
8	GISS-E2-H	NASA Goddard Institute for Space Studies	2.0 x 2.5	Schmidt, G.A.et.al., 2006.
9	GISS-E2-R	NASA Goddard Institute for Space Studies	2.0 x 2.5	Schmidt, G.A.et.al., 2006
10	HadGEM2-ES	Met Office Hadley Centre	1.2414 x 1.875	Collins, W.J.et.al.2011)
11	IPSL-CM5A-LR	Institut Pierre-Simon Laplace	1.875 x 3.75	Dufresne, J.L.et.al., 2013

Sl	Model	Institution	Resolution Lat x Long	Reference
12	IPSL-CM5A-MR	Institut Pierre-Simon Laplace	1.2587 x 2.5	Dufresne, J.L.et.al., 2013
13	MIROC-ESM	Atmosphere and Ocean Research Institute (The University of Tokyo), National Institute for Environmental Studies, and Japan Agency for Marine-Earth Science and Technology	2.8125 x 2.8125	Watanabe, S.et.al., 2011
14	MIROC-ESM-CHEM	Atmosphere and Ocean Research Institute (The University of Tokyo), National Institute for Environmental Studies, and Japan Agency for Marine-Earth Science and Technology	2.8125 x 2.8125	Watanabe, S.et.al.,2011
15	MIROC5	Japan Agency for Marine-Earth Science and Technology, Atmosphere and Ocean Research Institute (The University of Tokyo) and National Institute for Environmental Studies	1.4063 x 1.4063	Watanabe, S.et.al.,2010
16	MRI-CGCM3	Meteorological Research Institute	1.125 x 1.125	Yukimoto, S., 2012
17	NorESM1-M	Norwegian Climate Centre	1.875 x 2.5	Kirkevag, A., Iversen, T., Seland, O., debernard,J.B., Storelvmo, T., Kristjansson, J.E.,2008

2.6 Climate Change Scenarios

Long-term climate change projections require assumptions on human activities or natural effects that could alter the climate over decades and centuries. Defined scenarios are useful for a variety of reasons, e.g., assuming specific time series of emissions, land use, atmospheric concentrations or RF across multiple models allows for coherent climate model inter-comparisons and synthesis. Scenarios can be formed in a range of ways, from simple, idealized structures to inform process understanding, through to comprehensive scenarios produced by Integrated Assessment Models (IAMs) as internally consistent sets of assumptions on emissions and socioeconomic drivers (e.g., regarding population and socio-economic development).

2.6.1 Idealized Concentration Scenarios

As one example of an idealized concentration scenario, a 1% yr–1 compound increase of atmospheric CO_2 concentration until a doubling or a quadrupling of its initial value has been widely used in the past (Covey et al., 2003). An exponential increase of CO_2 concentrations induces an essentially linear increase in RF (Myhre et al., 1998) due to a 'saturation effect' of the strong absorbing bands. Such a linear ramp function is highly useful for comparative diagnostics of models' climate feedbacks and inertia. The CMIP5 inter-comparison project again includes such a stylized pathway up to a quadrupling of CO_2 concentrations, in addition to an instantaneous quadrupling case.

2.6.2 The Socio-Economic Driven SRES Scenarios

The SRES suite of scenarios were developed using IAMs and resulted from specific socio-economic scenarios from storylines about future demographic and economic development, regionalization, energy production and use, technology, agriculture, forestry and land use (IPCC, 2001). The climate change projections undertaken as part of CMIP3 and discussed in AR4 were based primarily on the SRES A2, A1B and B1 scenarios. However, given the diversity in models' carbon cycle and chemistry schemes, this approach implied differences in models' long lived GHG and aerosol concentrations for the same emissions scenario. As a result of this and other shortcomings, revised scenarios were developed for AR5 to allow atmosphere-ocean general circulation model (AOGCM) (using concentrations) simulations to be compared with those ESM simulations that use emissions to calculate concentrations.

2.6.3 Representative Concentration Pathway Scenarios and Their Extensions

Representative Concentration Pathway (RCP) scenarios (Moss et al., 2008; Moss et al., 2010; van Vuuren et al., 2011) are new scenarios that specify concentrations and corresponding emissions, but are not directly based on socio-economic storylines like the SRES scenarios. The RCP scenarios are based on a different approach and include more consistent short-lived gases and land use changes. They are not necessarily more capable of representing future developments than the SRES scenarios. Four RCP scenarios were selected from the published literature (Fujino et al., 2006; Smith and Wigley, 2006; Riahi et al., 2007; van Vuuren et al., 2008; Hijioka et al., 2008; Wise et al., 2009) and updated

for use within CMIP5 (Masui et al., 2011; Riahi et al., 2011; Thomson et al., 2011; van Vuuren et al., 2011a). The four scenarios are identified by the 21st century peak or stabilization value of the RF derived by the reference model (in W m^{-2}) (**Figure 2.6**): the lowest RCP, RCP2.6 (also referred to as RCP3-PD) which peaks at 3 W m^{-2} and then declines to approximately 2.6 W m^{-2} by 2100; the medium-low RCP4.5 and the medium-high RCP6 aiming for stabilization at 4.5 and 6 W m^{-2}, respectively around 2100; and the highest one, RCP8.5, which implies a RF of 8.5 W m^{-2} by 2100, but implies rising RF beyond that date (Moss et al., 2010). In addition there is a supplementary extension SCP 6 to 4.5 with an adjustment of emissions after 2100 to reach RCP 4.5 concentration levels in 2250 and thereafter. The RCPs span the full range of RF associated with emission scenarios published in the peer-reviewed literature at the time of the development of the RCPs, and the two middle scenarios where chosen to be roughly equally spaced between the two extremes (2.6 and 8.5 W m^{-2}). These forcing values should be understood as comparative labels representative of the forcing associated with each scenario, which will vary somewhat from model to model. This is because concentrations or emissions (rather than the RF) are prescribed in the CMIP5 climate model runs.

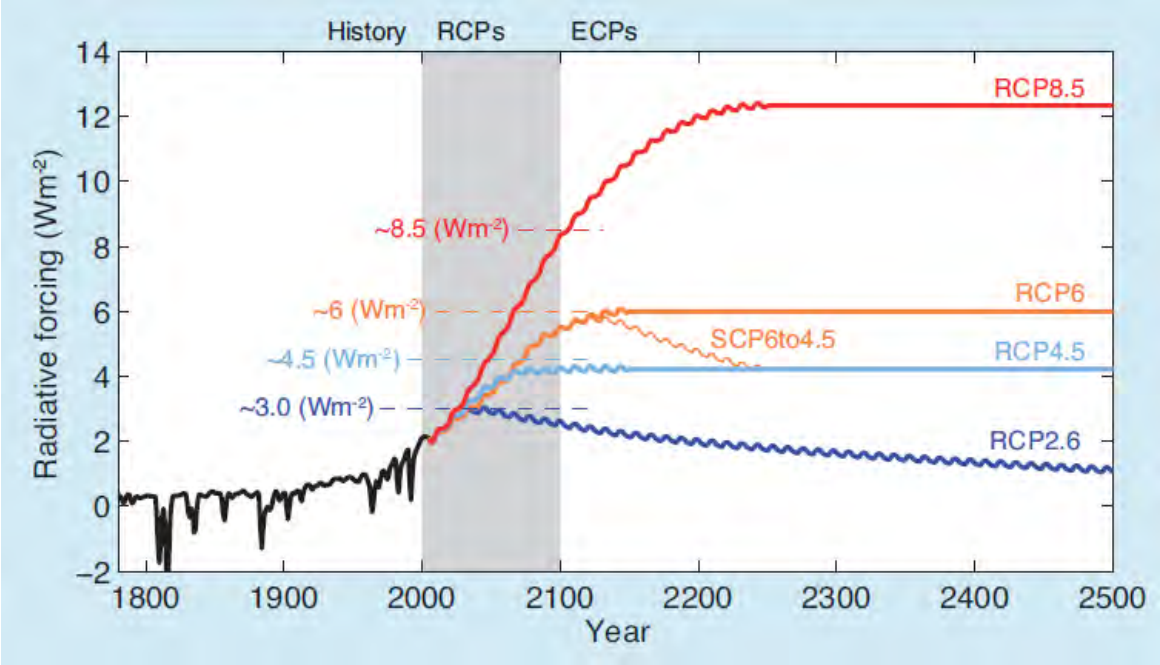

Figure 2.6: Total RF (anthropogenic plus natural) for RCPs and extended concentration pathways (ECP)—for RCP2.6, RCP4.5, and RCP6, RCP8.5, as well as a supplementary extension RCP6 to 4.5 (*Source: IPCC, 2013*)

Various steps were necessary to turn the selected ‘raw’ RCPs into emission scenarios from IAMs and to turn these into data sets usable by the climate modelling community, including the extension with historical emissions (Granier et al., 2011; Meinshausen et al., 2011), the harmonization (smoothly connected historical reconstruction) and gridding of land use data sets (Hurtt et al., 2011), the provision of atmospheric chemistry modelling studies, particularly for tropospheric ozone (Lamarque et al., 2011), analyses of 2000–2005 GHG emission levels, and extension of GHG concentrations with historical GHG concentrations and harmonization with analyses of 2000–2005 GHG concentrations levels (Meinshausen et al., 2011). The final RCP data sets comprise land use data, harmonized GHG emissions and concentrations, gridded reactive gas and aerosol emissions, as well as ozone and aerosol abundance fields

To aid model understanding of longer-term climate change implications, these RCPs were extended until 2300 (Meinshausen et al., 2011) under reasonably simple and somewhat arbitrary assumptions regarding post-2100 GHG emissions and concentrations. In order to continue to investigate a broad range of possible climate futures, the two outer RCPs, RCP2.6 and RCP8.5 assume constant emissions after 2100, while the two middle RCPs aim for a smooth stabilization of concentrations by 2150. RCP8.5 stabilizes concentrations only by 2250, with CO_2 concentrations of approximately 2000 ppm, nearly seven times the pre-industrial levels. As the RCP2.6 implies net negative CO_2 emissions after around 2070 and throughout the extension, CO_2 concentrations are slowly reduced towards 360 ppm by 2300.

Information on individual RCPs

RCP 2.6:

The RCP 2.6 is developed by the IMAGE modeling team of the Netherlands Environmental Assessment Agency. The emission pathway is representative for scenarios in the literature leading to very low greenhouse gas concentration levels. It is a so-called "peak" scenario: its radiative forcing level first reaches a value around 3.1 W/m2 mid-century, returning to 2.6 W/m2 by 2100. In order to reach such radiative forcing levels, greenhouse gas emissions (and indirectly emissions of air pollutants) are reduced substantially over time. The final RCP is based on the publication by Van Vuuren et al. (2007).

RCP 4.5:

The RCP 4.5 is developed by the MiniCAM modeling team at the Pacific Northwest National Laboratory's Joint Global Change Research Institute (JGCRI). It is a stabilization scenario where total radiative forcing is stabilized before 2100 by employment of a range of technologies and strategies for reducing greenhouse gas emissions. The scenario drivers and technology options are detailed in Clarke et al. (2007). Additional detail on the simulation of land use and terrestrial carbon emissions is given by Wise et al (2009).

RCP 6.0:

The RCP 6.0 is developed by the AIM modeling team at the National Institute for Environmental Studies (NIES), Japan. It is a stabilization scenario where total radiative forcing is stabilized after 2100 without overshoot by employment of a range of technologies and strategies for reducing greenhouse gas emissions. The details of the scenario are described in Fujino et al. (2006) and Hijioka et al. (2008).

RCP 8.5:

The RCP 8.5 is developed by the MESSAGE modeling team and the IIASA Integrated Assessment Framework at the International Institute for Applies Systems Analysis (IIASA), Austria. The RCP 8.5 is characterized by increasing greenhouse gas emissions over time representative for scenarios in the literature leading to high greenhouse gas concentration levels. The underlying scenario drivers and resulting development path are based on the A2r scenario detailed in Riahi et al. (2007).

2.6.4 Comparison of SRES and RCP Scenarios

The four RCP scenarios used in CMIP5 lead to RF values that span a range larger than that of the three SRES scenarios used in CMIP3. RCP4.5 is close to SRES B1, RCP6 is close to SRES A1B (more after 2100 than during the 21st century) and RCP8.5 is somewhat higher than A2 in 2100 and close to the SRES A1FI scenario. RCP2.6 is lower than any of the SRES scenarios. In **Figure 2.7**, the time evolution of the total anthropogenic (positive) and anthropogenic aerosol (negative) radiative forcing (RF) relative to pre-industrial (about 1765) between 2000 and 2300 for RCP scenarios and their extensions (continuous lines), and SRES scenarios (dashed lines) as computed by the Integrated Assessment Models (IAMs) has been shown graphically.

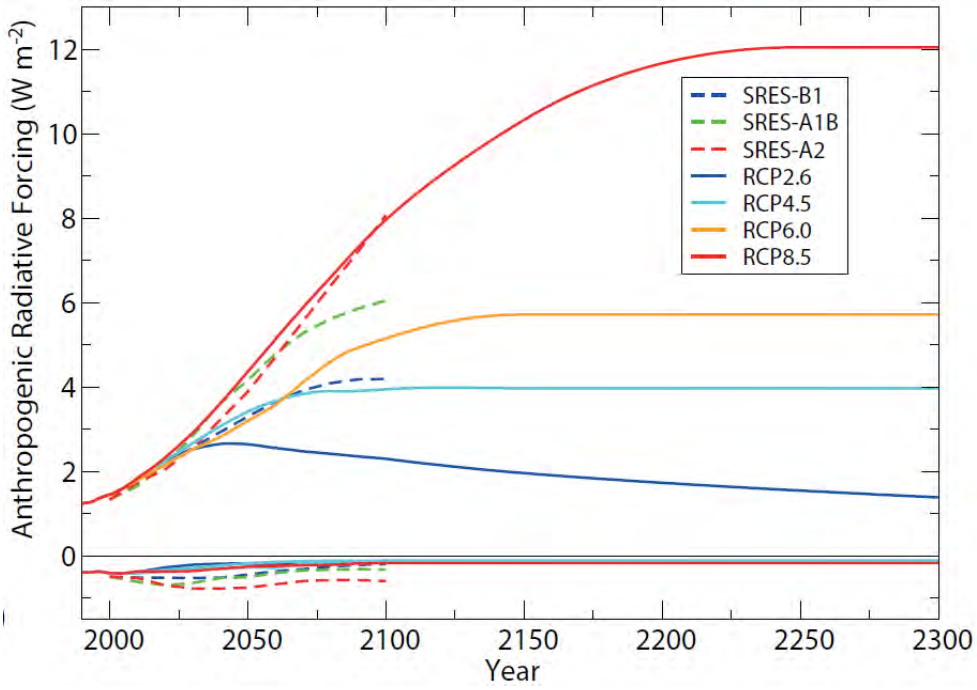

Figure 2.7: Time evolution of the total anthropogenic (positive) and anthropogenic aerosol (negative) radiative forcing (RF) relative to pre-industrial (about 1765) between 2000 and 2300 for RCP scenarios and their extensions (continuous lines), and SRES scenarios (dashed lines) as computed by the Integrated Assessment Models (IAMs) (*Source: IPCC, 2013*)

2.7 Climate Models

Climate models are the primary tools available for investigating the response of the climate system to various forcing, for making climate predictions on seasonal to decadal time scales and for making projections of future climate over the coming century and beyond. It is crucial therefore to evaluate the performance of these models, both individually and collectively. Under the World Climate Research Program (WCRP) the Working Group on Coupled Modelling (WGCM) established the Coupled Model Inter-comparison Project (CMIP) as a standard experimental protocol for studying the output of coupled atmosphere-ocean general circulation models (AOGCMs). CMIP provides a community-based infrastructure in support of climate model diagnosis, validation, inter-comparison, documentation and data access. This framework enables a diverse community of scientists to analyze Global Circulation Models (GCM) in a systematic fashion, a process which serves to facilitate model improvement. Virtually the entire international climate modeling community has participated in this project since its inception in 1995. The Program for Climate Model Diagnosis and Inter-comparison

(PCMDI) archives much of the CMIP data and provides other support for CMIP. PCMDI's CMIP effort is funded by the Regional and Global Climate Modeling (RGCM) Program of the Climate and Environmental Sciences Division of the U.S. Department of Energy's Office of Science, Biological and Environmental Research (BER) program.

2.8 Climate Change and change in Water availability in the Indian Subcontinent

Climate change has passed the phase of scientific curiosity and debate and has now become one of the developmental challenges for nations across the world. Scientific studies have established a changing climate, its impact on the natural resources and concomitantly on the lives and livelihoods of people. It is often quoted that such kinds of impacts will be more on people in the developing countries due to their heavy dependence on the natural resource base and lower resilience to environmental shocks. Climate change has an altogether different connotation for a country like India and Bangladesh due to its varied topography, consisting of diverse bio-geographical features including forests, coasts, mountains, mangroves, islands, etc. Further, the dependence of people, especially the poor, on the natural resource base also makes them more vulnerable to such changes. In India, a great deal of research has been undertaken to assess and bring forth the evidences of climate change and its impacts on human lives These studies have clearly indicated that a changing climate is manifesting itself in the form of unprecedented changes in almost all major ecosystems. From the receding glaciers to changing cropping patterns, studies have shown how the changing climate pattern is affecting the ecosystem and its services.

According to India's Initial National Communication (NATCOM) to United Nations Framework Convention on Climate Change (UNFCC), climate change is likely to adversely affect the water balance in different parts of India due to changes in precipitation and evapotranspiration and rising sea levels, leading to increased saline intrusion into coastal and island aquifers. The National Water Mission (NWM), a part of the National Action Plan on Climate Change (NAPCC) of India, identifies the threat to water resources in India due to climate change in terms of the expected decline in the glaciers and snow-fields in the Himalayas; increased drought like situations due to the overall decrease in the number of rainy days over a major part of the country; increased flood events due to the overall increase in the rainy day intensity; effect on groundwater quality in alluvial aquifers due to increased flood and drought events; impact on

groundwater recharge due to changes in precipitation and evapotranspiration; and increased saline intrusion of coastal and island aquifers due to rising sea levels (Earle, 2015).

The Himalayas comprise about 16.2 per cent of the total geographical area of the country. India's three main rivers – Indus, Brahmaputra and Ganga – which support a very large percentage of the Indian population, originate from here (Earle, 2015). The average water yield per unit area of the Himalayan rivers is almost double that of the peninsular systems, indicating the importance of snow and glacial melt water contribution from the high mountains (Kumar and Sharma, 2005). Moreover the water from the glacial melts is also crucial for sustaining the lives and livelihoods of the people living in the Himalayan region. The Himalayan snowline and the glacier boundaries are sensitive to a changing climate. According to the Indian Network for Climate Change Assessment (INCCA) report (MoEF, 2010), the annual temperature in this region is expected to increase from 0.9±0.6oC to 2.6±0.7oC in the 2030s. The water yield in the Himalayan region, mainly covered by the river Indus, is likely to increase by 5 per cent to 20 per cent in most of the areas, with some areas of Jammu and Kashmir and Uttarakhand showing an increase of up to 50 per cent with respect to the base year of the 1970s (ibid.). Increased glacial melt due to warming is predicted to affect river flows. Increased warming might result in increased flows initially with reduced flows later as the glacier disappears. The impact of climate change on river basins can be understood with the example of the Indus River Basin. The total annual run-off from the upper basin is likely to increase by 11 per cent to 16 per cent. It is estimated that although increased run-off could be advantageous for water supply and hydropower production it could aggravate problems of flooding, water logging and salinity in the upper basin.

The south-west monsoon system in India is the most important climatic phenomenon. Shifts from the normal regime can have catastrophic effects in the form of floods, droughts or famines. Though it has been established that there will be an impact on the rainfall pattern of the sub-continent, it is not yet certain as to what that will exactly be, with some models predicting increase while others showing a decreased rainfall pattern. INCCA, in its recent report, has given a comprehensive region-wise analysis of the predicted changes in the precipitation pattern in the country. It indicates clearly that climate variability in the future will present newer challenges. The experiences from around the country over the past few years reiterate these predictions. Sectors which are

climate sensitive, such as agriculture, are likely to be worst affected by these changes. In a recent study on climate change and its impact on flood and drought-affected areas of India, the World Bank notes that farm incomes and yields are likely to be adversely impacted due to changes in temperature and precipitation (World Bank, 2008). Although the linkages between the two have yet to be categorically established, it is believed that in the absence of any countermeasures, climate change is expected to influence future disaster risks through likely increase in weather and climatic hazards. It may also increase the vulnerability of communities to natural hazards due to ecosystem degradation, reductions in water resources and food availability, and changes in livelihoods, and push more people to higher levels of hazard exposure (ESCAP, 2010). What is perhaps significant is to realize that year to year climate variability (as opposed to secular climate change) in itself is a source of risk to life and livelihoods in many parts of the sub-continent. This manifests as floods, droughts and other forms of disasters and one of the key challenges in the water sector is to build resilience to such climate variability.

There is evidence to suggest that water budget estimates may be seriously overestimating the availability of water in the country. The business as usual approach followed in the water sector has given rise to unsustainable management and extractive water use regimes particularly with respect to groundwater. The rivers and water bodies are already under tremendous pressure to meet the demands from various sectors while maintaining their ecological integrity. Climate variability, now a characteristic feature of the subcontinent, is more pronounced than ever, challenging people's resilience and increasing pressure on water bodies.

The per capita water resource availability for the people of the Indian subcontinent has declined considerably over the years and of particular concern is the disparity in water footprints of the rich and the poor. The government and local communities have responded well to many imminent challenges but a paradigm shift in the way water is perceived as a resource will be required to build a robust future course of action.

2.9 Review of Physically Based Hydrological Modeling

Hydrologic modeling involves formulating the mathematical models to represent the hydrologic processes such as, precipitation, snowmelt, interception, evapotranspiration, infiltration, sub-surface flow, and surface flow, as well as the interaction between them.

Hydrologic modeling can be challenging because it involves highly nonlinear processes, complex interactions and high spatial variability at basin scale. Starting from the mid of the nineteenth century, the evolution of hydrologic modeling is continuing from lumped conceptual models to physically based distributed models with the development of understanding the physical processes, computational efforts and data retrieving facilities. Lumped conceptual hydrologic models consider three basic processes within a river basin: the loss of water from storage to atmosphere; storage of water in soil, vegetation, aquifer, and in rivers; routing of flow over the surface (Gosain et.al., 2009). Physically based hydrologic models are based on known scientific principles of energy and water fluxes whereas, conceptual models are based on conceptual storages and model parameters that require calibration. In physically based hydrologic modeling the hydrologic process of water movement are modeled either by the finite difference approximation of the partial differential equation representing the mass, momentum and energy balance or by empirical equations (Abbott et.al., 1986). Typically the primary components of hydrologic cycle related to the land phase are taken into consideration. These are: interception, snowmelt, evapotranspiration, sub-surface runoff, groundwater flow, surface runoff and channel routing.

Hydrologic models can be classified according to the physical processes involved in modeling as conceptual and physically based (Refsgaard, 1996). In conceptual models each of the hydrologic processes, are represented by simplified mathematical relationships, where as in physically based model the detail physical processes can be represented in a deterministic way by representations of mass, momentum and energy conservation (Refsgaard, 1996). According to the spatial description of the watershed process, hydrologic models can be classified as lump and distributed models. In a lumped model the spatial variability of watershed characteristics are ignored, while in a distributed model the spatial variability of vegetation, soil, topography, etc. are taken into account. The conceptual models are usually lumped while the physically based model in practice has to be distributed in manner (Refsgaard, 1996).

2.9.1 Modeling Concepts of Hydrologic Processes

In physically based hydrologic modeling the hydrologic process of water movement are modeled either by the finite difference approximation of the partial differential equation

representing the mass, momentum and energy balance or by empirical equations (Abbott et.al., 1986).

Typically the primary components of hydrologic cycle related to the land phase are taken into consideration. These are: interception, snowmelt, evapotranspiration, sub-surface runoff, groundwater flow, surface runoff and channel routing. A number of physically based hydrologic models have been reviewed and modeling concepts of these physical processes used by various hydrologic models will be discussed in the following sections. Selected model acronyms and principal reference(s) are listed in **Table 2.4**

Table 2.4: Selected physically based hydrologic model, spatial description and discretization type *(Source: Alam, 2015)*

Model Acronym	Model Definition	Principle Reference(s)	Semi/Fully Distributed	Discretization type*
TOPMODEL	TOPography based hydrological MODEL	Beven and Kirby (1976,1979) Beven et.al. (1995)	Semi	HRU
WATBAL		Knusden et.al. (1986)	Semi	OG
SHE	European Hydrologic System	Abbot et.al. (1986a, 1986b)	Fully	OG
ISBA	Interaction Soil Biosphere Atmosphere	Nolihan and Planton (1989) Nolihan and Mahfouf (1995)	Fully	OG
IHDM	Institute of Hydrology Distributed Model	Beven et.al. (1987) Calver and Wood (1995)	Fully	HRU
THALES		Grayson et.al. (1992a; 1995)	Fully	IE
SLURP	Semi-distributed Land Use-based Runoff Processes	Kite (1995)	Semi	GRU
MIKE SHE	MIKE System Hydrologique European	Refsgaard and Storm (1995)	Fully	OG
SWAT	Soil and Water Assessment Tool	Arnold et.al. (1998a)	Semi	HRU
WATFLOOD/SPL9	Waterloo Flood Forecasting Model	Kouwen (1988) Kouwen (2000) Kouwen and Mousavi (2002)	Fully	OG
HRCDHM	Hydrologic Research Centre Distributed Hydrologic Model	Carpenter et.al. (2001)	Semi	HRU

Model Acronym	Model Definition	Principle Reference(s)	Semi/Fully Distributed	Discretization type*
DPHM-RS	Semi-distributed Physically based Hydrologic Model using Remote Sensing and GIS	Biftu and Gan (2001, 2004)	Semi	HRU
R.WATER.FEA	Vieux and Gaver (1994)		Fully	IE
tRIBS	TIN-based Real-time Integrated Basin Stimulator	Ivanov et.al., 2004	Flly	TIN
TOPNET	Bandaragoda et.al. (2004)		Semi	HRU
MISBA	Modified Interaction Soil Biosphere Atmosphere	Kerkhoven and Gan (2006)	Fully	OG
LISTFLOOD		Van der Knijff et.al. (2010) De Roo et.al. (2000)	Fully	OG
HydroGeoSphere		Therrien et.al. (2005; 2010)	Fully	OG
PAWS	Process-based Adaptive Watershed Simulator	Shen and Phanikumar (2010)	Fully	OG
CREST	The Coupled Routing and Excess Storage	Wang et.al. (2011)	Fully	OG

2.9.2 Advantages and Limitations of Physically Based Hydrologic Modelling

Lumped conceptual hydrologic models consider three basic processes within a river basin: the loss of water from storage to atmosphere; storage of water in soil, vegetation, aquifer, and in rivers; routing of flow over the surface (Gosain et.al., 2009). Focus on the physically based distributed hydrologic modeling started in order to minimize or overcome the deficiencies of the conceptual models. Conceptual models are controlled by various parameters to represent the hydrologic processes. Parameters of these models are estimated either by manual curve fitting or by optimizing the objective functions, thus making less or no physical interpretation of the fitted parameters. Therefore, unrealistic parameter values may be obtained through errors in measurements (Abbott et al., 1986). In lumped conceptual models the mathematical representation of hydrologic processes are only an approximate representation of the real world. So the errors in parameter estimation also can be raised from model structure (Beven, 1989). The calibration of conceptual models requires long meteorological and hydrological records which are not always available, especially for the un-gauged catchments (Gosain et.al., 2009). Spatial

heterogeneities of landuse, soil, and input variables are not considered in lumped conceptual models (Abbott et al., 1986a). The calibration and validation of lumped conceptual models depends on the accuracy of both inputs and outputs. So, uncertainty is involved in estimating the input variables, especially the evapotranspiration may cause significant changes in calibration and validation processes (Beven, 1989). Different set of parameter values may result equal quality of good results in a lumped conceptual model (Beven, 1989). As discussed in the previous paragraph, the development of physically based hydrologic model was initiated to overcome the deficiencies associated with the lumped conceptual models, by using parameter values with physical interpretation and considering their spatial variability (Abbott et al., 1986a). However, the physics on which the equations of physically based hydrologic models are based is the small scale physics of homogeneous system and in application these models lump up the small scale physics to the model grid scale without considering any theoretical framework (Beven, 1989).

Calibration of most physically based hydrologic models is usually performed by the comparison of predicted and observed hydrograph which is a necessary test but cannot be considered a sufficient test of model that implies the internal response of catchment (Beven, 1989). In application of physically based hydrologic models, the context of their original purpose of development is often lost when they are applied beyond the scope of their capabilities (Grayson et.al., 1992a). Development of some physically based model is not dynamic nor is it in conjunction of a field program (Dunne, 1983). A summary of advantages and limitations of physically based distributed hydrologic models over lumped conceptual models discussed in the aforementioned paragraphs is listed in below in **Table 2.5**.

Table 2.5: Advantages and limitations of physically based distributed hydrologic models over lumped conceptual models *(Source: Islam, 2011)*

Advantages Over Lumped Conceptual Model
• Parameters in physically based models are based on physics • Physically based are developed from well established scientific laws at micro-scale to water behavior at the meso-scale or regional scale • Consider the spatial heterogeneities of land use, soil, and input variables. • Can consider the effects of the land use changes on the hydrologic cycle.

Advantages Over Lumped Conceptual Model
• Less (or no) calibration is needed.
Limitations
• Lump up the small scale physics to the model grid scale without considering any theoretical framework. • Calibration by the comparison of the predicted and observed hydrograph cannot be considered a sufficient test of model that implies the internal response of catchment. • Context of original purpose of development is often lost when models applied beyond the scope of their capabilities. • Development of some physically based model is not dynamic nor it is in conjunction of a field program • Many models are developed from limited data sources.

2.10 Studies Related to Changes in Water Balance due Climate Change in Bangladesh

The "Surface Water Assessment of Bangladesh and Impact of Climate Change" study had been carried out by Institute of Water Modelling in connection with the Integrated Water Resources Assessment of Bangladesh (IWM, 2014a). The study considered the following thematic area of surface water for its assessment and analysis:

- Surface water resources assessment and water balance study of five hydrological regions (NW, NC, NE, SW and SE) of Bangladesh
- Country wide flooding analysis (does not include EH region)
- Salinity problem in the SW region
- Low flow analysis of major rivers of Bangladesh
- Water demand and availability status of major irrigation projects of the country

In the study, a climate change impact assessment had been carried out after conducting a 'base line' study on the chosen surface water thematic areas of Bangladesh. Climate change scenarios of 2030 and 2050 projection year were identified first followed by a detail investigation to find out the probable impacts of climate change on the chosen thematic areas of surface water resources of Bangladesh.

It was mentioned in the study that the rainfall is expected to decrease in the dry season (Feb – Apr) during a CC 2030 and 2050 dry climate change condition. The prediction shows that rainfall will decrease by 18 percent in CC 2030 and 11 percent in CC 2050 for a dry year condition. In the post-monsoon and winter season, the rainfall will also decrease substantially in a dry year climate change condition. The decrease could be about 8 and 10 percent, respectively during this period in a CC 2030 and CC 2050 dry condition. Monsoon rain will slightly decrease or remain almost same as base condition during a dry year climate change scenario of 2030 and 2050. On the other hand, about 14 to 120 percent increase in rainfall is predicted in November, December and January for an average or wet year during CC 2030 and CC 2050 condition. This high increase in winter rainfall could give a misleading impression if it is not realized contextually. Basically, the rainfall is insignificant during this period and a small increase in rainfall amount provides a large percentage of change. The dry and pre-monsoon rain is expected to increase significantly for an average or wet hydrological year. The increase could be around 6 – 25 percent in April, 37 – 45 percent in May according to the prediction of CC 2030 and CC 2050 condition. With the exception of June, monsoon rain will slightly decrease or remain same during an average or wet year of climate change condition. June rain, however, is expected to increase by 15 and 26 percent in CC 2030 and CC 2050 condition, respectively. For a dry year climate change condition, the evaporation rate may decrease up to 4 percent during dry and first part of pre-monsoon season while it will increase up to 7 percent for rest of the year. On the other hand, the evaporation rate will increase in all seasons and it may vary from 2.5 to 9 percent for an average or wet year climate change condition. In the North-West region which is located just downstream of the Teesta River Basin, the increase in rainfall due CC 2030 or CC 2050 will eventually increase total runoff (11 – 12 percent) and recharge (5 – 6 percent) despite increase in evapotranspiration (5 – 7 percent). The cross-boundary river inflows of North West region will increase 3 – 6 percent for CC 2030 and CC 2050 condition, respectively.

To summarize, the “Surface Water Assessment of Bangladesh and Impact of Climate Change” study was a comprehensive study that assessed the changes in the water balance due to climate change for all the regions of Bangladesh.

IWM along with Indian Institute of Technology (IIT), Guwahati had carried out another study entitled “Physical Assessment of the Brahmaputra River” in 2014 which analyzed

available climatic and hydrologic data to carry out a physical assessment of the basin (IWM, 2014b). The analysis also looked at possible climate change impacts on temperature, evapotranspiration, rainfall, and river flows in the basin. By analyzing the outputs from twenty two General Circulation Models (GCMs), it was found that:

- Temperatures are expected to increase from 1.3° C to 2.4° C by 2050, and from 2.0° C to 4.5° C by 2100 in the basin;
- Monthly evapotranspiration is likely to increase by 5% to 18% by 2050, and from 7% to 36% by 2100, especially in the months of winter;
- Average change in monthly rainfall are likely to vary from 14% decrease to 15 % increase by 2050, and 28 % decrease to 22 % increase by 2100;
- Average monthly flow at a downstream station at Chilmari in Bangladesh is expected to change by -1% to 15% by 2050, and by 5% to 20% by 2100; and
- Generally, A1B1 and A2 impact predictions are similar, which tend to be more severe than impacts in the B1 emission scenario

Alam el al, 2015 assessed the impact of Climate Change on the hydrology of the Brahmaputra River Basin. They developed a semi-distributed hydrological model of the Brahmaputra River Basin (BRB) using Soil Water Assessment Tool (SWAT) which had been calibrated and validated for the stream flow measured at the Bahadurabad station for the periods of l98l to 2010 and satisfactory goodness-of-fit statistics were found. Synthetic approach of climate change modeling has been applied to assess the changes in water availability due to future potential changes in temperature and precipitation in BRB. Twenty hypothetical climate change scenarios (perturbed temperatures and precipitation: precipitation from -20% to +20% at 10% interval and temperature change of 0°C to 4°C at 2°C interval) were applied to the calibrated and validated model in order to investigate the sensitivity BRB annual stream flow under the impact of climate change. The results revealed that the changes in annual stream flow due to changes in precipitation and temperature are linear. It appears that with respect to the climate normal (1981- 2010) the changes in average annual stream flow (keeping temperature unchanged) are +12.83% per +10% change in precipitation. In contrast, stream flow response to the increase in temperature (keeping precipitation unchanged) is -2.49% per °C.

2.11 Studies Related to Changes in Water Balance due Climate Change Globally

Over the years several researchers have looked into the case of potential changes in the water balance of a region due to the change in climate. Giang et al studied the impacts of climate change in Uppar Ca River. The Ca River originates in the Loi Mountains of Laos, crosses Laos PDR's Xiangkhouang Province, flows into Vietnam and through the province of Nghe An, and joins the La River before emptying into the Gulf of Tonkin at the Cua Hoi estuary. The impact of climate change on the seasonality of water resources in the Upper Ca River Watershed was assessed using downscaled global climate models coupled with the SWAT model in this study. The results indicated that temperature and evapotranspiration will increase in all months of future years. The area could warm as much as 3.4∘C in the 2090s, with an increase of annual evapotranspiration of up to 23% in the same period. An increase in the seasonality of precipitation (both an increase in the wet season and a decrease in the dry season) was found in this study. The greatest monthly increase of up to 29% and the greatest monthly decrease of up to 30% are expected in the 2090s according to the authors. Due to this projected climate change condition, a change in the river flow discharge was also observed. **Figure 2.8** illustrates the relative monthly change projected by the three climate change scenarios B1, B2, and A2 and displayed for the three future time periods of the 2030s, 2060s, and 2090s. There is a clear trend in changes throughout the year. Discharge is projected to decrease for the first six months of the year, from January to June, and increase for the other six months, from July to December. The magnitude of changes varies depending on the month and scenario. Note, however, that November and December belong to the dry season, whereas May and June belong to the wet season. Therefore, in the dry season, there are four months with decreases and two months with increases in discharge. On the other hand, discharge increases for four of the six months of the wet season and decreases for the other two months.

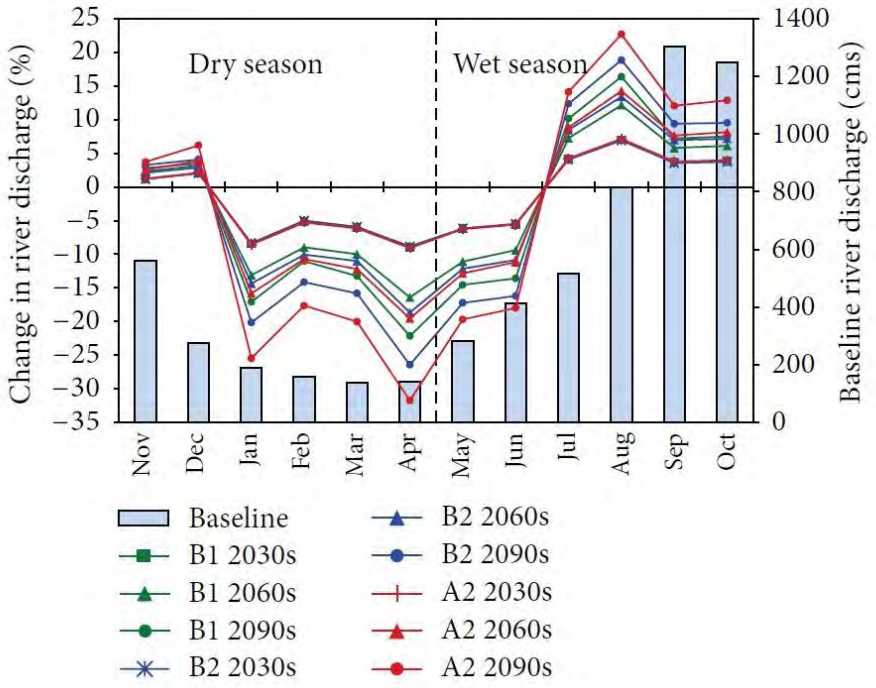

Figure 2.8: Monthly change in river discharge at Yen Thuong Station (line chart) relative to the average data of the baseline period (column chart). (*Source: Giang et al, 2014*)

The increase in discharge for all months from July to December can be explained by the large increases in precipitation for these months. However, the shapes of the increases in discharge and precipitation are not homogeneous. This is because of differences in temperature change and therefore differences in the rate of evapotranspiration change, in addition to the differences in the amount of precipitation between the months. On the other side of the graph, the most substantial decrease can be found in April (9.1% in the 2030s, 19.6% in the 2060s, and 31.8% in the 2090s, according to scenario A2), followed by January, March, and May. The decrease in discharge in January, March, April, and May corresponds to the decrease in precipitation in these months. It is noticeable that discharge decreases in February and June, despite the increase in precipitation in these months. In February, the increase of about 1% of a small precipitation amount (about 20mm) cannot compensate for the increase of PET driven by the temperature rise, resulting in a discharge decrease. June is one of the hottest months with an average maximum temperature of about 38^0C and an average PET of more than 100 mm. The increase in PET in this month is possibly more significant than the increase in precipitation; the river discharge therefore decreases. The differences in the trends in precipitation change and discharge change in June may also be due to the time-lag between the precipitation events and the stream discharges. In addition to evaporation,

saturation is also an important factor. When it rains, it takes time for the ground to become saturated, but once it has become saturated, any additional rainfall then runs over the land into streams. However, the increase in temperature in the month of June can cause an increase in the ground infiltration rate, resulting in a decrease in the amount of water running into streams. Overall, annual discharge is projected to increase, meaning that there will be more water in the watershed annually, but there is also likely to be a problem with uneven distribution of water resources: a large volume of water in the wet season and a scarcity of water in the dry season. This indicates the possibility of more frequent floods in the wet season and droughts in the dry season.

Mitra and Mishra undertook a similar kind of study in 2014 for the Baitarni river basin located in eastern India. Stream flow and sediment yield response to climate change in the Baitarni river basin has been investigated employing SWAT (Soil and Water Asessment Tool) model. Climate change impact analyses were performed by assuming scenarios of increased temperature ($+2^0$C, $+4^0$C and $+6^0$C), varied rainfall (±20% at ±5% increment) and increased atmospheric carbon dioxide (CO_2) concentrations (330 ppm, 495 ppm and 660 ppm) and by extending historical rainfall (1974 to 2004) trend in future from 2005 to 2099. The trend analysis has shown that average annual rainfall at the Baitarni river basin has increased by 8.8 mm per year in the last 30 years which has resulted to an increase in stream flow in the river basin. Climate change sensitivity showed an increasing stream flow to independent increase in rainfall whereas showed decreasing stream flow to decreased rainfall and increased temperature in the basin. The increased atmospheric CO_2 concentrations, independently, showed an increase in stream flow. The analysis shows that the water availability at the Baitarni river basin is expected to increase in future under linear increase in rainfall since historic and expected increasing rainfall trend persisting in future. The predicted future scenarios developed by SWAT model gave the normalized daily rainfall distribution and was unable to catch the expected extreme rainfall conditions. This characteristic of predicted rainfall showed that the method used to study and estimate future water resources does not hold good for the estimation of sediment yield.

Gurung, 2013 used SWAT to assess the impact of climate change on water balance and crop yield in the West Seti River basin. The projected climate result showed that the average daily maximum temperature will change by -0.62°C to +0.66°C per decade and minimum temperature will change by -1.14°C to +0.03°C per decade in this study area.

This shows an average day becomes hotter and night becomes colder. The result of the model simulation under current climate conditions shows declining trends of actual ET and crop yields in this study area. The projected model results show that summer precipitation will decrease except on the maize fields and winter precipitation will increase; whereas actual ET will increase for all crops except in millet under future climate scenario. As a result, summer crop yields will decrease and winter crop yields will increase under projected climate change scenarios. However, there is large degree of uncertainty in the simulated results due to disagreement among the projected future climate scenarios (Bharati et al., 2012) and this uncertainty can reliably be reduced by using only a selection of GCMs that shows high intermodal similarity for the current and future climate (Weiland et al., 2012).

Yan et al, 2015 used Variable infiltration capacity (VIC) model to assess the impact of climate change on seasonal discharge and extreme flows. For the assessment he used the bias-corrected results of five different climate models under the IPCC scenarios RCP4.5 and 8.5. He emphasized to assess variations in low flow across the basin, because it is suffering from water shortage and salt water intrusion in the dry season. Results indicate a reduction in average low flow under the five climate models. The reduction varies across the basin and is between 6 and 48% for RCP4.5. River discharge in the dry season is projected to decrease throughout the basin. In the wet season, river discharge tends to increase in the middle and lower reaches and decrease in the upper reach of the Pearl River basin. The variation of river discharge is likely to aggravate water stress. Especially the reduction of low flow is problematic as already now the basin experiences temporary water shortages in the delta.

Dahal et al, 2016 while estimated the impact of climate change on water availability in Bagmati basin, Nepal suggested that understanding potential hydrologic influences of projected climate change is important for management of water resources. He developed a calibrated hydrological using SWAT then used the temperature and precipitation outputs from a global climate model (GCM) were used to drive the calibrated SWAT model in order to study the impacts of climate change. The GCM used in this study is from IPCC Fifth Assessment report. This study demonstrates the temporal differences in hydrologic responses to future climate changes in Bagmati basin, Nepal. The climate projection indicates an increase in annual precipitation in the basin, even though most of the precipitation will be concentrated within the summer monsoon. No appreciable

change in the seasonality of rainfall was observed. The increase in precipitation results in an increase in annual water yield in future. Evapotranspiration is modeled to increase during the pre-monsoon dry summer, possibly indicating longer dry periods.

Karlssona et al, 2016 combined the effects of climate models, hydrological model structures and land use scenarios for a 486 km^2 catchment in Denmark and to evaluate the sensitivity of the results to the choice of hydrological model. Three hydrological models, NAM, SWAT and MIKE SHE, were constructed and calibrated using similar methods. Each model was forced with results from four climate models and four land use scenarios. The results revealed that even though the hydrological models all showed similar performance during calibration, the mean discharge response to climate change varied up to 30%, and the variations were even higher for extreme events (1th and 99th percentile). Land use changes appeared to cause little change in mean hydrological responses and little variation between hydrological models. Differences in hydrological model responses to land use were, however, significant for extremes due to dissimilarities in hydrological model structure and process equations. The climate model choice remained the dominant factor for mean discharge, low and high flows as well as hydraulic head at the end of the century.

Zuo et al, 2016 on the other hand assessed the effects of changes in land use and climate on runoff and sediment yields from a watershed in the Loess Plateau of China. His team investigated the Huangfuchuan River basin (HFCRB) of the Loess Plateau by combined usage of statistical tests, hydrological modeling, and land-use maps. The temporal trends and abrupt changes in runoff and sediment loads during 1954–2012 are detected by using non-parametric Mann–Kendall and Pettitt tests. The land-use changes between 1980 and 2005 are determined by using transition matrix analysis, and the effects of land-use and climate changes on water and sediment yields are assessed by using the Soil and Water Assessment Tool (SWAT) hydrological model and four scenarios, respectively. The results show significant decreasing trends in both annual runoff and sediment loads, whereas slightly decreasing and significantly increasing trends are detected for annual precipitation and air temperature, respectively. 1984 is identified as the dividing year of the study period. The land-use changes between 1980 and 2005 show significant effects of the Grain for Green Project in China. Both land-use change and climate change have greater impact on the reduction of sediment yield than that of water. Water and sediment yields in the upstream region show more significant decreases than those in the

downstream region under different effects. The results obtained in this study can provide useful information for water resource planning and management as well as soil and water conservation in the Loess Plateau region.

2.12 Studies Related to Hydrological Modelling of the Teesta River Basin

Teesta being a very important trans-boundary river, has been under the scrutiny of many researchers over the past few years. In this section some of those researches have been discussed. For example, Ganju et al 2012 studied the design flood of all the hydro-power development projects in the cascade in an integrated and consistent manner. In the study a distributed hydrological model has been developed for design flood review study of projects in Teesta basin in an integrated manner. All the physiographic parameters required to develop unit hydrographs for different sub-catchments of distributed model has been estimated by GIS processing of STRM DEM. In the absence of a long term data availability and predominant orographic conditions in the area, the design storm for each sub catchment of distributed hydrological model has been finalized by taking characteristic maximum one day rainfall depth for different topographical regions. The design flood for different projects has been estimated using hydro meteorological approach and a distributed hydrological model set up on HEC-HMS. His team succeeded in estimating the design flow of the major hydropower projects with the aid of the hydrological model.

Chakrabarty and Mandal (2015) prepared a similar kind of hydrological model with HEC-HMS but connected the hydrological model outputs with HEC-RAS and Flow-2D to simulate the hydraulics characteristics of the Teesta Basin for a flash flood. The main object was to construct a direct unit hydrograph for an excess rainfall by estimating the stream flow response at the outlet of a watershed. Specifically, the methodology was based on the creation of a spatial database in GIS environment and on data editing. The model output showed, with an input rainfall intensity above 400 mm per day for three days the flood runoff simulation models shows outbursts of lakes and check dam individually or in combination with run-off causing severe damage to the downstream settlements. Model output shows that 313 Sq. km area were found to be most vulnerable to flash flood includes Melli, Jourthang, Chungthang, and Lachung and 655sq. km. as moderately vulnerable includes Rangpo,Yathang, Dambung,Bardang, Singtam, Teesta Bazarand Thangu Valley. The model was validated by inserting the rain fall data of a

flood event took place in August 1968, and 78% of the actual area flooded reflected in the output of the model. Lastly preventive and curative measures were suggested to reduce the losses by probable flash flood event.

Pradhan et al, 2010 also estimated the Rainfall Runoff using Remote Sensing and GIS in and around Singtam, East Sikkim. The author of the research believed that the use of remote sensing and GIS technology can be used to overcome the problem of conventional method for estimating runoff caused due to rainfall. In the paper, modified Soil conservation System (SCS) CN model is used for rainfall runoff estimation that considers parameter like slope, vegetation cover, area of watershed. Estimated runoff is compared with the runoff calculated with the actual rainfall data for the year 2009, in general good correlation has been found between observed and computed runoff. The author also said that the analysis can be extended further to assess the impact of change in land cover over a period of time on rainfall runoff and impact of change in runoff on morphology of river Teesta.

2.13 SWAT Model

The Soil and Water Assessment Tool (SWAT) is a public domain model jointly developed by USDA Agricultural Research Service (USDA-ARS) and Texas A&M AgriLife Research, part of The Texas A&M University System. SWAT divides a watershed into subwatersheds. Each subwatershed is connected through a stream channel and further divided into Hydrologic Response Unit (HRU). HRU is a unique combination of a soil and a vegetation type in a subwatershed, and SWAT simulates hydrology, vegetation growth, and management practices at the HRU level.

2.13.1 Water Balance

Water balance is the driving force behind everything that happens in the watershed. To accurately predict the movement of pesticides, sediments or nutrients, the hydrologic cycle as simulated by the model must conform to what is happening in the watershed. The simulation of hydrologic cycle can be separated into land phase and water or routing phase. Land phase controls the amount of water, sediment, nutrient and pesticide loading to the main channel in each subbasin whereas routing phase defines the movement of water, sediments, etc. through the channel network of the watershed to the outlet.

Schematic of pathways available for water movement in SWAT is shown in the **Figure 2.9**. It involves various elements such as snow, canopy storage, infiltration, evapotranspiration, lateral subsurface flow, surface runoff, transmission losses, return flow etc.

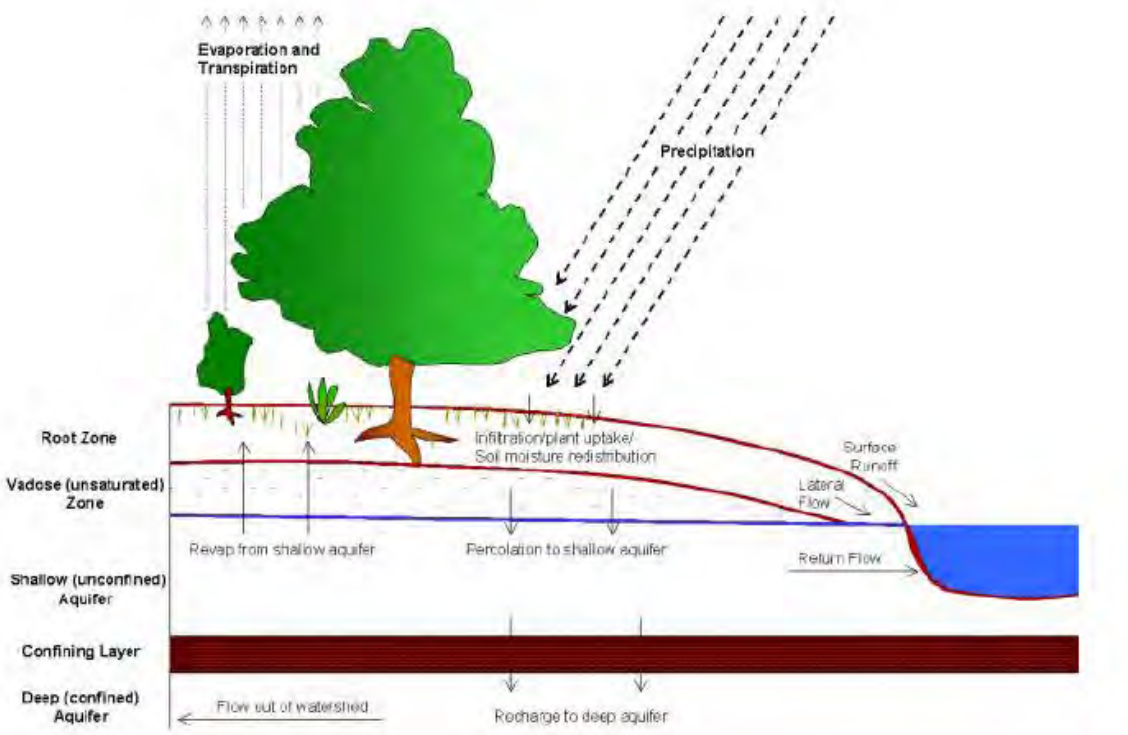

Figure 2.9: Hydrologic process in SWAT *(Source: Alam, 2015)*

Land phase of the hydrologic cycle:

Hydrologic cycle simulated by swat is based on the water balance equation

$$SW_t = SW + \sum_{i=1}^{t} (R_i - Q_i - ET_i - P_i - QR_i) \quad (2.3)$$

Where SW_t is the final soil water content (mm H_2O), SW is the initial soil water content on day i (mm H2O), Q*i* is the amount of surface runoff on day i (mm H_2O), ET_i is the amount of evapotranspiration on day i (mm H_2O), P_i is the amount of water entering the vadose zone from the soil profile on day i(mm H2O), and QR_i is the amount of return flow on day i(mm H_2O).

Snow:

Swat classifies precipitation as rain or freezing rain/snow using the average daily temperature.

Snow cover: This component of swat can handle simple uniform cover to complex non-uniform cover due to shading, drifting, topography and land cover. User defines a threshold snow depth above which snow coverage will always extend over 100% of the area.

Snow melt: snow melt is controlled by air and snow pack temperature, melting rate, and the areal coverage of snow. If snow is present, it is melted on days when the maximum temperature exceeds 0C using a linear function of the difference between the average snow pack-maximum air temperature and the base or threshold temperature for snow melt. Melted snow is treated the same as rainfall for estimating runoff and percolation.

Lumped conceptual hydrologic models consider three basic processes within a river basin: the loss of water from storage to atmosphere; storage of water in soil, vegetation, aquifer, and in rivers; routing of flow over the surface (Gosain et.al., 2009). Focus on the physically based distributed hydrologic modeling started in order to minimize or overcome the deficiencies of the conceptual models. Conceptual models are controlled by various parameters to represent the hydrologic processes. Parameters of these models are estimated either by manual curve fitting or

Canopy Storage:

Canopy storage is the water intercepted by vegetative surfaces (the canopy) where it is held and made available for evaporation. When using the curve number method to compute surface runoff, canopy storage is taken into account in the term initial abstractions. However, if methods such as Green & Ampt are used to model infiltration and runoff, canopy storage must be modeled separately. SWAT allows the user to input the maximum amount of water that can be stored in the canopy at the maximum leaf area index for the land cover. This value and the leaf area index are used by the model to compute the maximum storage at any time in the growth cycle of the land cover/crop. When evaporation is computed, water is first removed from canopy storage.

Infiltration

Infiltration refers to the entry of water into a soil profile from the soil surface. As infiltration continues, the soil becomes increasingly wet, causing the rate of infiltration to decrease with time until it reaches a steady value. The initial rate of infiltration depends

on the moisture content of the soil prior to the introduction of water at the soil surface. The final rate of infiltration is equivalent to the saturated hydraulic conductivity of the soil. Because the curve number method used to calculate surface runoff operates on a daily time-step, it is unable to directly model infiltration. The amount of water entering the soil profile is calculated as the difference between the amount of rainfall and the amount of surface runoff. The Green & Ampt infiltration method does directly model infiltration, but it requires precipitation data in smaller time increments.

Evapotranspiration

Evapotranspiration is a collective term for all processes by which water in the liquid or solid phase at or near the earth's surface becomes atmospheric water vapor. Evapotranspiration includes evaporation from rivers and lakes, bare soil, and vegetative surfaces; evaporation from within the leaves of plants (transpiration); and sublimation from ice and snow surfaces. The model computes evaporation from soils and plants separately as described by Ritchie (1972). Potential soil water evaporation is estimated as a function of potential evapotranspiration and leaf area index (area of plant leaves relative to the area of the HRU). Actual soil water evaporation is estimated by using exponential functions of soil depth and water content. Plant transpiration is simulated as a linear function of potential evapotranspiration and leaf area index.

Potential evapotranspiration:

Potential evapotranspiration is the rate at which evapotranspiration would occur from a large area completely and uniformly covered with growing vegetation which has access to an unlimited supply of soil water. This rate is assumed to be unaffected by micro-climatic processes such as advection or heat-storage effects. The model offers three options for estimating potential evapotranspiration: Hargreaves (Hargreaves et.al., 1985), Priestley-Taylor (Priestley and Taylor, 1972), and Penman-Monteith (Monteith, 1965). The three PET methods included in swat vary in the amount of required inputs. The Penman-Monteith method requires solar radiation, air temperature, relative humidity and wind speed. The Priestley-Taylor method requires solar radiation, air temperature and relative humidity. The Hargreaves method requires air temperature only.

Lateral Subsurface Flow

Lateral subsurface flow, or interflow, is stream flow contribution which originates below the surface but above the zone where rocks are saturated with water. Lateral subsurface

flow in the soil profile (0-2m) is calculated simultaneously with redistribution. A kinematic storage model is used to predict lateral flow in each soil layer. The model accounts for variation in conductivity, slope and soil water content.

Surface Runoff

Surface runoff, or overland flow, is flow that occurs along a sloping surface. Using daily or sub daily rainfall amounts, SWAT simulates surface runoff volumes and peak runoff rates for each HRU.

Surface Runoff Volume:

It is computed using a modification of the SCS curve number method (USDA Soil Conservation Service, 1972) or the Green & Ampt infiltration method (Green and Ampt, 1911). In the curve number method, the curve number varies non-linearly with the moisture content of the soil. The curve number drops as the soil approaches the wilting point and increases to near 100 as the soil approaches saturation. The Green & Ampt method requires sub-daily precipitation data and calculates infiltration as a function of the wetting front matric potential and effective hydraulic conductivity. Water that does not infiltrate becomes surface runoff. SWAT includes a provision for estimating runoff from frozen soil where a soil is defined as frozen if the temperature in the first soil layer is less than 0°C. The model increases runoff for frozen soils but still allows significant infiltration when the frozen soils are dry.

Peak Runoff Rate:

Peak runoff rate predictions are made with a modification of the rational method. In brief, the rational method is based on the idea that if a rainfall of intensity i begins instantaneously and continues indefinitely, the rate of runoff will increase until the time of concentration, tc, when all of the sub basin is contributing to flow at the outlet. In the modified Rational Formula, the peak runoff rate is a function of the proportion of daily precipitation that falls during the sub basin tc, the daily surface runoff volume, and the sub basin time of concentration. The proportion of rainfall occurring during the sub basin tc is estimated as a function of total daily rainfall using a stochastic technique.

Return Flow

Return flow, or base flow, is the volume of stream flow originating from groundwater. SWAT partitions groundwater into two aquifer systems: a shallow, unconfined aquifer

which contributes return flow to streams within the watershed and a deep, confined aquifer which contributes return flow to streams outside the watershed (Arnold et.al., 1995). Water percolating past the bottom of the root zone is partitioned into two fractions—each fraction becomes recharge for one of the aquifers. In addition to return flow, water stored in the shallow aquifer may replenish moisture in the soil profile in very dry conditions or be directly removed by plant. Water in the shallow or deep aquifer may be removed by pumping.

Routing Phase of Hydrologic Cycle

Once swat determines the loading of water, sediment, nutrients and pesticides to the main channel, the loading are routed through the stream network of the watershed using a command structure similar to that of HYMO (Williams and Hann, 1973). Additionally swat also models the transformation of chemicals in the stream and streambed.

Routing in the Main Channel or Reach

As water flows downstream, a portion may be lost due to evaporation and transmission through the bed of the channel. Another potential loss is removal of water for agricultural or human use. Flow may be supplemented by the fall of rainfall or addition of water from point source. In swat flow is routed using variable storage coefficient method developed by Williams (1969) or the Maskinghum routing method.

Variable Storage Routing

The variable storage routing method was developed by Williams (1969) and used in the HYMO (William and Hann, 1973) and ROTO (Arnold et.al., 1995) models. For a given reach segment, storage routing is based on the continuity equation

$$V_{in} - V_{out} = \Delta V_{stored} \qquad (2.4)$$

Where V_{in} is the volume of inflow during the time step (m^3 H_2O), V_{out} is the volume of outflow during the time step (m^3 H_2O). ΔV_{stored} is the change in volume of storage during time step (m^3 H_2O). After rearranging the equation it can be written as

$$Q_{out,2} = SC\ (q_{in,ave} + V_{stored,1} / \Delta t) \qquad (2.5)$$

SC is the storage coefficient, $q_{in,ave}$ is the average of $q_{in,1}$ and $q_{in,2}$ where $q_{in,1}$ is the inflow rate at the beginning of the time (m^3/s), $q_{in,2}$ is the inflow rate at the end of the time step (m^3/s), $q_{out,2}$

Muskinghum Routing

The Muskingum method is a commonly used hydrologic routing method in situations requiring a variable storage-discharge relationship (Chow et.al., 1988). The Muskingum method models the storage volume of flooding in a river channel using a combination of wedge and prism storage (see schematic below). The key parameters in Muskingum routing are K (travel time) and X (weighting coefficient). The value of X depends on the shape of the wedge storage to be modeled, and the value of X ranges from 0 for reservoir type storage to 0.5 for a full wedge. In natural streams, X is between 0 and 0.3 with a mean value near 0.2 (Chow et.al., 1988). K is the time required for an incremental flood wave to traverse its reach, and it may be estimated as the observed time of travel of peak flow through the reach (Chow et.al., 1988). If observed inflow and outflow hydrographs are available for a river reach the values of K and X can be determined to provide the best fit (or narrowest loop) relative to the observed flows.

It is necessary to enter a bankfull discharge, Manning's N parameter, slope, length, width, number of segments to represent the reach, an averaging weighting coefficient (X), and weighting coefficient for celerity. The weighting coefficient for celerity is the weight that should be given to the celerity calculated for the bankfull discharge. The weighting coefficient should be between 0 and 1. A weight of 1 uses the bankfull discharge celerity; a weight of zero uses only the celerity calculated for discharge at 10 percent of bankfull. In any case, the weighted estimate of celerity is used for all routing, regardless of changes in inflow. This differs from variable parameter Muskingum Cunge routing, where the celerity is calculated with each change in flow.

2.13.2 Hydrology

Rainfall Intensity

The rainfall intensity is the average rainfall rate during the time of concentration. Based on this definition, it can be calculated with the equation

$$I=R_{tc} / t_{conc} \quad (2.6)$$

Where I is the rainfall intensity (mm/hr) , R_{tc} is the amount of rain falling during the time of concentration (mm H_2O), and t_{conc} is the time of concentration for the subbasin (hr).

Percolation

Percolation is calculated for each soil layer in the profile. Water is allowed to percolate if the water content exceeds the field capacity water content for that layer and the layer below is not saturated. The volume of water available for percolation in the soil layer is calculated

$$SW_{ly,access}=SW_{ly}-FC_{ly} \quad \text{if } SW_{ly}>FC_{ly} \qquad (2.7)$$
$$SW_{ly,access}=0 \quad \text{if } SW_{ly}<= FC_{ly}$$

Where $SW_{ly,access}$ is the drainable volume of water on a given day (mm H_2O), SW_{ly} is the water content of the soil layer on a given day (mm H_2O). The amount of water that moves from one layer to the underlying layer is calculated using storage routing methodology.

Lateral Flow

Lateral flow will be significant in areas with soils having high hydraulic conductivities in surface layers and an impermeable semi permeable layer at a shallow depth. In such a system, rainfall will percolate vertically until it encounters the impermeable layer. The water then ponds above the impermeable layer forming a saturated zone of water, i.e. a perched water table. This saturated zone is the source of water for lateral subsurface flow.

Swat incorporates a kinematic storage model for subsurface flow developed by Sloan et al (1983) and summarized by Sloan and Moore (1984). This model simulates subsurface flow in a two dimensional cross-section along a flow path down a steep hillslope.

Groundwater System

An aquifer whose upper boundary is the water table whereas a confined aquifer is bounded above and below by geologic formations whose hydraulic conductivity are significantly lower than that of the aquifer.

Shallow Aquifer

The water balance for the shallow aquifer is:

$$aq_{sh,i} = aq_{sh,i-1} + w_{rchrg,sh} - Q_{gw} - w_{revap} - w_{pump,sh} \qquad (2.8)$$

where $aq_{sh,i}$ is the amount of water stored in the shallow aquifer on day i (mm H_2O), $aq_{sh,i-1}$ is the amount of water stored in the shallow aquifer on day i-1 (mm H_2O), $w_{rchrg,sh}$ is the amount of recharge entering the shallow aquifer on day I (mm H_2O), Q_{gw} is the groundwater flow, or base flow, into the main channel on day i (mm H_2O), w_{revap} is the amount of water moving into the soil zone in response to water deficiencies on day (mm H_2O) and $w_{pump,sh}$ is the amount of water removed from the shallow aquifer by pumping on day i (mm H_2O).

Deep Aquifer

The water balance for the deep aquifer is:

$$aq_{dp,i} = aq_{dp,i-1} + w_{deep} - w_{pump,dp} \quad (2.9)$$

where $aq_{dp,i}$ is the amount of water stored in the deep aquifer on day i (mm H_2O), $aq_{dp,i-1}$ is the amount of water stored in the deep aquifer on day i-1(mm H_2O), w_{deep} is the amount of water percolating from the shallow aquifer into the deep aquifer on day i (mm H_2O), and $w_{pump,dp}$ is the amount of water removed from the deep aquifer by pumping on day i (mm H_2O). If the deep aquifer is specified as the source of irrigation water or water removed for use outside the watershed, the model will allow an amount of water up to the total volume of the deep aquifer to be removed on any given day.

Transmission Loss

During periods when a stream receives no groundwater contributions, it is possible for water to be lost from the channel via transmission through the side and bottom of the channel. Transmission losses are estimated with the equation

$$t_{loss}=K_{ch} \times T_T \times P_{ch} \times L_{ch} \quad (2.10)$$

Where t_{loss} are the channel transmission losses (m^2 H_2O), K_{ch} is the effective hydraulic conductivity of the channel alluvium (mm/hr), T_T is the flow travel time (hr), P_{ch} is the wetted perimeter (m), and L_{ch} is the channel length (km). Transmission losses from the main channel are assumed to enter bank storage or the deep aquifer

Evaporation Loss

Evaporation losses from the reach are calculated:

$$E_{ch}=co_{efev} \times E_o \times L_{ch} \times W \times f_r\Delta t \quad (2.11)$$

Where E_{ch} is the evaporation from the reach for the day (mm H_2O), co_{efev} is an evaporation coefficient, E_o is the potential evaporation (mm H_2O), L_{ch} is the channel length (km), W is the channel width at water level (m), and $f_r\Delta$ is the fraction of the time step in which water is flowing in the channel.

The evaporation coefficient is a calibration parameter for the user and is allowed to vary between 0 and 1. The fraction of the time step in which water is flowing in the channel is calculated by dividing the travel time by the length of the time step.

Bank Storage

The amount of water entering bank storage on a given day is calculated

$$bnk_{in}= t_{loss} \times(1-fr_{trans}) \quad (2.12)$$

Where bnk_{in} is the amount of water entering bank storage (m^3H_2O), t_{loss} are the channel transmission losses (m^3 H_2O), and fr_{trans} is the fraction of transmission losses portioned to the deep aquifer.

Bank storage contributes flow to the main channel or reach within the subbasin. Bank flow is simulated with a recession curve similar to that used for groundwater. The volume entering the reach from bank storage is calculated

$$V_{bnk}=bnk \times (1-exp[-\alpha_{bnk}]) \quad (2.13)$$

Where V_{bnk} is the volume of water added to the reach via return flow from bank storage (m^3 H_2O), bnk is the total amount of water in bank storage (m^3 H_2O), and α_{bnk} is the bank flow recession constant or constant of proportionality.

Channel Water Balance

Water storage in the reach at the end of the time step is calculated:

$$V_{stored,2} = V_{stored,1} + V_{in} - V_{out} – t_{loss} - E_{ch} + div + V_{bnk} \quad (2.14)$$

Where $V_{stored,2}$ is the volume of water in the reach at the end of the time step (m^3 H_2O), $V_{stored,1}$ is the volume of water in the reach at the beginning of the time step (m^3 H_2O), V_{in} is the volume of water flowing into the reach during the time step(m^3 H_2O), V_{out} is the volume of water flowing out of the reach during the time step (m^3 H_2O), t_{loss} is the volume of water lots from the reach via transmission through the bed(m^3 H_2O), E_{ch} is the evaporation from the reach for the day (m^3 H_2O), div is the volume of water added or removed from the reach for the day through diversions (m^3 H_2O), and V_{bnk} is the volume of water added to the reach via return low from bank storage (m^3 H_2O). As the transmissions losses, evaporation and other water losses for the reach segment are calculated, the amount of outflow to the next reach segment is reduced by the amount of the loss.

2.13.3 SWAT Advantages

- Physically based
- Requires generally available information as input
- Computationally efficient
- Capable of being used on ungauged watersheds
- Enables users to study long-term impacts.

CHAPTER THREE
METHODOLOGY

3.1 Methodology

Assessment of climate change impact on the flow of any river basin using hydrological model involves several steps. Numerous amount of preprocessing and post-processing is one of the major difficulties faced by the researchers. In the present work initially several types of data such as, Digital Elevation Model, land use pattern, soil distribution, climate data and flow time series were collected to setup a semi-distributed model using SWAT. Steps followed in the present research can be described as following:

Step 1-Data Collection: This include DEM, land use pattern, soil distribution, climate data and flow time series

Step 2-Model Setup: Model setup which includes watershed delineation, weather data setup, HRU definition and selection of calculation methods.

Step 3-Model Development: Sensitivity analysis of the calibration parameters, calibration using the selected parameters, validation of the model and evaluation of the performance

Step 4-Scenario Selection: Selection of scenarios for climate change and upstream development impact assessment.

Step 5- Impact Assessment: Run the model with high resolution projected data and analyzed the impact of climate change as well as input the upstream development scenario to simulate its impact on the flow of Teesta river Basin

3.2 Data Collection

The literature review was carried out to better understand the river systems, the existing condition, the challenges and opportunities of the Teesta River basin. Based on the previous study reports, Journals, research papers relevant to the objective of data acquisition is to support the mathematical modelling process with requisite hydrometric,

hydro-geological and topographic data and to establish a digital database. For this study, six different types of data were acquired for the model development process. The details of the collected data are shown in **Table 3.1.**

Table 3.1: Details of the collected data

Data Type	Source	Station Name	Time Period	Remarks
DEM	Shuttle Radar Topography Mission (SRTM)		-	DEM with resolution of 90m
River Network	USGS Hydrosheds		-	-
Land Use	The USGS Land Cover Institute (LCI)		-	-
Soil data	FAO/UNESCO Soil Map of the World		-	The FAO soil types were manually included in the SWAT database, so they can be recognized by the program.
Climatic Data	NASA Prediction of Worldwide Energy Resource (POWER) and Tropical Rainfall Measuring Mission (TRMM)		1998-2013	Precipitation data was taken from the TRMM archive which provides the data from 1998-2013. Other climatic parameters such as Temperature, Wind Speed and Relative Humidity was retrieved from NASA POWER project.
Discharge Data	Bangladesh Water Development Board (BWDB)	Dalia (u/s of Teesta Barrage)	1985-2013	Discharge & Water Level data of Dalia point was collected from BWDB
Water Level			1996-2012	

3.2.1 Digital Elevation Model (DEM)

DEM data are required to provide the basic topographic information to the model. The DEM is used extensively for watershed delineation and to find out the drainage pattern of a given watershed. The DEM was collected from Shuttle Radar Topography Mission (SRTM). The SRTM DEM has a resolution of 90m x 90m. The DEM of the study area is shown in **Figure 3.3.**

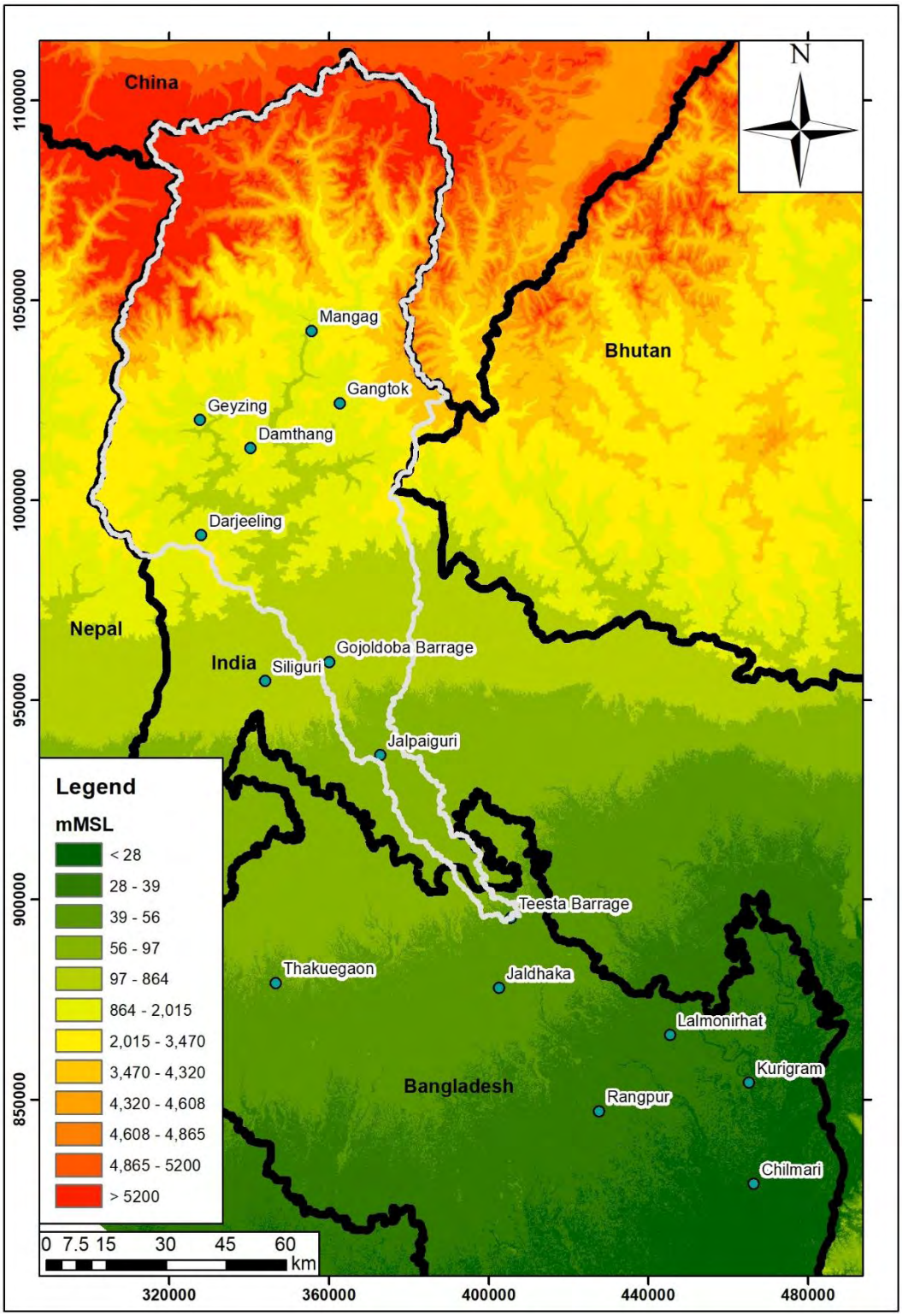

Figure 3.1: Digital Elevation Model (DEM) of the study area

3.2.2 River Network Data

River network helps the model identify the natural streams in the area so that it can set up its watershed based on the location and pattern of the natural streams. Although the model itself may be able to delineate the river network from the given DEM data,

providing the river network data makes the catchment delineation process much more accurate. The River Network data was downloaded from USGS Hydrosheds. The river network of the study area is shown in **Figure 3.3.**

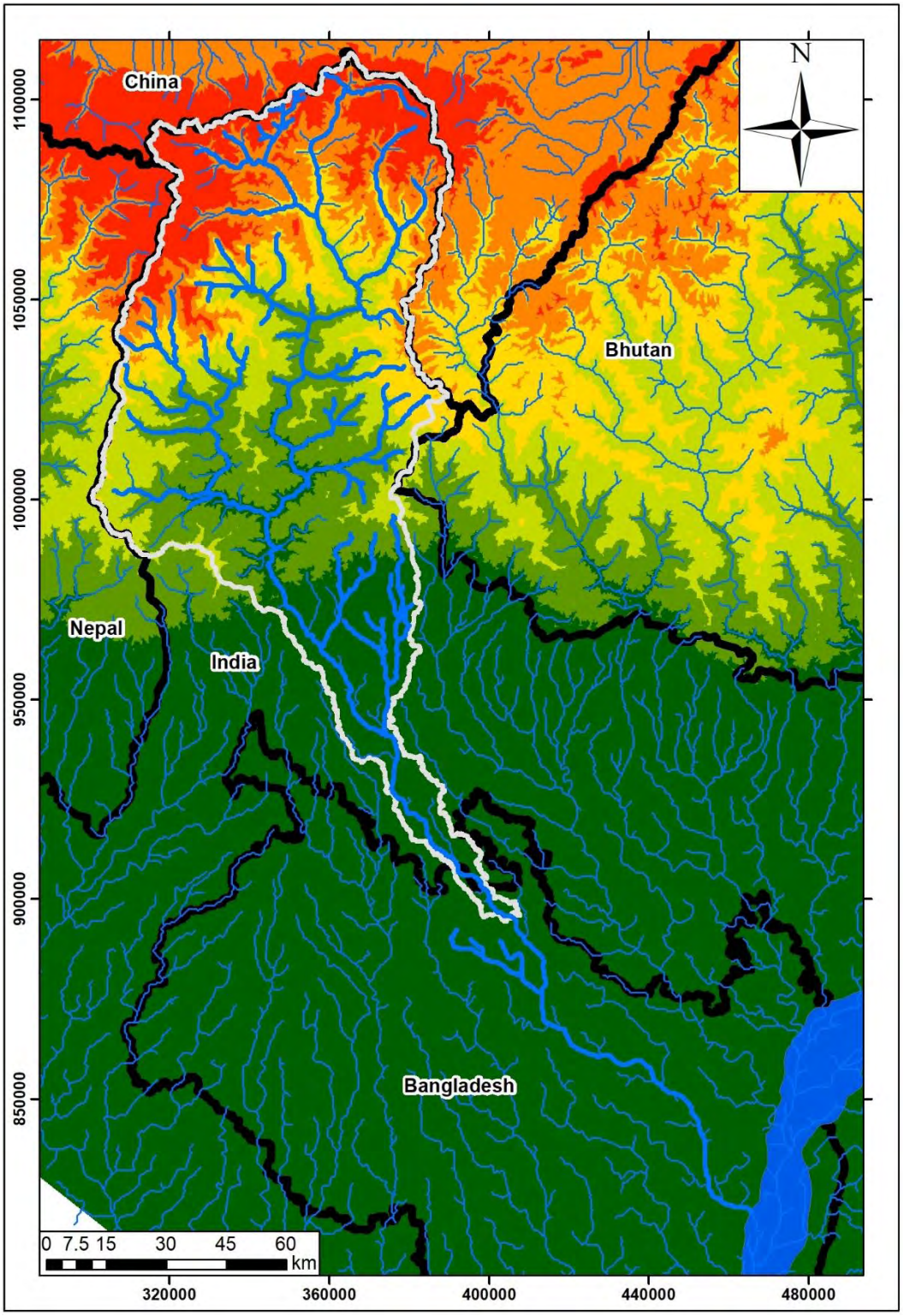

Figure 3.2: River Network of the study area

3.2.3 Soil Type Data

Soil Type data is required to set up the ground water part of the hydrological model which plays a very key role for the hydrological model calibration. The amount of infiltration as well as percolation with in the soil structure determines the amount of surface runoff of the region thus is an integral part of the hydrological cycle. For the purpose of this study "Soil map of the world" prepared by FAO (Food and Agriculture Organization) - UNESCO (United Nations Educational, Scientific and Cultural Organization) of the United Nations (FAO). The project for a joint FAO/UNESCO Soil Map of the World was undertaken following a recommendation of the International Society of Soil Science. It is the first attempt to prepare, on the basis of international cooperation, a soil map covering all the continents of the world in a uniform legend, thus enabling the correlation of soil units and the comparison of soils on a global scale. The project, which started in 1961, fills a gap in present knowledge of soils and soil potentialities throughout the world, and provides a useful instrument in planning agricultural and economic development. This map is at a scale of 1: 5000000 and based on the compilation of available soil survey material and on field correlation. **Figure 3.3** shows the extracted portion of the "Global soil Map" for the study area. It is worth mentioning that the along with the map, the "Global Soil Map" also provides a comprehensive data about its soil characteristics which can be incorporated in the model for better model output.

3.2.4 Land type and land use Data

Land use data allows the swat model characterize the initial parameters of the watersheds as well define the behavior of the catchment in case of precipitation. The presence of urban areas or forest area greatly changes the soil characteristics and the model will try to emulate the changing condition with the land use data type. The Land use data was downloaded from U.S Geological Survey (USGS) Land Cover Institute (LCI) website. The Land Use map has a resolution of 90m x 90m. The Land type and Land Use data of the study area is shown in **Figure 3.4**.

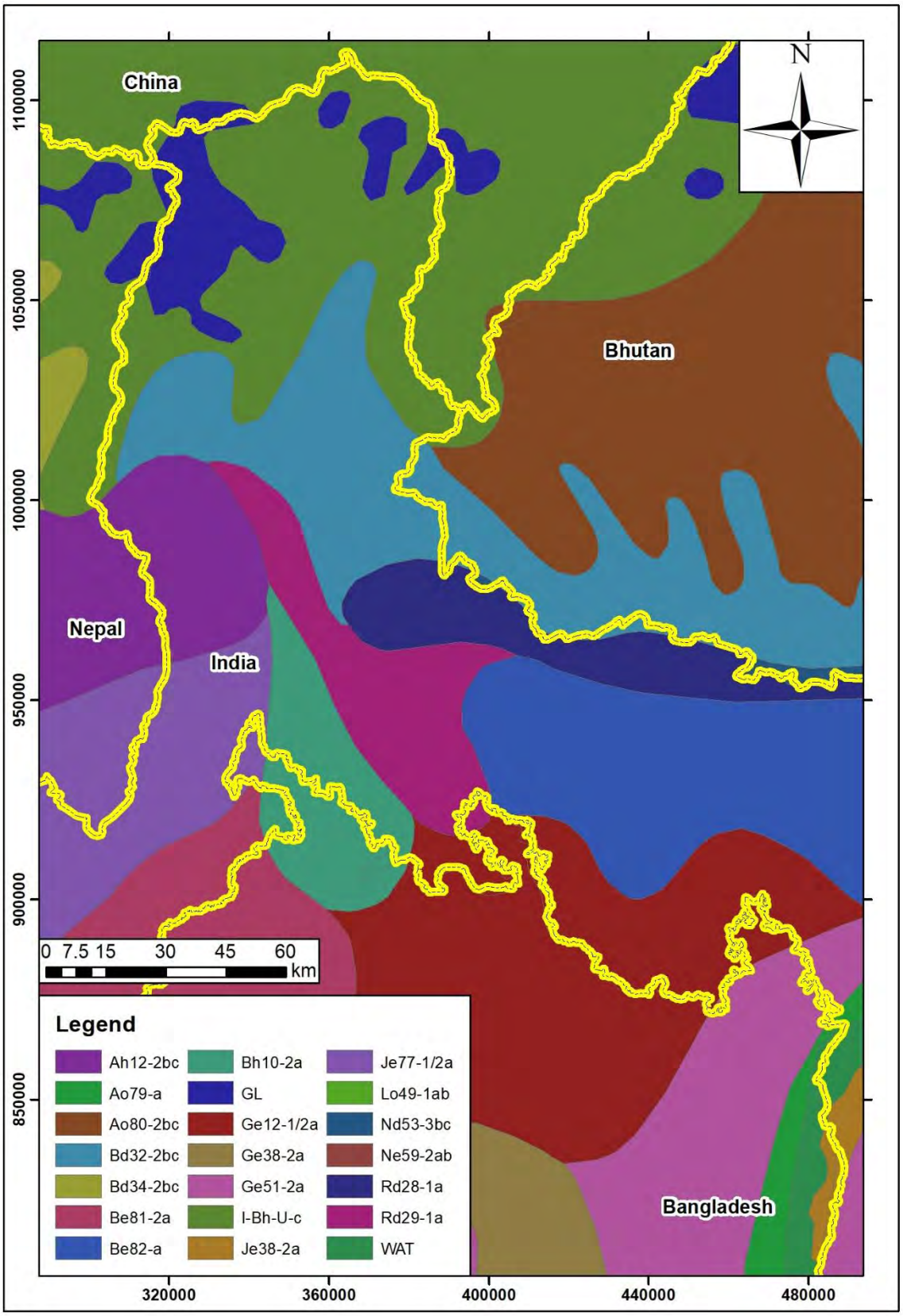

Figure 3.3: Soil classification type of the study area

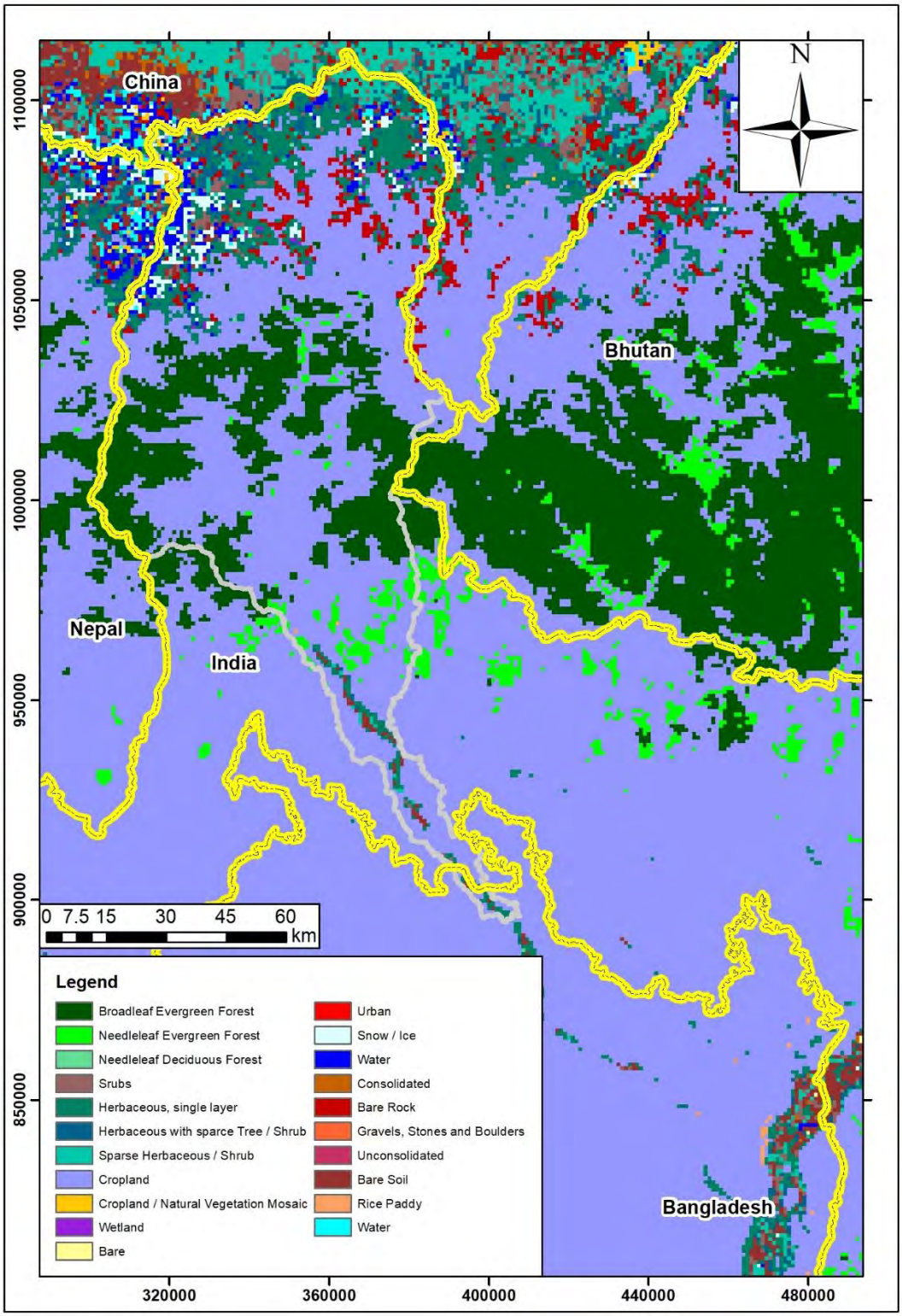

Figure 3.4: Land type and land use pattern of the study area

3.2.5 Weather and climatic data

Weather and climatic data are the heart of any hydrological model. It is these data that feed in the model about the daily precipitation and evaporation as well as define how the model is going to react.

The precipitation data for the model was acquired from the Tropical Rainfall Measuring Mission (TRMM). The Tropical Rainfall Measuring Mission (TRMM) is a joint mission between NASA and the Japan Aerospace Exploration (JAXA) Agency to study rainfall for weather and climate research. The TRMM satellite ended collecting data on April 15, 2015. Launched in late November 1997, with a design lifetime of 3 years, the TRMM satellite produced over 17 years of valuable scientific data. TRMM carried 5 instruments: a 3-sensor rainfall suite (PR, TMI, VIRS) and 2 related instruments (LIS and CERES). TRMM delivered a unique 17-year dataset of global tropical rainfall and lightning. The TRMM daily precipitation data comes at a gridded format at an interval of 0.25 degrees and the collected data ranges from 1998-2013.

Other climatic datasets such as daily mean temperature, relative humidity and wind speed data was downloaded from NASA POWER project. The Prediction of Worldwide Energy Resource (POWER) project was initiated to improve upon the current SSE data set and to create new data sets from new satellite systems and forecast modeling data. In the late 1990's, the Surface Meteorological and Solar Energy (SSE) project was initiated through NASA's Applications program to provide internet-based access to parameters specifically tailored to assist in the design of solar and wind powered renewable energy systems. The goal of the SSE-project was to make NASA's satellite data more readily accessible to the renewable energy community where such data was demonstrated to enhance the output of existing Discussion Support Systems (Stackhouse, et. al. 2002).The POWER project’s aim was to improve these SSE data and make them available for researches working in the field of sustainable development and renewable energy. The collected climatic datasets has a spatial distance of 1 degree and ranges from 1997-2013.

3.2.6 Discharge data

Discharge data is required to calibrate and validate the model. The discharge generated by the model due to precipitation and or snow melt must be checked against a set of observed discharge data. The discharge data of Dalia point, upstream of Teesta Barrage which is situated in Nilphamari district near the Bangladesh-India border has been collected from Bangladesh Water Development Board (BWDB) for the period of 1985-2013.

3.2.7 Water Level data

Water Level data was collected to carry out secondary data analysis to see the trend of water availability of Teesta basin. The water level data of Dalia point, upstream of Teesta Barrage has been collected from Bangladesh Water Development Board (BWDB) for the period of 1996 to 2012.

3.3 Model Development

The physically based hydrological model Soil and Water Assessment Tool (SWAT) of Amold and Allen (1996) selected for study. This study operates on daily time step and uses physiographical data such as elevation, soil use, meteorological data and river discharge. The hydrological processes included in the model are evapotranspiration (ET), surface runoff, infiltration, percolation, shallow and deep aquifers flow, and channel routing. The effects of spatial variations in topography and land use, soil and other characteristics of watershed hydrology are incorporated by dividing a basin into several sub-basins based on drainage areas of tributaries and then the sub-basins are further divided into a number of Hydrological Response Units (HRUs) based on land cover and soils. Each HRU is assumed to be spatially uniform in terms of land use, soil, topography and climate. The subdivision of the watershed enables the model to reflect differences in evapotranspiration for various crops and soils. Moreover this discretization of basin into HRU allows a detailed simulation of the hydrological processes. All the computations are performed at HRU level (Mengistu, 2012). The hydrological cycle as simulated by SWAT is based on the water balance equation which is given below:

$$SW_t = SW_0 + \sum_{i=1}^{t}(R_{day} - Q_{surf} - E_a - w_{seep} - Q_{gw}) \quad (3.1)$$

Where SW_t is the final soil water content, SW_0 is the initial soil water on day I, t is the time in days, R_{day} is the amount of precipitation on day I, Q_{surf} is the amount of surface runoff on the day I, E_a is the amount of evapotranspiration on day I, W_{seep} is the amount of water entering the vadose zone from the soil profile on day I and Q_{gw} is the amount of flow on the day I (All units except the time are presented as mm of water).

The Arc-GIS extension of SWAT called “ArcSWAT” had been used as the hydrological modelling tool for the purpose of this study.

3.3.1 Model Setup:

To setup the hydrological model using SWAT, the first step would be to delineate the river basin. The "Automatic Watershed Delineation" tool of ArcSWAT was used for this purpose. The "Automatic Watershed Delineation" uses the DEM as well as the river network provided by the user to delineate the watersheds of the catchment. In case the presence of large reservoirs in the catchment, the user can also incorporate that though the "Automatic Watershed Delineation". After completion of these processes, the ArcSWAT delineated the Teesta River Basin which had an area of 9,993 sq. km. The Teesta river basin was further subdivided into 43 sub-basins. The delineated Teesta River Basin along with all of its sub-basins are shown in **Figure 3.5**.

After watershed delineation, the sub-basins are further divided into a number of Hydrological Response Units (HRUs) based on land cover, soil type and slope of the watershed. After providing the land cover and soil type data and calculating the slope of the watershed from DEM, the entire Teesta basin was divided into 360 HRUs.

Once the discretization into HRU level was completed, weather datasets such as daily precipitation, mean daily temperature, wind speed and relative humidity was applied for the base model (1995-2013). The first three years of the simulation (1995-1998) served as the warm-up period of the model and model outputs beginning from 1999 was considered for the base model. The potential evapotranspiration (PET) estimates was calculated using Penman/Monteith method while for rainfall distribution, the skewed normal distribution was used.

SWAT can use two types of channel routing method, variable storage method and Muskingum method. The variable storage method was developed by Williams (1969) and used in the HYMO (Williams and Hann, 1973) and ROTO (Arnold et al, 1995) model. The storage routing here is calculated using a dimensionless storage coefficient (SC) which is updated every time step iteratively. Muskingum method on the other hand models the storage volume in a channel length as a combination of wedge and prism storages. When a flood wave advances into a reach segment, inflow exceeds outflow and a wedge of storage is produced. As the flood wave recedes, outflow exceeds inflow in the reach segment and a negative wedge is produced. In addition to the wedge storage, the reach segment contains prism of storage formed by a volume of constant cross-section

along the reach length. After a few trial and error processes, variable storage method was chosen for the developed hydrological model as it provided better results.

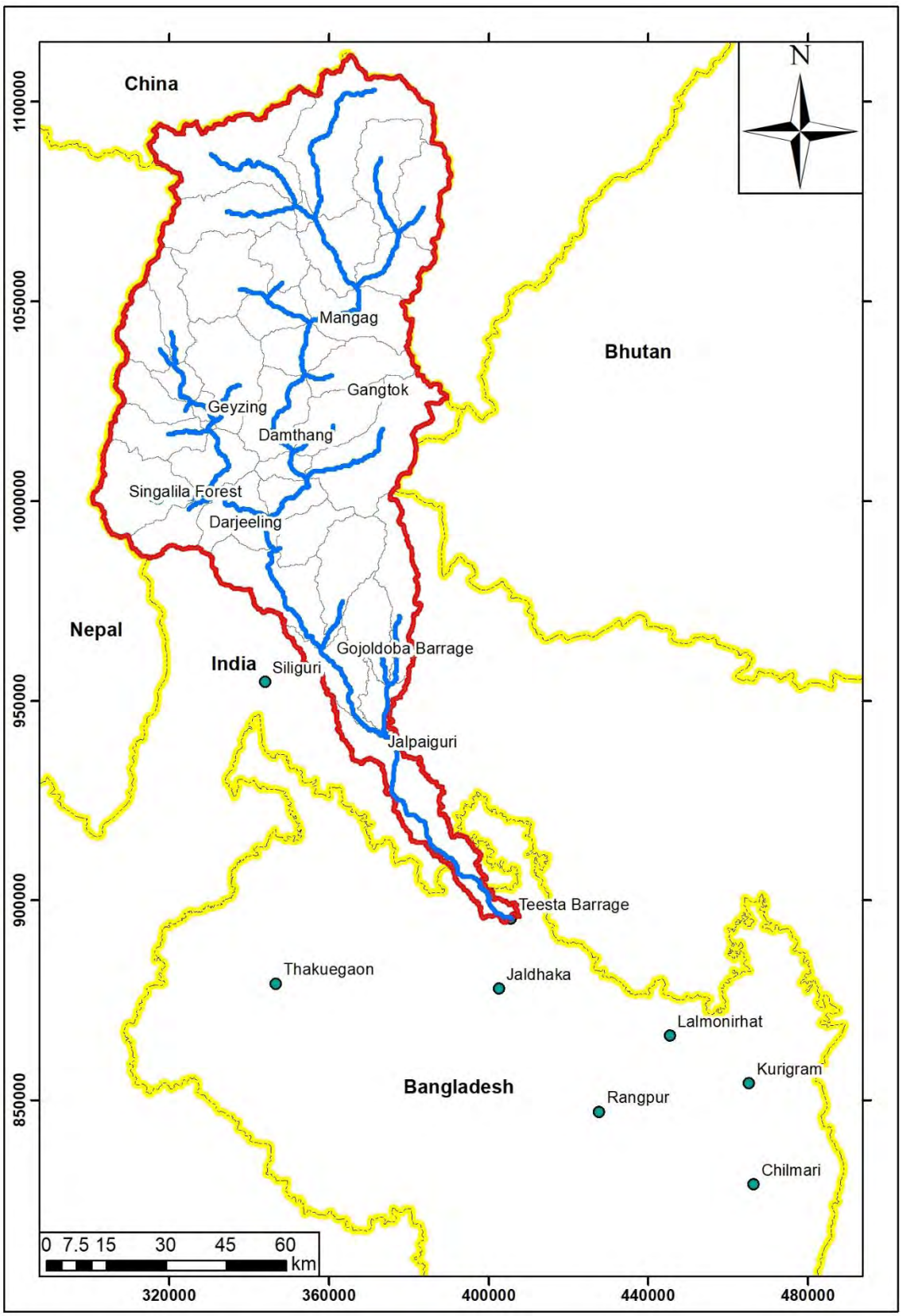

Figure 3.5: Teesta River basin delineated with the aid of ArcSWAT

3.3.2 Model Calibration and Validation:

Calibration means adjustment of the model parameters so that simulated and observed data will match within the desired accuracy. Model parameters may require adjustment due to a number of reasons. There are numerous parameters in hydrological models which can be classified as physical parameters (i.e. parameters that can be physically measurable from the properties of watershed) and process parameters (i.e, parameters represents properties which are not directly measurable) (Sorooshian and Gupta, 1995). In reality, all models require some degree of calibration to fine tune the predictive ability of the model. After some test simulations it was clear that four parameters had greater influence on the shape and magnitude of the output hydrographs. They are:

SCS Curve Number Calculation

SCS (Soil Conservation Service) Curve Number (CN) is an empirical parameter used or predicting direct runoff or infiltration from rainfall excess. There are actually two ways that the program can calculate the surface runoff, one is the SCS Curve number method (1972) the other is the Green & Ampt infiltration method (1911). However the Green & Ampt infiltration method requires sub daily in precipitation data which is very hard to get. That is why SCS curve number method of surface runoff calculation was used.

The main parameter for the curve number calculation is CN2 which is the initial SCS runoff curve number for moisture condition II. The SCS CN is function of the soil's permeability, land use and antecedent soil water condition. The CN has a range from 30 to 100. Lower numbers indicate low runoff potential while larger numbers are for increasing runoff potential. So, the lower the curve number, the more permeable the soil is.

It is worth mentioning that the CN2 parameter is highly sensitive. With the slightest change of this parameter the SWAT model completely changes the simulated runoff magnitude. Initially the SWAT model assigns a CN2 value based on the soil data and land use pattern but more often than not a user needs to change this value for better calibration. The default value of CN2 is 60-95 while final calibrated value was 70-92, so only minor changes from the initial value of CN2 was required for model calibration.

Ground Water Delay Time

The ground water delay time parameter of the SWAT model actually represent the lag time between the times that the water exits the soil profile and enters the shallow aquifer. This parameter cannot be directly measured but will mainly depend on the depth of the water table and the hydraulic properties of the geologic formation in the vadose (region of aeration above the water table) and ground water zones. It terms of model behavior, increasing the ground water delay time actually increases the base flow of the model and generates more flow in the dry periods, damping out the hydrograph a lot. While the default value is 31 days, during the calibration process, the value of Ground Water Delay time was chosen as 32 Days.

Baseflow recession constant

The baseflow recession constant is a direct index of ground water flow response to change in charge (Smedema and Rycroft, 1983). The value may vary from 0.1 to 0.3 with slow response to recharge and from 0.9-1 for land with rapid response. Although the baseflow recession constant may be calculated, it requires a lot of data on baseflow contribution into the main channel as well as data of recharge rate of shallow aquifer and storage of the shallow aquifer. Thus it will be a very hard job to calculate the baseflow recession constant.

In the swat model environment, the baseflow recession constant has a significant effect on the shape of the hydrograph. The default value of the parameter was set to 0.048 which represent a very slow responding soil. Increasing the base flow recession constant will make the slope of the hydrograph a lot steeper, meaning that peaks will be reached faster and the recession limb of the hydrograph will also be a lot steeper hence meaning quicker drainage. The default value of baseflow recession constant, which is 0.048 was used in the developed calibrated model of the Teesta basin.

Ground water Revap

Water may move from the shallow aquifer into the overlying unsaturated zone. In periods when the material overlying the aquifer is dry, water in the capillary fringe that separate the saturated and unsaturated zone will evaporate and diffuse upward. As this water gets

removed, more water from the underlying aquifer will replace the evaporated one. This process is modeled by SWAT using the "GW_REVAP" parameter. The default value of GW_REVAP 0.02 was taken during calibration.

The details about the calibration parameter default value and selected values are shown in **Table 3.2**.

Table 3.2: Model Calibration Parameters

Parameter	Default Value	Suggested Range	Calibrated Value
SCS Curve Number	60-95	30-98	70-92
Ground Water Delay	31	0-500	32
Baseflow Recesion	0.048	0-1	0.048
GW REVAP	0.02	0.02-0.2	0.02

Validation:

Validation is the process of determining the degree to which a model or simulation is an accurate representation of the real world from the perspective of the intended uses of the model or simulation. Once the model parameters have been finalized during calibration process, the model is simulated with that set of parameter for a different time frame to see the models performance. If the model performs well in predicting the output for the different timeframe it can be said to be validated.

Calibration is generally done with the latest available data series. As a result the final eight years of available data series that is from 2006-2013 has been used for calibration. After finalizing the parameters the model was simulated for the entire time frame and the first seven years of the simulation from 1999-2005 was chosen as the validation period for the model. In calibration and validation stage of the model, the performance of the model is evaluated both statistically as well as graphically. The model generated mean monthly discharge and observed mean monthly discharge at Dalia point is shown in **Figure 3.6**.

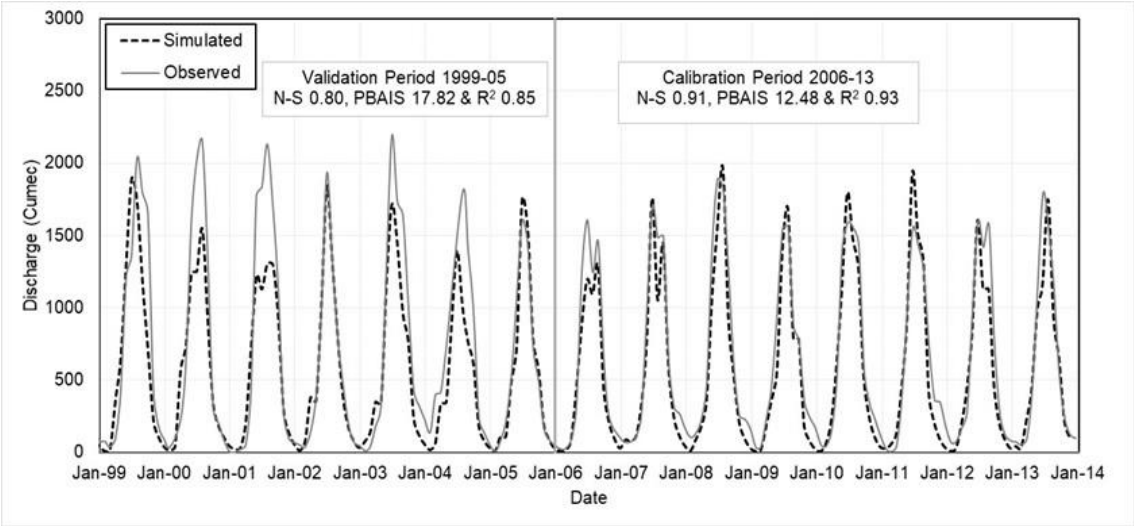

Figure 3.6: Monthly observed and simulated flows at Dalia point for calibration and validation of the model

3.3.3 Model Performance Evaluation

Statistically the performance of the model has been evaluated using the Nash-Sutcliffe Efficiency value (NSE), the coefficient of determination (proportion of the variance in the observations explained by the model, R^2), percent bias (PBIAS) and the ration of the root mean square error between the simulated and the observed values to the standard deviation of the observations (RSR). The statistically model performance is given in **Table 3.3.** As can be seen from the table, the NSE values for calibration and validation period is 0.91 and 0.80 respectively. The coefficient of determination (R^2) was found to be 0.93 and 0.85 for calibration and validation period. While the RSR and PBAIS was determined as 12.48 and 0.30 for calibration stage and 17.82 and 0.44 for validation stages respectively.

Table 3.3: Statistical performance of the developed Teesta river basin model

Period		Observed Mean (m^3/s)	Simulated Mean (m^3/s)	Model Performance Parameter			
				N-S	PBAIS	RSR	r^2
Calibration	"2006-2013"	634.46	549.48	0.91	12.48	0.30	0.93
Validation	"1999-2005"	684.64	576.52	0.80	17.82	0.44	0.85

3.4 Climate Model and Scenario Selection

For the CMIP5 twenty eight different institutions have sixty one different GCM models, with each GCM model providing completely different output from the other one. Working with all those sixty one models becomes quite challenging. Thus selecting proper scenarios becomes very important. Analyzing GCM simulated precipitation, maximum temperature and minimum temperature for the Teesta basin thus becomes crucial to identify the warmest, coolest, driest, wettest scenarios. To analyze the precipitation data, the rainfall at 88 different points were compared for different GCM and RCP scenarios. For temperature the GCM data were compared at 63 different stations. Precipitation, max temperature and min temperature obtained from different GCMs were average for two periods, viz. 2040-2069 (2050s) and 2070-2099 (2080s). Changes of precipitations and temperature from the base period were analyzed separately for all the periods. Finally, selection of scenarios were done based on the changes at the end of 21st century which is represented by 2080s

For the purpose of this study two GCMs were chosen. They are HADGEM2 ES model developed by The Hadley Centre and CSIRO MK 3.6.0 GCM model developed by Commonwealth Scientific and Industrial Research Organization (CSIRO). A brief description the models are provided below:

3.4.1 HADGEM2 ES Model

The Hadley Centre Global Environmental Model version 2 (HadGEM2) family of models has been designed for the specific purpose of simulating and understanding the centennial scale evolution of climate including biogeochemical feedbacks. Along with inclusion of the complex earth system (ES) into the underlying model physical model, the HadGEM2 has been introduced with large-scale hydrology module (LSH) in order to improve the soil moisture, and hence the vegetation distribution, and provide additional functionality such as simulation of wetland area required for interactive methane emissions. LSH (Clark and Gedney, 2008; Gedney and Cox, 2003) is based on the TOPMODEL approach (Beven and Kirkby, 1979) whereby soil moisture and runoff are affected by local topography as well as meteorology, vegetation and soil properties.

The river scheme is based on TRIP (Oki and Sud, 1998) as in HadGEM1. It includes river transport dynamics, driven by fluxes of surface and subsurface runoff. TRIP operates on 1o x 1o grid which is higher resolution than land surface or atmosphere model. Rivers provide significant freshwater input to the oceans thereby forcing the oceans regionally through changes to density. The inclusion of the TRIP river flow model allows the inclusion of this regional ocean forcing, which is an important component of both Earth system and atmosphere-ocean models. The total HadGEM2-ES simulated discharge to the oceans is 1.07 Sv, within the observational range of 1.035 to 1.27 Sv (Dai and Trenberth, 2002) but tending to the low side. The scale used here is Sverdrup (Sv) which corresponds to 106 m^3/s or a change in sea level of ~10m per century. **Figure 3.7** compares the simulated regional discharge from HadGEM2-ES and an observational dataset of ocean discharge from Dai et al. (2009). HadGEM2-ES simulates the point of river discharge in a slightly different location to the observations due to the smoothed land-sea mask of the ocean model. However, the major rivers such as the Amazon, Ganges/Brahmaputra and Mississippi are all well simulated.

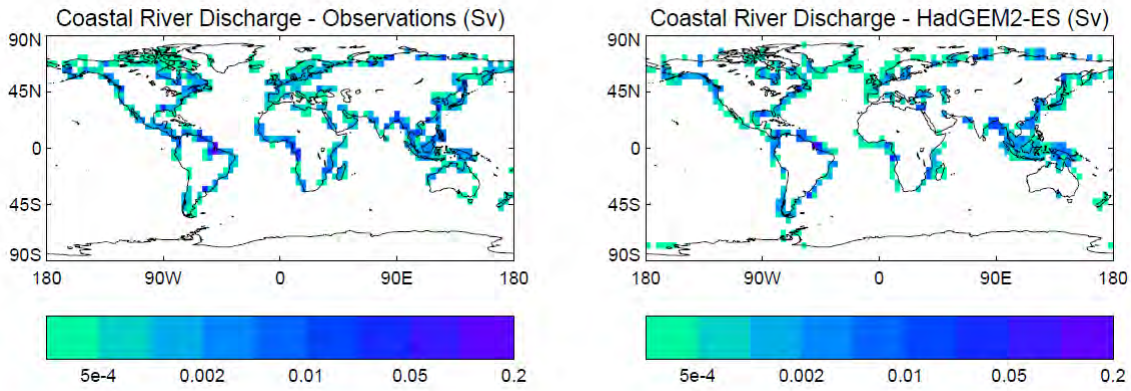

Figure 3.7: Mean annual (1948–2004) discharge (Sv) from 4o x 5o (Lat x Long) coastal box estimated from available gauge records and reconstructed river flow (Dai et al., 2009) and simulated discharge from HadGEM2 (*Source: Collins et al., 2011*)

3.4.2 CSIRO MK 3.6.0 Model

The CSIRO-Mk3.6.0 model, hereafter called Mk3.6, is an upgrade from the CSIRO-Mk3.5 GCM (Gordon et al., 2010). Details of the model are given by Rotstayn et al. (2010). The atmospheric component has a horizontal resolution of approximately 1.9°x1.9° and every atmospheric grid-point iscoupled to two ocean grid-points. This enhanced north-south resolution in the ocean component is expected to increase the capacity for the ocean to simulate important tropical and extra-tropical seasonal

interactions. The atmosphere has 18 vertical levels whereas the ocean has 30 levels with most found in the upper 1500m. By far the most important improvement of the Mk3.6 model from its predecessor is the inclusion of an interactive aerosol scheme that also required an update to the radiation scheme used in the model (Rotstayn et al., 2010). This allows for the investigation of the impact of a number of aerosol agents on climate. For example, a recent study by Rotstayn et al. (2011) investigated the impact of mineral dust on Australian rainfall by turning it on and off in two experiments. The study found that an accurate simulation of the El Niño-Southern oscillation (ENSO)-rainfall relationship over Australia might require realistic representation of processes associated with sources and deposition of Australian dust.

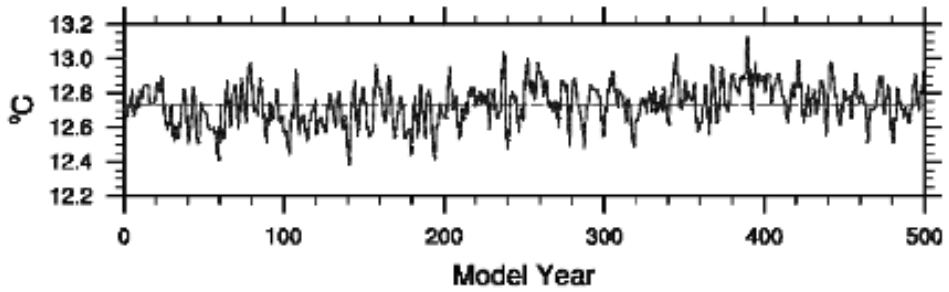

Figure 3.8: Global average surface air temperature (°C) for the CSIRO-Mk3.6.0 pre-industrial control experiment. The dashed line is the 500 year average (*Source: Gordon et al., 2010*)

To have confidence in a climate model's ability to realistically simulate present and future climate conditions it is necessary for it to be able to respond in a satisfactory manner when driven by pre-industrial (year 1850) forcings. An important indicator of this is the stability of the model solution which includes negligible drift in important climate indices and one devoid of irregular behavior. **Figure 3.8** shows globally averaged annual surface temperature from the pre-industrial control experiment, which appears to be stable during the 500 year long experiment. **Figure 3.9** shows the ocean potential temperature and salinity (practical salinity units). The ocean temperature drift in the Mk3.6 is 0.02°C/century, which is comparable to other coupled climate models. The salinity drift is also and indicates the global precipitation and evaporation are not perfectly balanced in the model, at least on these time-scales.

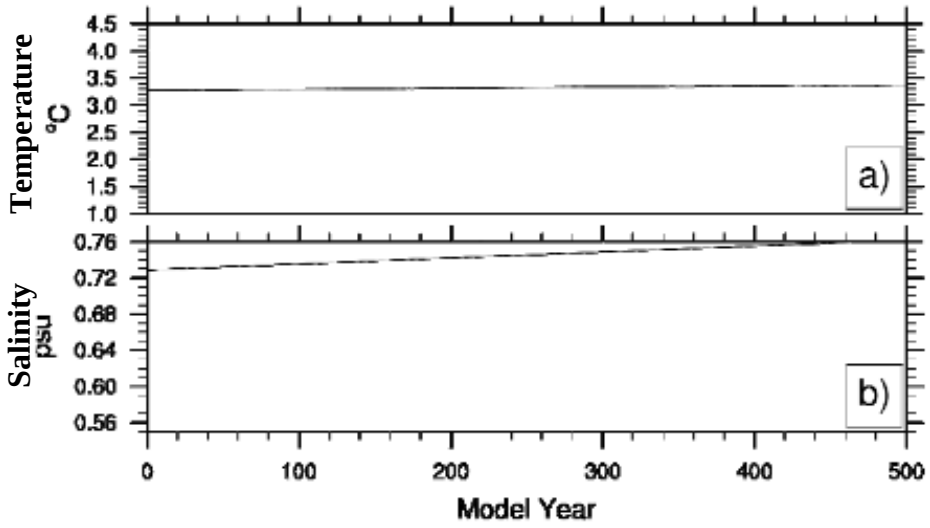

Figure 3.9: Global average volume weighted a) ocean potential temperature (°C) and b) salinity (psu-34.0) for the CSIRO-Mk3.6.0 pre-industrial control experiment (*Source: Gordon et al., 2010*)

3.4.3 Statistical Downscaling (Delta Method) CMIP5 Data

There has been significant scientific discord over what the best resolution for forecasting the impacts of climate change on agriculture and biodiversity is. Several researchers state that original GCM resolution should be kept in order to manage, understand and not bias or alter uncertainties produced by GCMs themselves; however, a coarse resolution of 100 or 200km (or even more) is simply not practical particularly in the tropics, where orographic and climatic conditions vary significantly across relatively small distances. Given the time and processing capacity required for applying these equations in a single cell (taking into account its interactions with neighbor cells), GCM cells cannot be unlimitedly small; rather, they are restricted to a size of 100-300km. Downscaling techniques allow researchers to obtain regional predictions of climatic changes, ranging from smoothing and interpolation of GCM anomalies (e.g. Tabor and Williams, 2010, among others), to neural networks, and regional climate modeling (Giorgi, 1990). The different downscaling techniques vary in accuracy, output resolution, computational and time requirements, and climatic science robustness (i.e. theoretical background). Regional Climate Models provide 20 to 50km surfaces by re-modeling GCM outputs and are thus only applicable to a limited number of GCMs (for which boundary conditions are available), and require considerable processing capacity, time and storage for obtaining a single scenario-by-period output, thus making it barely feasible to get RCM outputs for most assessment offices and researchers.

Statistical downscaling, on the other hand, provides an easy-to-apply and much more rapid method for developing high resolution climate change surfaces for high resolution regional climate change impact assessment studies. However, climatologists have lambasted the procedure for degrading data, since downscaling tends to reduce variances (and thus alter uncertainties) and to give off a false sense of increased accuracy, when in actuality, it only provides a smoothed surface of future climates. However, the price of not disaggregating, interpolating, smoothing, downscaling, or doing whatever possible to increase GCM resolution to a finer scale, could be greater than the inherent degradation of GCM data involved with these approaches.

In this study, results from a simple downscaling method (named delta method), based on the sum of interpolated anomalies to high resolution monthly climate surfaces from WorldClim (Hijmans et al., 2005). The method produces a smoothed (interpolated) surface of changes in climates (deltas or anomalies) and then applies this interpolated surface to the baseline climate (from WorldClim), taking into account the possible bias due to the difference in baselines. The method assumes that changes in climates are only relevant at coarse scales and that relationships between variables are maintained towards the future. While these assumptions might hold true in a number of cases, they could be wrong in highly heterogeneous landscapes where topographic conditions cause considerable variations over relatively small distances. The method makes the following gross assumptions:

1. Changes in climates vary only over large distances (i.e. as large as GCM side cell size)
2. Relationships between variables in the baseline ("current climates") are likely to be maintained towards the future

The process consists of the following steps:

1. Gathering of baseline data (current climates corresponding to WorldClim)
2. Gathering of full GCM timeseries
3. Calculation of 30 year running averages for present day simulations (1961-1990) and 7 future periods

4. Calculation of anomalies as the absolute difference between future values in each of the 3 variables to be interpolated (minimum and maximum temperature, and total precipitation)
5. Interpolation of these anomalies using centroids of GCM cells as points for interpolation
6. Addition of the interpolated surfaces to the current climates from WorldClim, using absolute sum for temperatures, and addition of relative changes for precipitation
7. Calculation of mean temperature as the average of maximum and minimum temperatures

For this study, the statistically downscaled HadGEM2-ES model and CSIRO MK 3.6.0 Model, downscaled by CGIAR's (Formally known as Consultative Group on International Agricultural Research) research program on Climate Change, Agriculture and Food Security (CCAFS). The data is available on the internet for research purposes.

3.5 Upstream Control Structure Scenario Selection

Teesta River basin's unique challenge is the presence of multiple human interventions such as dams and barrages in the Upper Teesta Basin. The details of the structures have been discussed in **Article 2.2**. Approximately 30 major hydropower projects have been planned on the river, with a planned capacity of over 5,000 megawatts of electricity (Parsai, 2013). Along with that the presence of flow diversion structures like the Gozoldoba Barrage severely disrupts the natural flow of the Teesta River. In this study, the effect of some of important structures were incorporated to see its impact on the surface water availability at the Dalia point. Based on the location, size of the dam as well as probable impact on water availability at Dalia, three different structures were selected for the purpose of the study. Of all the current and future structures on the Teesta river basin, the most important of them all is the Gozoldoba barrage, where a major portion of the water is being diverted. Thus the Gozoldoba barrage was incorporated in the study to see the impact of possible impact of the barrage. The other two structures are further upstream of the basin. One of them is the Teesta Stage III hydropower project which has been commissioned by the Sikkim state government in 2017. Since the massive 1200 MW project only began operation last monsoon, the effect of the dam on the water availability of Teesta becomes an important issue for the future studies. Thus

it was considered in this study. Another one considered for the study is the Rammam III hydropower plant which is an ongoing project in West Bengal. The construction of Rammam III has begun in 2015 and expected to become operational by 2020. This new project will also have some effect on the water availability of Teesta River at Dalia point. The location of these structures are shown in **Figure 3.7**.

To incorporate Gozoldoba barrage of the Teesta River, different flow diversion scenarios have been considered in this study. Six different flow diversion scenarios varying from 10% up to 60% (at 10% increment) flow diversion scenarios have been considered for this purpose. Here 20% flow diversion means 20% of the total available flow at the structure during base condition will be diverted through the structures side canal during the lean flow season (i.e. October – April) and 80% of the flow will be allow to flow downstream.

To incorporate the hydroelectric projects Teesta III and Rammam III, a different type of flow scenario was considered. Six flow diversion scenarios varying from 5% up to 30% (at 5% increment) flow was extracted from the stream during monsoon (June to September). The amount extracted during monsoon was later released during lean season (October to May) to simulate the effect of hydroelectric power project.

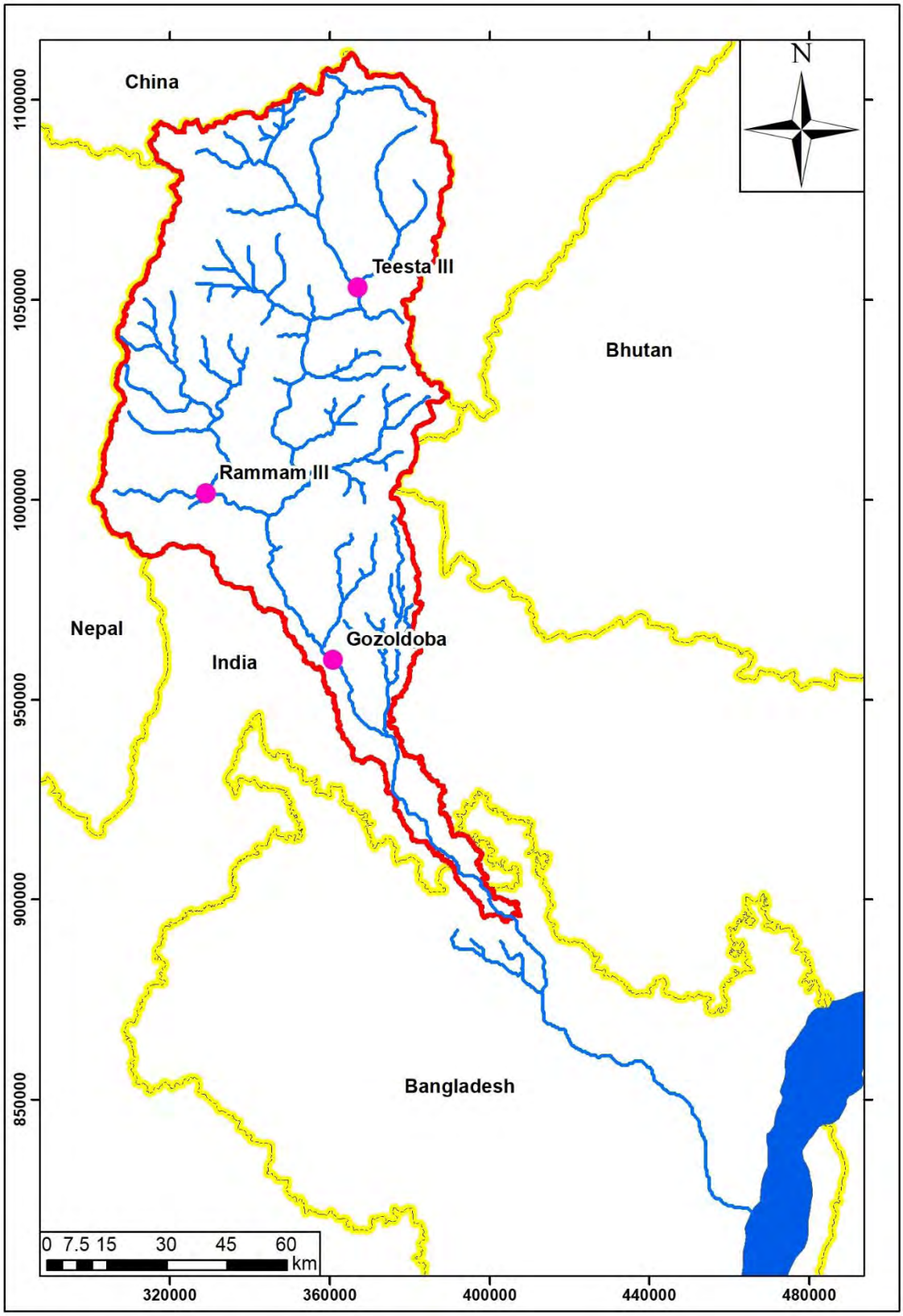

Figure 3.10: Upstream control structures considered for the study

CHAPTER FOUR
ANALYSIS AND RESULTS

The analysis of the secondary data, analysis of downscaled GCM data to develop climate change scenarios as well as the model generated results for different climate change scenarios and different flow diversion scenarios (projecting upstream developments) has been discussed briefly in this chapter.

4.1 Historical Flow and Water Level Analysis of Teesta River at Dalia Point

Discharge data for 28 years (1985-2012) and water level data of 17 years (1996-2012) has been analyzed to find out the trend of flow of the Teesta river basin. Extreme value analysis of the annual maximum discharge data was also carried out to find the flood events of the corresponding flood event.

The annual maximum flow at the Dalia point, u/s of the barrage is shown in **Figure 4.1**. It can be seen from the Figure that the maximum annual flow has occurred during 1998, the second highest flow can be observed during 1987. However the most salient feature of the figure is the trend line, represented with the dotted line which shows significant decline of annual maximum flow over the years. Similar plot has been prepared for the annual average or mean flow which is shown in **Figure 4.2**. The figure also shows a declining trend line which indicates that water availability in the Teesta River at Dalia point is on the decline over the past three decades.

The annual minimum flow of the Teesta River at Dalia is shown in **Figure 4.3**. As the discharge of the Teesta river basin is highly controlled, no specific trend can be identified from the minimum discharge graph. But it can be observed that the annual minimum discharge drops below 10 cumec almost every year indicating very low water availability during the lean season.

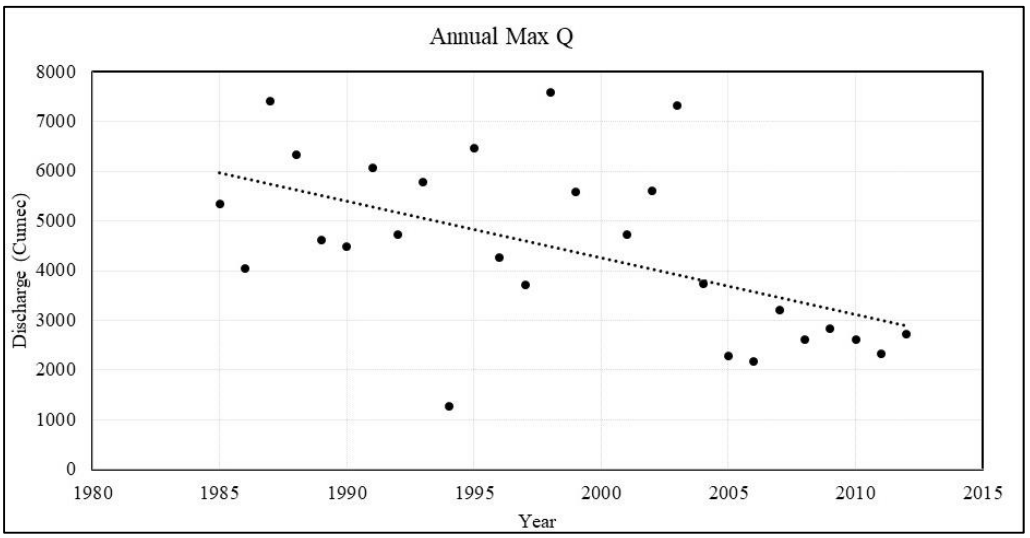

Figure 4.1: Annual Maximum Flow of Teesta River at Dalia point

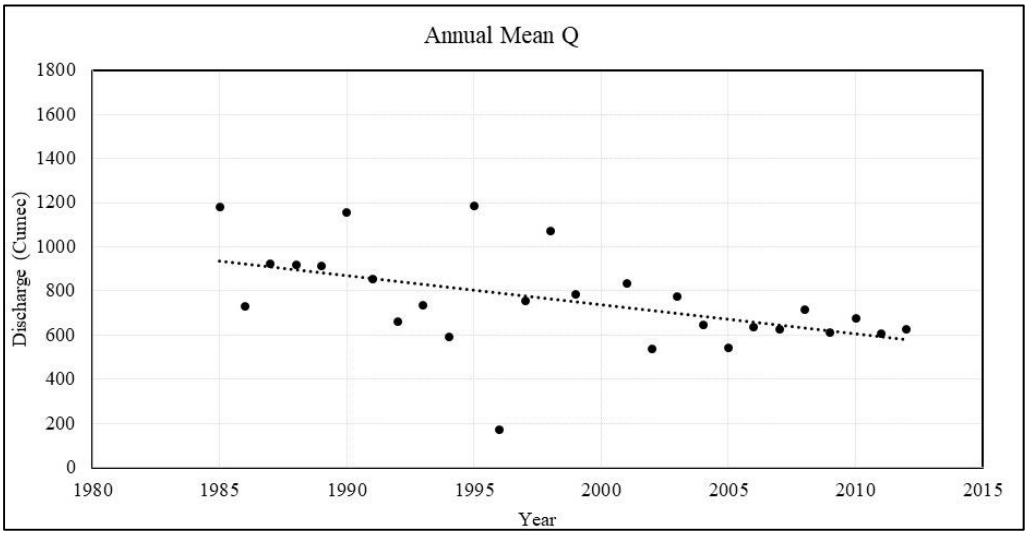

Figure 4.2: Annual Mean Flow of Teesta River at Dalia point

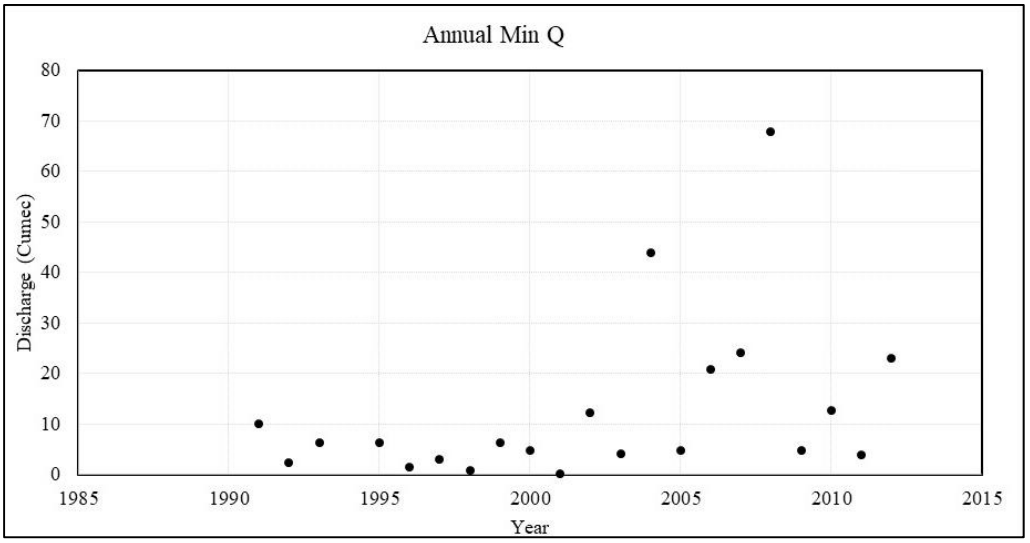

Figure 4.3: Annual Minimum Flow of Teesta River at Dalia point

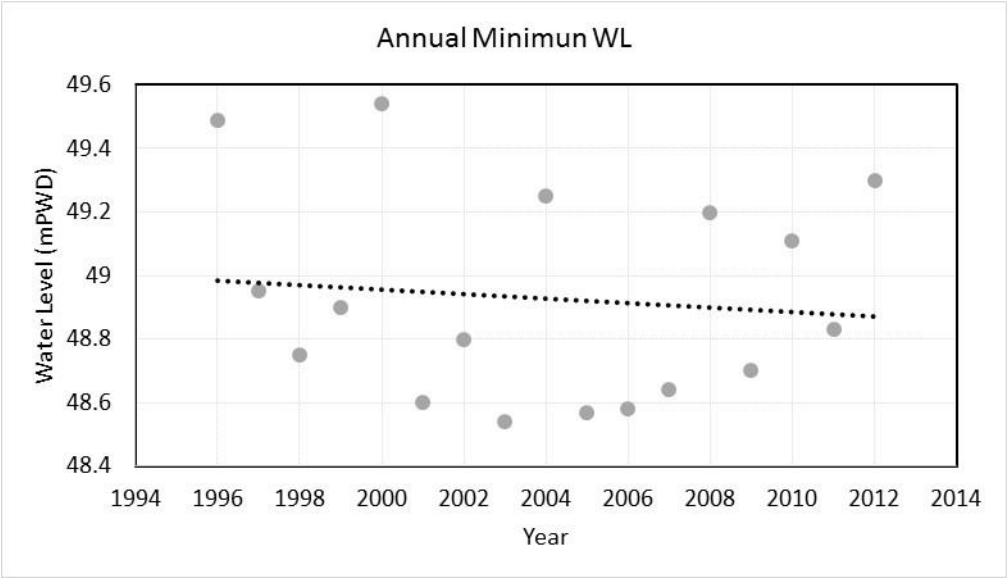

Figure 4.4: Annual Minimum Water Level of Teesta River at Dalia point

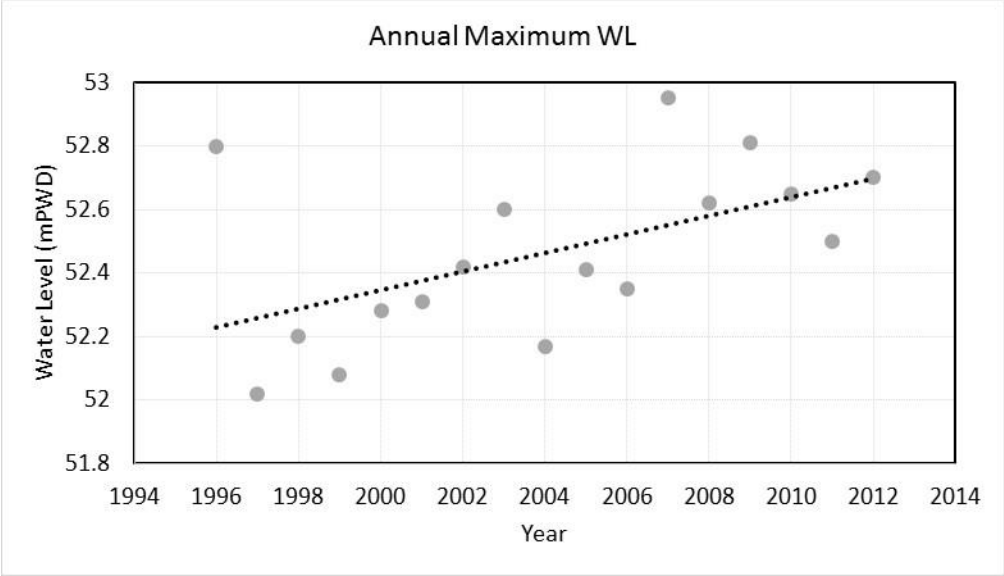

Figure 4.5: Annual Maximum Water Level of Teesta River at Dalia point

The annual minimum water level and annual maximum water level at the Dalia point, upstream of the barrage is shown in **Figure 4.4** and **Figure 4.5**. From the figures, it is clearly visible that the maximum water level at Dalia point is increasing but the minimum water level is decreasing. This means the water availability in the dry season is decreasing in the Teesta River, but the intensity of the flood is increasing in the monsoon. Comparing **Figure 4.5** and **Figure 4.1**, we can see that although the maximum flow of the Teesta River is decreasing, the maximum water level is increasing which indicates siltation of the Teesta River.

Along with that Extreme value analysis of the annual maximum flow data has been carried out. The frequency analysis was carried out for three different distribution methods, Gumbel, Log-Normal and Log-Pearson method. The results of the frequency analysis for 2.33, 5, 10, 25 and 100 year return period are shown in **Table 4.1**. Chi-square test was carried out for all the distributions to find the best fit, the result of which are shown in **Table 4.2**. From the Table it can be seen that Log-Pearson method has fits best with the given.

Table 4.1: Frequency Analysis for annual maximum Flow

Return Period (yr)	Gumbel (Cumec)	Log Normal (Cumec)	Log Pearson (Cumec)
2.33	4570.94	4246.03	4318.87
5	5786.21	5915.01	5937.87
10	6776.04	7033.80	6946.29
25	8026.68	8460.26	8155.44
50	8954.48	9532.19	9013.90
100	9875.43	10609.66	9835.66

Table 4.2: Chi-Square test for different distributions

Chi-Square	Gumbel	Log Normal	Log Pearson
	413.150027	383.5706168	269.8168814

4.2 Analyzing the downscaled GCM Data

The acquired downscaled GCM data has been analyzed at different point of the Teesta Basin to find the wettest, driest, coolest and warmest model scenarios for each of the RCPs. The precipitation data have been analyzed at eighty eight (88) different points and the temperature data have been analyzed at sixty three (63) different points. The analyzing points for Precipitation and temperature are shown in **Figure 4.6** and **Figure 4.7**.

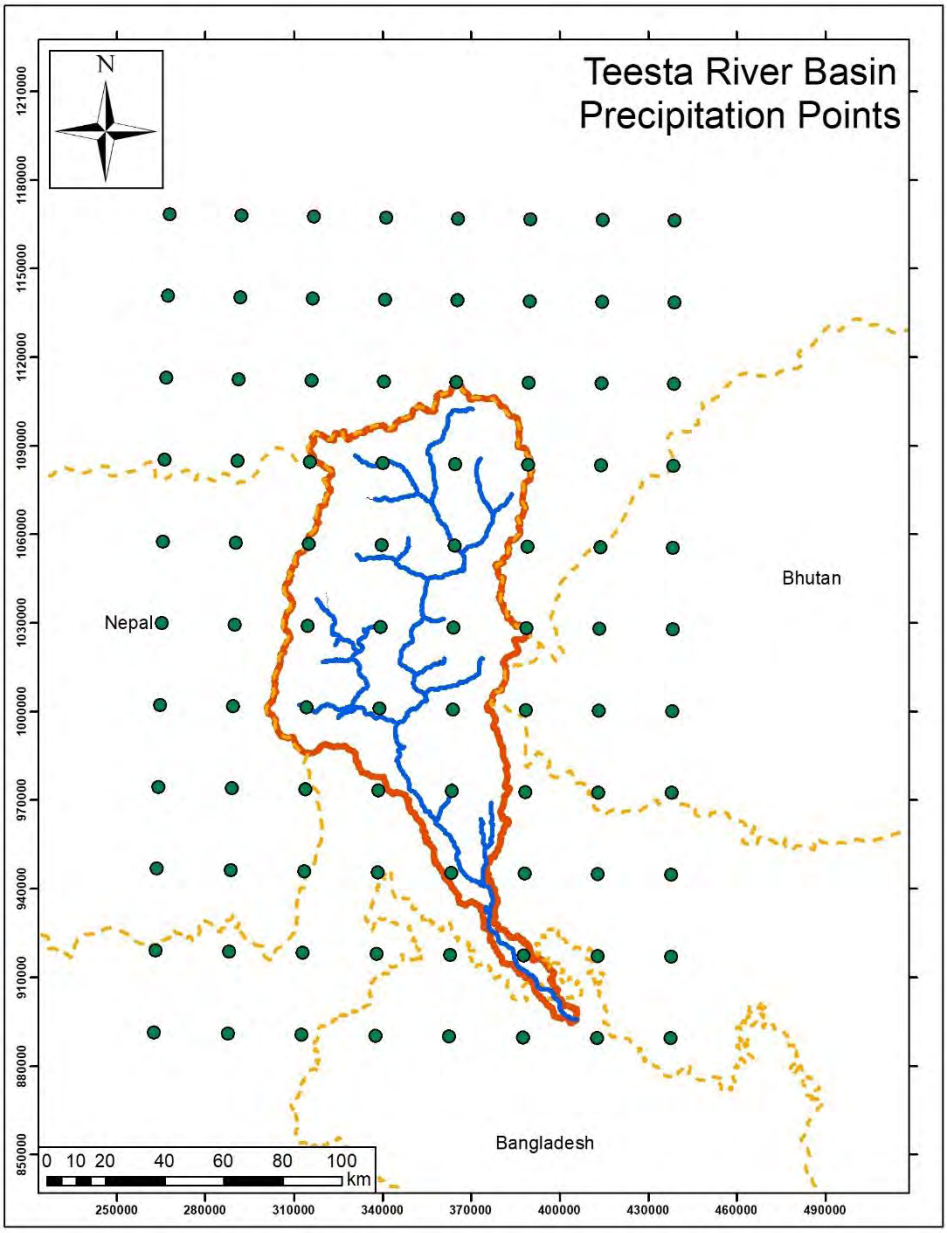

Figure 4.6: Analyzing points for Precipitation

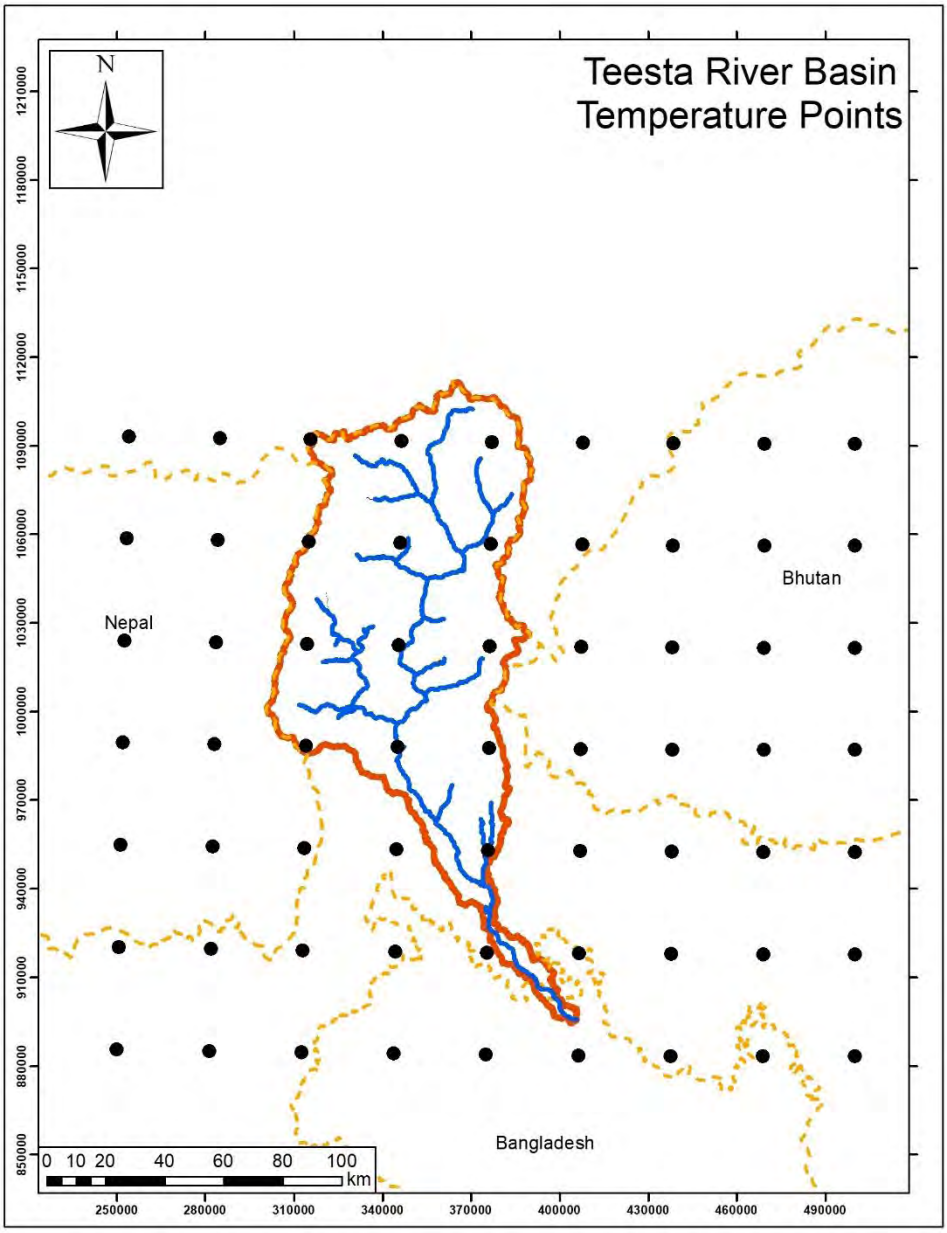

Figure 4.7: Analyzing points for Temperature

4.2.1 RCP 2.6

The changes in precipitation for RCP 2.6 is shown in **Table 4.3.** The result is separated in two periods, 2050s (2040-2069) and 2080s (2070-2099). Monthly mean precipitation data for each model is compared with base period data (1960-1990). Here the change is denoted with ΔP which is the difference between model simulated and base data divided by base data and represented in percent. So,

$$\Delta P = \frac{(P_{rcp} - P_{Base})}{P_{Base}} X\ 100 \qquad (4.1)$$

Table 4.3: Precipitation change (%) for RCP 2.6

Model	2050s	2080s
HAD GEM - 2 ES	-9.10	-1.76
CSIRO MK - 3.6.0	3.57	6.60

From the Table it can be seen that the changes in precipitation varies from 6.60% to -9.10%. The interesting thing of note here is that for the HAD GEM – 2 ES model the precipitation for both the time period has decreased while the precipitation has increased for CSIRO MK 3.6.0 for both the time frame.

The changes in temperature for RCP 2.6 is shown in **Table 4.4**. From the table it can be seen that the maximum temperature for both model increases to about 2.24°C by the end of the century. The minimum temperature increases about 1.50°C for HAD GEM 2ES model by 2050 and 1.57°C by 2080s while it increases nearly 2°C for CSIRO MK 3.6.0 model.

Table 4.4: Temperature increase for RCP 2.6

Model	T_{max}		T_{min}	
	2050s	2080s	2050s	2080s
HAD GEM - 2 ES	2.24	2.24	1.47	1.57
CSIRO MK - 3.6.0	2.14	2.24	1.77	1.97

4.2.2 RCP 4.5

The changes in precipitation for RCP 4.5 is shown in **Table 4.5** while the increase in temperature for RCP 4.5 is shown in **Table 4.6**. It can be seen from the tables that the precipitation increases for both the models due to RCP 4.5. Maximum increase in precipitation occurs in HAD GEM -2 ES in the 2080s while the minimum increase in precipitation also occurs in HAD GEM – 2 ES in the 2050s. As for the temperature as much as 3.54°C increase in maximum temperature may occur by 2080s in the Teesta River basin as predicted HAD GEM 2ES. The same model predicts that the minimum temperature may also increase by 2.87°C by the end of the century.

Table 4.5: Precipitation change (%) for RCP 4.5

Model	2050s	2080s
HAD GEM - 2 ES	1.19	11.71
CSIRO MK - 3.6.0	7.64	5.87

Table 4.6: Temperature increase for RCP 4.5

Model	T_{max}		T_{min}	
	2050s	2080s	2050s	2080s
HAD GEM - 2 ES	2.64	3.54	2.07	2.87
CSIRO MK - 3.6.0	2.44	3.64	1.17	1.37

4.2.3 RCP 6

The changes in precipitation for RCP 6 is shown in **Table 4.7** while the increase in temperature for RCP 6 is shown in **Table 4.8.** It can be seen from the tables that in 2050s, the HAD GEM model predicts that precipitation will decrease by nearly 14% but will continue to increase after that increasing to about 4.55% by the end of the century. The CSIRO model however predicts a much wetter scenario where the precipitation will increase by 2.79% by midcentury and 6.52% by the end of the century. As for the temperature, the maximum temperature is predicted to increase by 3.14°C by both the models in the 2080s while the minimum monthly temperature is predicted to increase by 2.57°C and 2.97°C by the HAD GEM and CSIRO model respectively.

Table 4.7: Precipitation change (%) for RCP 6

Model	2050s	2080s
HAD GEM - 2 ES	-13.64	4.55
CSIRO MK - 3.6.0	2.79	6.52

Table 4.8: Temperature increase for RCP 6

Model	T_{max}		T_{min}	
	2050s	2080s	2050s	2080s
HAD GEM - 2 ES	2.34	3.14	1.67	2.57
CSIRO MK - 3.6.0	1.94	3.14	1.87	2.97

4.2.4 RCP 8.5

The changes in precipitation for RCP 8.5 is shown in **Table 4.9** while the increase in temperature for RCP 8.5 is shown in **Table 4.10.** In RCP 8.5, Precipitation decreases in HAD GEM model for the 2050s compared to the base condition. But sharp increase in precipitation can be seen in both of the GCM for the 2080s. As for the temperature, highest increase in temperature can be seen in this RCP. Maximum temperature increases as much as 5.34°C (HAD GEM 2ES, 2080s) while the minimum temperature increases as much as 4.87°C (CSIRO MK 3.6.0, 2080s) in this RCP condition.

Table 4.9: Precipitation change (%) for RCP 8.5

Model	2050s	2080s
HAD GEM - 2 ES	-1.56	9.39
CSIRO MK - 3.6.0	8.78	11.33

Table 4.10: Temperature increase for RCP 8.5

Model	T_{max}		T_{min}	
	2050s	2080s	2050s	2080s
HAD GEM - 2 ES	3.24	5.34	2.57	4.27
CSIRO MK - 3.6.0	2.94	4.84	2.87	4.87

4.2.5 Selection of Scenarios

From the analyzed downscaled GCM data, **Figure 4.8** has been produced which shows ΔT_{max} vs ΔP Plot for 2080s. From the Figure, it can be seen that maximum temperature increases for HAD GEM ES 2 model for its RCP 8.5 scenario, while the maximum precipitation occurs for HAD GEM ES 2 model for its RCP 4.5 scenario. The HAD GEM ES 2 model for its RCP 2.6 scenario is the only one where the precipitation actually decreases comparing to the base condition. And minimum increase of temperature occurs for CSIRO MK 3.6.0 model for its RCP 2.6 scenario. These four model outputs will serve as the four scenarios for 2080s model. The chosen scenarios are shown in **Table 4.11**.

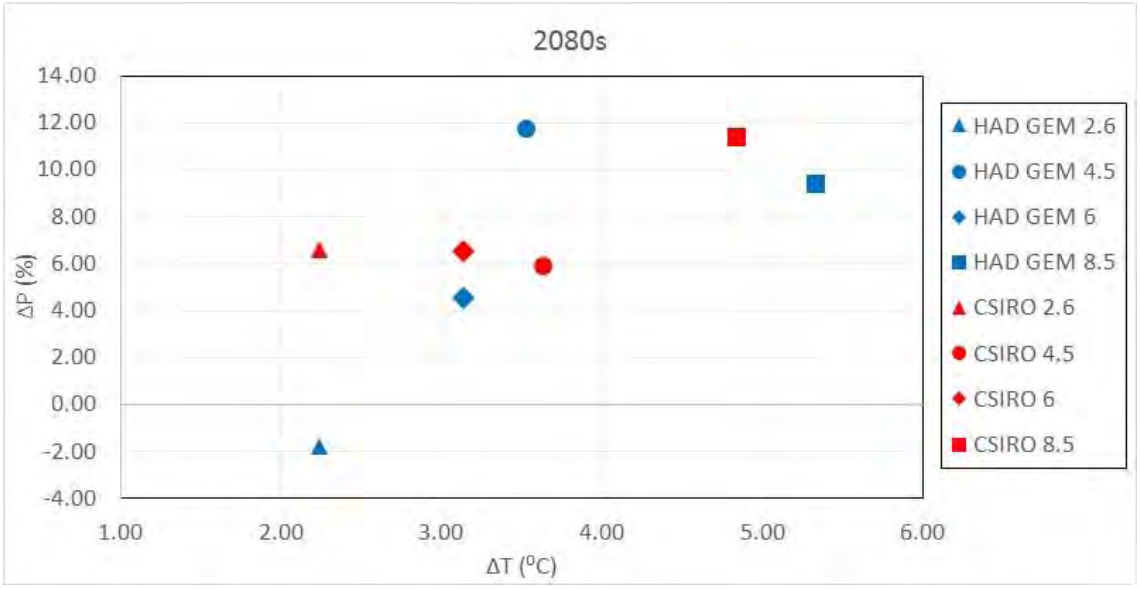

Figure 4.8: ΔT_{max} vs ΔP Plot for the 2080s

Table 4.11: Selected Scenarios

Scenario	Model	RCP	Δ Value
Wettest	HAD GEM 2 ES	4.5	ΔP = 11.71%
Driest	HAD GEM 2 ES	2.6	ΔP = -1.76%
Warmest	HAD GEM 2 ES	8.5	ΔT = 5.34 ^{0} C
Coolest	CSIRO MK 3.6.0	2.6	ΔT = 2.24 ^{0} C

4.3 Water Balance of the Teesta Basin

The hydrological model of the Teesta River basin has been simulated for base condition (1995-2013) as well as four different climate change scenarios as mentioned in **Article 4.2**. The water balance of each of the model analyzed and compared.

4.3.1 Base Model

The water balance of the Teesta Basin for base model condition is shown in **Table 4.12.** It can be seen that July is the wettest month (520.94 mm) and December is the driest month (4.31 mm) in the Teesta Basin. The surface runoff also shows similar pattern to the precipitation data in the monsoon season with highest runoff occurring in the month of July (249.77 mm). However the lowest runoff occurs in the month of January when the runoff drops to 0.58 mm. While the lowest percolation occurs in January (0.27 mm), the groundwater contribution to the stream i.e. base flow is lowest in the month of March when it reduces to 1.17 mm. The similar trend is also present during the peak of the percolation and base flow. The peak percolation occurs during the month of July (127.09 mm) while the peak groundwater contribution to stream occurs couple of months later in September (98.85 mm). The evapotranspiration of the model domain varies from 5 mm (January) to 49.32 mm (July). The water yield of the Teesta basin reaches its maximum in the month of July (410.4 mm) while lowest water yield occurs in the month of February when it falls to 5.95 mm. The water balance of the Teesta River Basin has been presented graphically in **Figure 4.9**, which can better illustrate the temporal changes of each parameter of the water balance.

Table 4.12: Water Balance of the Teesta Basin for Base Condition (1995-2013)

Month	Water Balance Parameter (mm)							
	Rain	Snow	Surface Runoff	Lateral Flow	Base Flow	Perco	ET	Yield
Jan	10.15	4.53	0.58	0.77	6.41	0.27	5	9.87
Feb	16.54	7.5	1.77	1.37	1.29	0.79	7.22	5.95
March	48.05	16.72	8.49	6.73	1.17	5.32	15.73	17.55
April	122.43	18.4	32.71	24.43	4.95	25.70	30.83	62.54
May	189.32	11.26	61.26	42.14	18.46	55.99	45.43	122.16
June	370.82	1.92	157.19	62.85	38.63	96.35	47.87	258.69
July	520.94	0.85	249.77	85.76	72.61	127.09	49.32	410.4
Aug	447.51	0.91	193.69	82.05	96.93	117.49	45.01	375.85
Sep	276.9	2.33	106.24	55	98.85	77.71	36.45	264.9
Oct	107.08	9.33	41.16	19.62	84.13	22.71	24.95	149.63
Nov	10.74	4.91	0.38	1.44	48.29	0.95	11.57	53.43
Dec	4.31	2.11	0.23	0.53	22.81	0.35	6.25	26.31
Sum	2124.79	80.77	853.47	382.69	494.53	530.73	325.63	1757.28

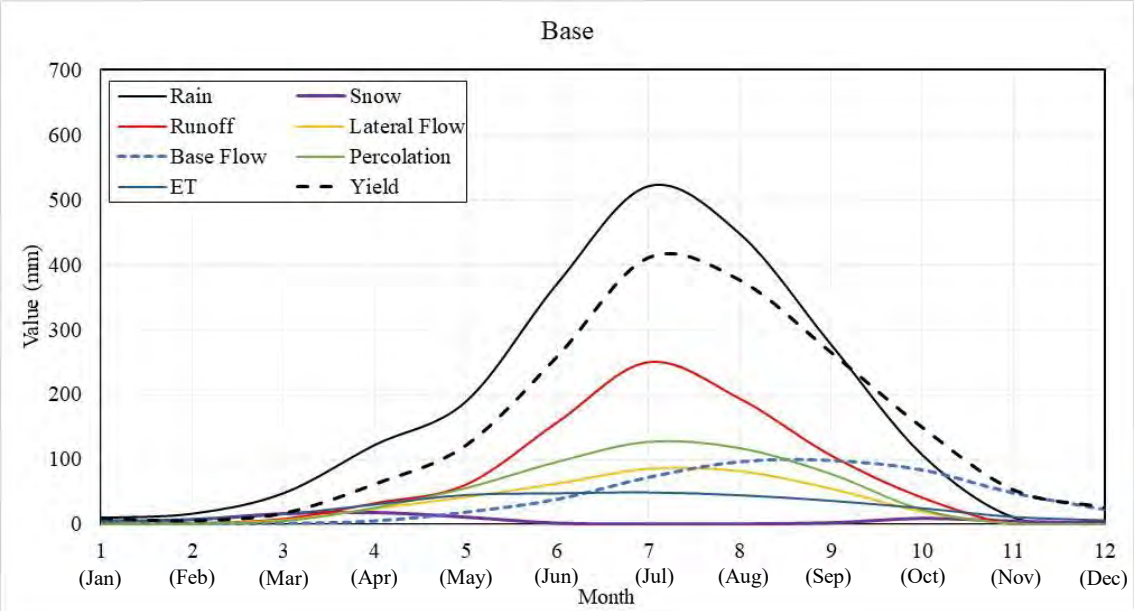

Figure 4.9: Water Balance of the Teesta Basin for Base Condition (1995-2013)

4.3.2 Wettest Scenario

The water balance of the Teesta Basin for the wettest scenario is shown in **Table 4.13**. The wettest scenario for the Teesta River basin was found to be HAD GEM 2ES for its RCP 4.5 scenario. Substantial changes from the base condition can be seen for the wettest scenario in the 2080s. The cumulative value of all the parameters has increased

substantially comparing to the base condition. The driest month in terms of precipitation has shifted from December to January. The least surface runoff (0.99 mm) occurs in the month of February comparing to January for base condition. Similar trend can be see for lateral flow and percolation both of whose minimum value has shifted by one month. But the evapotranspiration, lateral flow and yield minimum as well as the maximum values occurs in the same month as the base condition. The temporal changes of the water balance parameters for the wettest scenario is shown in **Figure 4.10**.

The interesting trend that has emerged from the **Table 4.13**, is that although the total precipitation has increased by more than 15% (16.3%), the rainfall in the lean season (i.e. December to April) has decreased a lot. In the base condition, total rainfall in the lean season is 201.48 mm. But for the wettest scenario, the total rainfall is calculated as 174.67 mm. That means although the annual rainfall has increased by 16%, the lean season has seen a 13% decrease in rainfall, meaning that the monsoon has become more wetter but the dry season has become more drier even in the wettest scenario.

Table 4.13: Water Balance of the Teesta Basin for the Wettest Scenario

Month	Water Balance Parameter (mm)							
	Rain	Snow	Surface Runoff	Lateral Flow	Base Flow	Perco	ET	Yield
Jan	9.66	6.79	1.99	1.18	8.32	2.19	6.4	13.92
Feb	14.07	9.39	0.99	1.23	2.81	1.56	7.93	6.75
March	32.77	15.52	4.62	4.8	2.21	5.56	16.7	12.97
April	98.61	3.11	25.47	19.29	4.67	15.98	34.72	49.94
May	186.56	1.55	62.84	37.63	13.28	46.72	49.56	113.76
June	551.9	0.24	280.84	79.85	35.42	120.03	51.81	395.56
July	603.61	0	307.07	94.98	79.48	136.52	52.62	484.39
Aug	495.44	0.04	222.22	88.93	105.67	122.05	49.78	420.68
Sep	344.44	1.23	148.34	63.59	106.43	88.37	40.08	322.97
Oct	86.67	0.77	35.04	16.93	90.41	17.88	26.79	147.57
Nov	27.3	12.24	3.67	3.02	50.85	4.20	12.08	61.08
Dec	19.56	8.89	4.68	1.93	24.84	2.58	7.19	34.23
Sum	2470.59	59.77	1097.77	413.36	524.39	563.64	355.66	2063.82

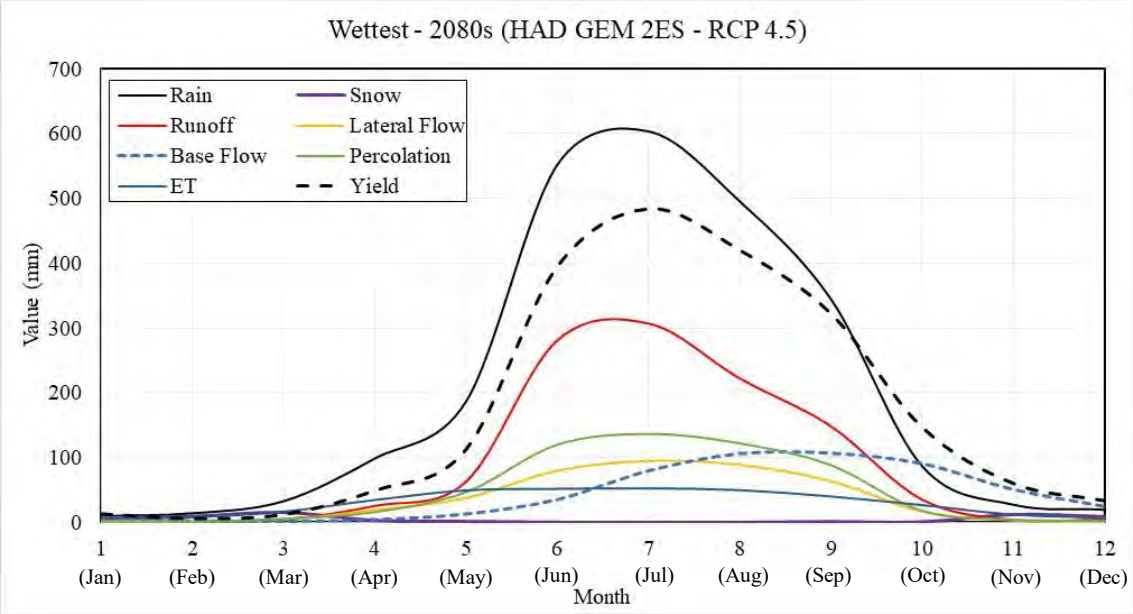

Figure 4.10: Water Balance of the Teesta Basin for Wettest Scenario (2080s)

4.3.3 Driest Scenario

The water balance of the Teesta Basin for the driest scenario is shown in **Table 4.14.** January appears as the driest month from the table with 7.11 mm of rain fall. Highest rainfall is predicted to fall in the month of July (570.90 mm) but the magnitude even for the driest condition is higher than the base condition. The least amount of surface runoff occurs in February (0.55 mm) while the highest occurs in July (281.62 mm). The ground water flow reaches its lowest in March (1.31 mm) and its peak in September (101.26 mm). The temporal changes of the water balance parameters for the wettest scenario is shown in **Figure 4.11.**

Comparing the lean season flow for the driest scenarios, we can see a similar trend but a much more drier lean season. We can see that the annual precipitation even for the driest scenario has increased by 3.5%. However the total precipitation in the lean season is found to be 157.59 mm (in base condition 201.48 mm). That means the precipitation in the lean season decreases by 21.78%. So, for the driest scenario the precipitation in the Teesta Basin is expected to increase in the wet seasons, while decrease substantially for the dry season.

Table 4.14: Water Balance of the Teesta Basin for the Driest Scenario (2080s)

Month	Water Balance Parameter (mm)							
	Rain	Snow	Surface Runoff	Lateral Flow	Base Flow	Perco	ET	Yield
Jan	7.11	4.17	1.01	0.6	6.98	0.63	5.23	10.73
Feb	9.39	6.51	0.55	1	1.76	1.01	6.7	4.89
March	39.62	10.48	6.8	6.03	1.31	4.35	16.37	15.35
April	92.65	3.26	24.22	20.1	4.19	19.01	33.4	48.99
May	159.99	1.43	47.81	33.76	13.49	40.68	47.82	95.37
June	402.64	0.4	179.62	65.37	31.07	98.24	50.3	275.59
July	570.9	0.05	281.62	92.1	69.26	132.54	51.64	445.44
Aug	474.06	0.22	208.17	86.89	97.70	119.67	48.14	395.99
Sep	317.98	1.42	130.16	61.11	101.26	84.19	39.09	296.97
Oct	92.57	2.17	37.38	17.65	86.83	19.21	26.19	146.61
Nov	23.5	14.64	1.9	2.18	49.34	3.43	11.62	56.77
Dec	8.82	5.53	0.69	0.75	23.85	0.82	6.34	28.07
Sum	2199.23	50.28	919.93	387.54	487.03	523.77	342.84	1820.77

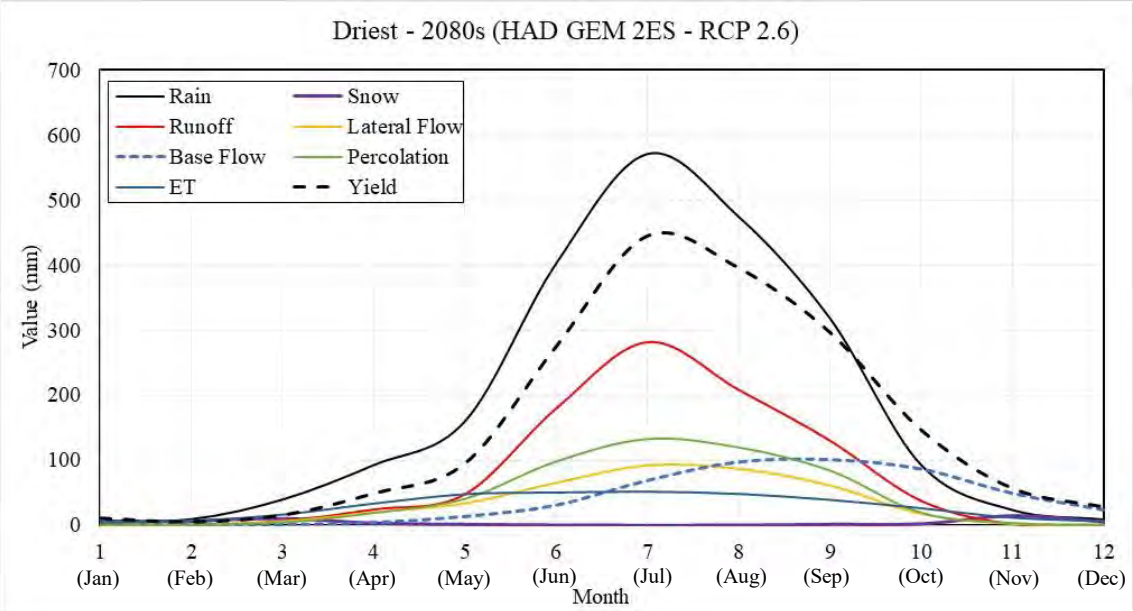

Figure 4.11: Water Balance of the Teesta Basin for Driest Scenario (2080s)

4.3.4 Warmest Scenario

The water balance of the Teesta Basin for the warmest scenario is shown in **Table 4.15**, while the temporal changes of the water balance parameters for the warmest scenario is shown in **Figure 4.12**. It can be seen from the Table that the rain fall has increased by 12% in the warmest scenario comparing to the base condition (i.e. annual rainfall 2379.04 mm comparing to 2124.79 mm). The surface runoff as well as the subsurface flows also

increased in this scenario. But the standout for the driest condition is the Evapotranspiration which is highest among all the scenarios considered in this study. Since evapotranspiration is a function of temperature, this increase is understandable.

The total rainfall in the lean season for the warmest scenario is 194.95 mm, which shows a 3% decrease in lean season precipitation. Hence, the warmest scenario also predicts a wetter monsoon and drier lean season.

Table 4.15: Water Balance of the Teesta Basin for the Warmest Scenario (2080s)

Month	Water Balance Parameter (mm)							
	Rain	Snow	Surface Runoff	Lateral Flow	Base Flow	Perco	ET	Yield
Jan	12.01	7.71	1.72	1.42	9.35	2.22	7.29	14.88
Feb	33.99	19.26	5.71	2.65	3.69	4.06	9.92	13.74
March	33.24	17.23	6.19	5.06	3.80	7.77	18.55	16.43
April	93.46	8.45	20.88	17.28	6.36	16.67	35.72	45.24
May	199.95	2.21	69.76	39.24	14.44	48.75	51.83	123.02
June	465.59	0.01	221.32	71.95	35.03	107.80	53.35	328.18
July	566.05	0	280.43	90.75	74.56	129.18	55.78	448.64
Aug	499.85	0	227.37	87.93	99.99	121.19	51.84	418.46
Sep	326.83	0.39	135.76	61.98	102.52	84.31	41.52	305.26
Oct	83.74	0.23	34.11	16.09	87.12	17.03	27.89	142.15
Nov	42.08	13.74	9.06	5.31	49.22	7.25	13.06	67.01
Dec	22.25	9.57	6.94	2.97	25.11	4.17	8.02	37.73
Sum	2379.04	78.80	1019.25	402.63	511.20	550.39	374.77	1960.74

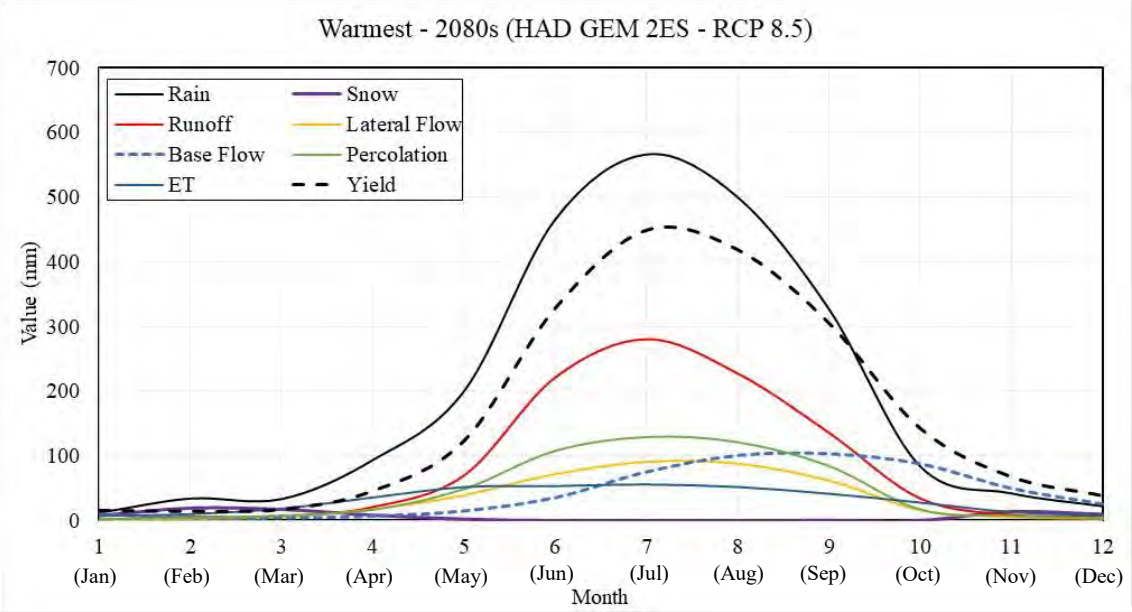

Figure 4.12: Water Balance of the Teesta Basin for Warmest Scenario (2080s)

4.3.5 Coolest Scenario

The water balance of the Teesta Basin for the coolest scenario is shown in **Table 4.16**, while the temporal changes of the water balance parameters for the coolest scenario is shown in **Figure 4.13.** The evapotranspiration for this scenario is found to be 353.03 mm which is higher than base condition but substantially lower than the warmest scenario. The precipitation in the month of December, January and February is 29.4 mm, which is 5% lower than the base condition precipitation of these three months. However the annual precipitation sees an increase of 13%. So, the coolest scenario also experiences a drier lean season and wetter monsoon season.

Table 4.16: Water Balance of the Teesta Basin for the Coolest Scenario (2080s)

Month	Water Balance Parameter (mm)							
	Rain	Snow	Surface Runoff	Lateral Flow	Base Flow	Perco	ET	Yield
Jan	6.23	3.17	0.81	0.74	8.73	0.79	5.82	12.66
Feb	13.07	5.29	1.86	1.83	2.22	1.70	7.74	7.64
March	59.06	20.33	10.86	7.9	1.93	6.59	17.65	21.95
April	132.54	15.44	38.78	27.53	6.51	30.26	33.64	73.4
May	197.16	4.69	64.6	42.52	20.63	54.46	49.87	128.21
June	373.97	0.15	161.72	62.35	38.70	92.16	51.81	262.95
July	549.01	0.04	268.96	88.91	71.42	128.31	52.79	431.58
Aug	545.11	0.1	256.97	93.32	98.30	130.03	48.84	451.73
Sep	347.3	1.88	149.22	64.81	105.00	89.70	38.72	323.91
Oct	159.22	11.7	71	26.15	93.02	30.92	26.87	195.22
Nov	18.23	7.35	1.37	3.15	55.89	3.08	12.49	64.03
Dec	10.1	4.61	1.24	1.07	27.69	1.07	6.79	32.98
Sum	2411.00	74.75	1027.39	420.28	530.04	569.07	353.03	2006.26

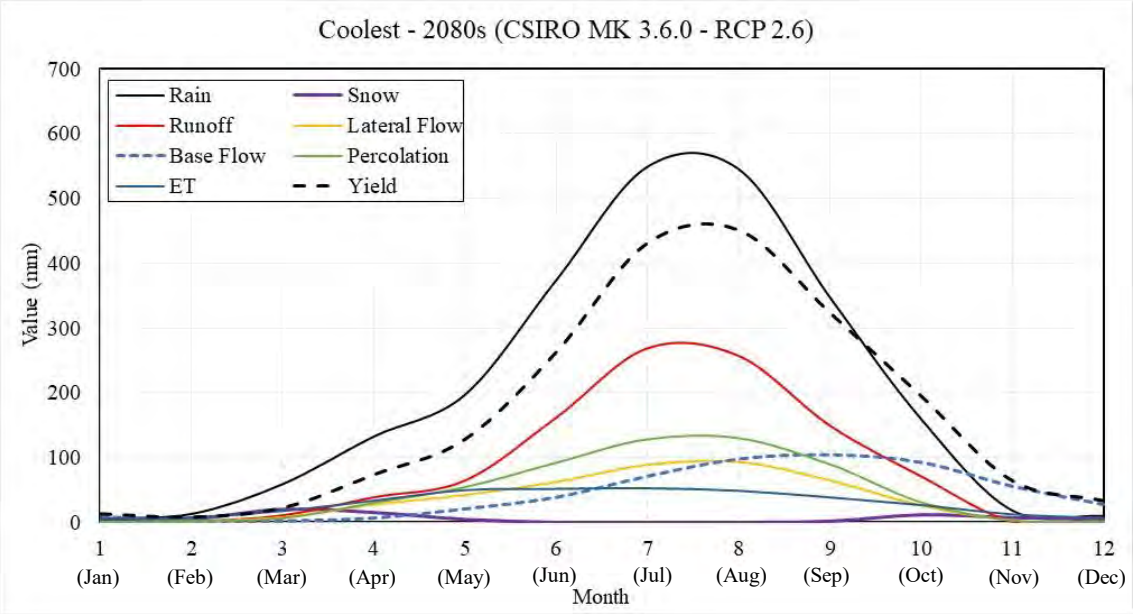

Figure 4.13: Water Balance of the Teesta Basin for Coolest Scenario (2080s)

4.3.6 Scenario Comparison

Figure 4.14 shows changes in precipitation with respect to base condition for different climate change scenarios. All the graphs generally shows similar kind of trend, decreasing rainfall in the dry season and increasing rainfall for the monsoon season. For the wettest scenario, the precipitation increases by 48% in the month of June comparing to the base condition but still predicts 30% less precipitation for the month of March. The driest scenarios predicts a 43% decrease of rainfall in February but still predicts 14% higher precipitation in the month of September. The similar trend can be more or less observed for the Warmest and Coolest scenarios. So analyzing the changes of precipitation due to climate change scenarios, it can be said that, the lean season will get more drier and the monsoon season will get more wetter due to climate change.

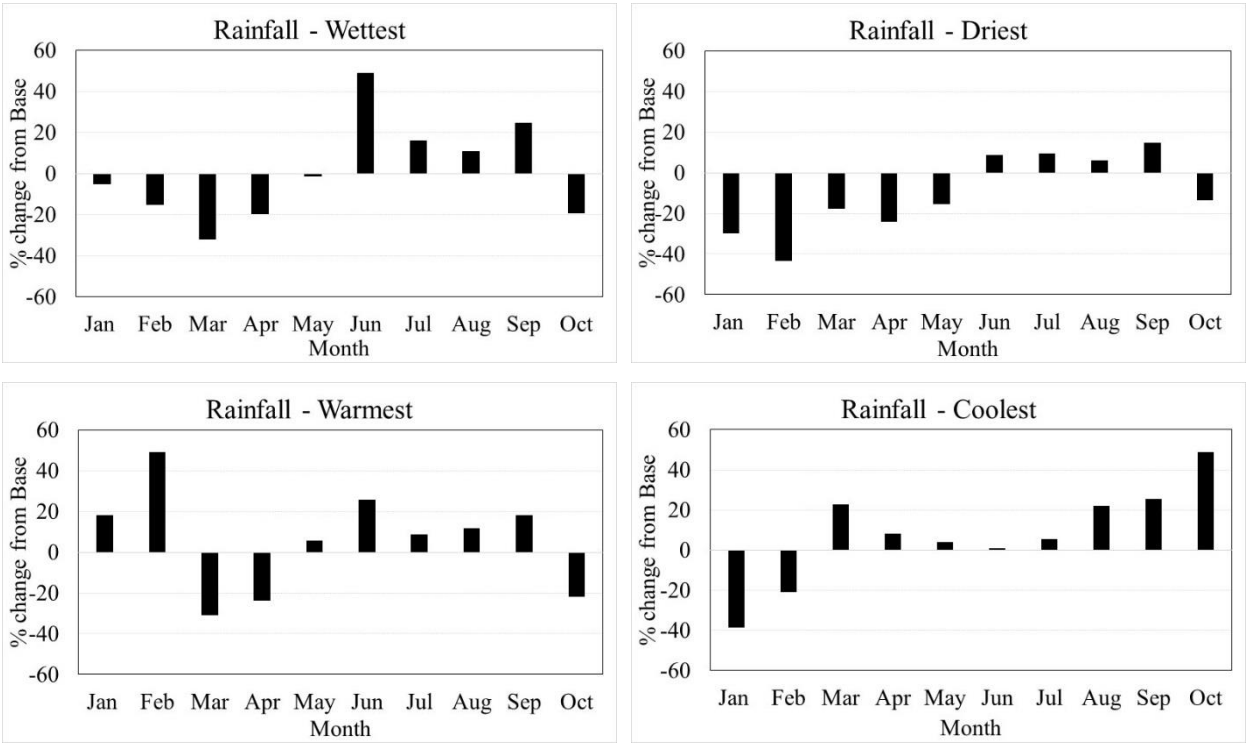

Figure 4.14: % Changes in Rainfall for different Climate Change Scenarios

The changes in Surface runoff has also been prepared for different climate change conditions which is shown in **Figure 4.15**. Except the coolest scenario, where the surface runoff has increase all throughout the year, the general trend for the changes in surface runoff, is that is has increased in the monsoon season and decreased in the lean season. It can be seen that the surface runoff has decreased by 70% for the driest condition in the month of February. Even for that dry lean season, the monsoon flows may increase by as much as 15% creating a more unbalanced condition in the future. As for the wettest scenario, in which the surface runoff increases by nearly 80% in the month of July while the lean season sees as much as 45% decrease in surface runoff in the month of February and March. So, from the analyzed surface runoff data it can be said that lesser water would be available in the dry season due to the effect of climate change.

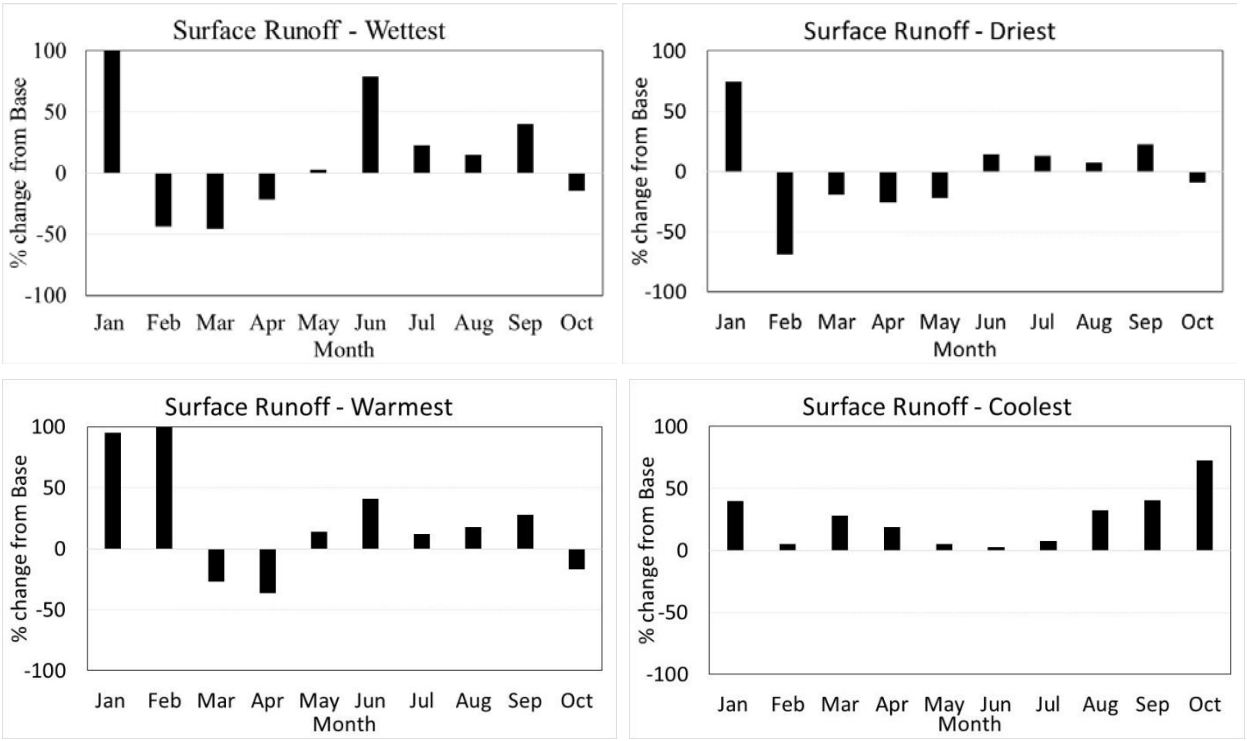

Figure 4.15: % Changes in Surface Runoff for different Climate Change Scenarios

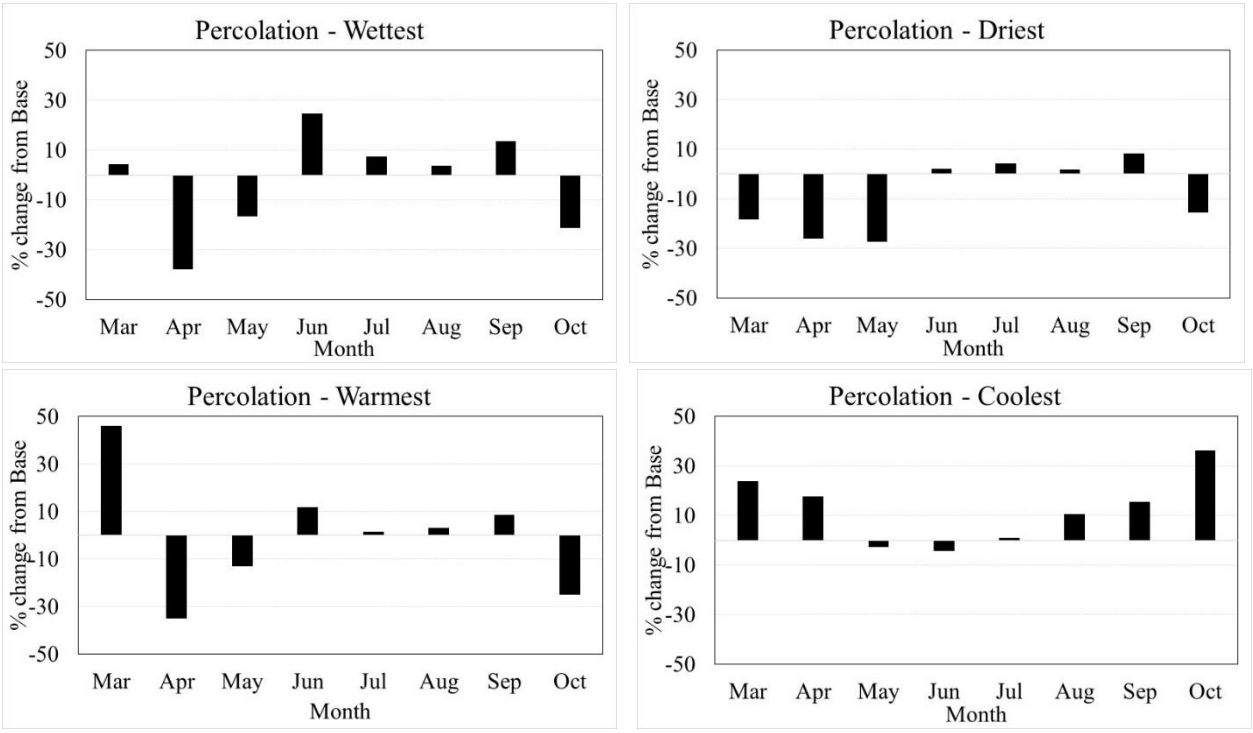

Figure 4.16: % Changes in Percolation for different Climate Change Scenarios

The similar plots have been prepared for percolation as well which is shown in **Figure 4.16**. Omitting the graph of the coolest scenario, all the scenarios show a general trend, the percolation drops drastically in the lean season. While for the driest and the warmest scenario, the percolation sees only a marginal increase in the monsoon months. The

coolest climate change scenario shows a complete different trend for percolation comparing to the other scenarios. It shows an increase in percolation in the dry season while the rate of percolation drops slightly in the peak monsoon season, increasing again in the post monsoon season.

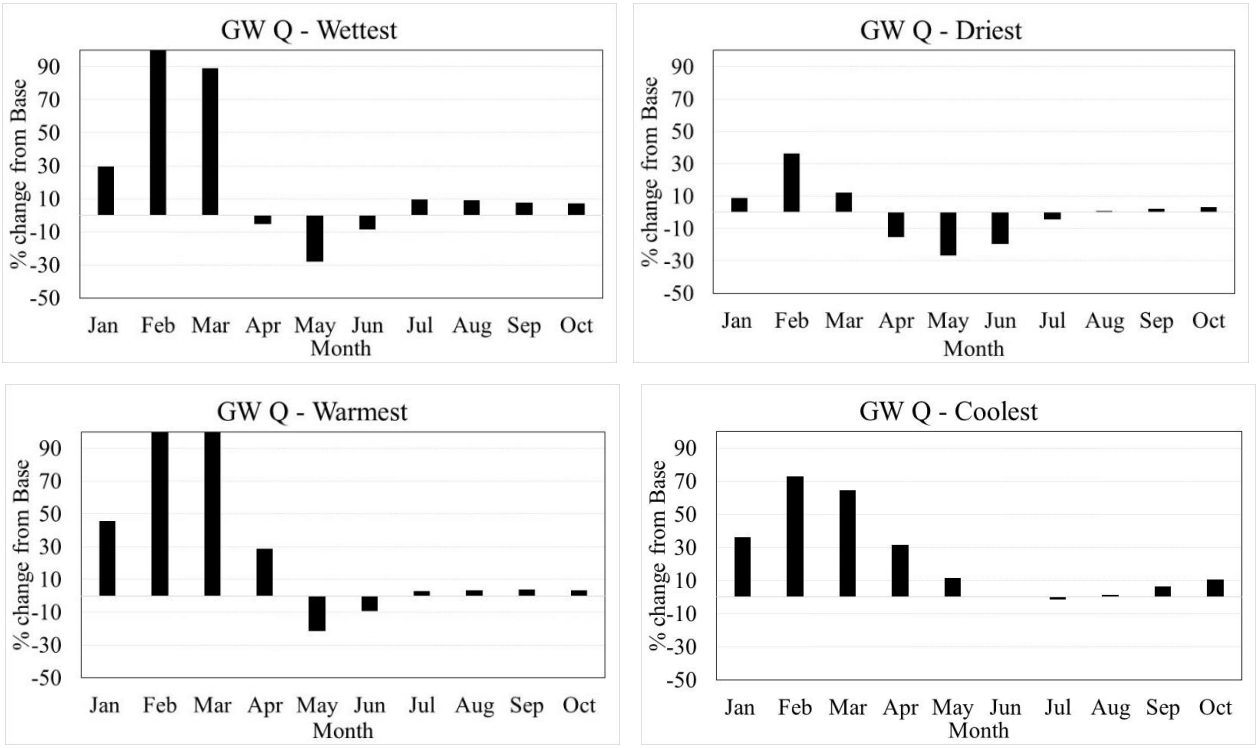

Figure 4.17: % Changes in Ground Water Flow for different Climate Change Scenarios

Figure 4.17 shows changes in ground water flow in to the stream (Base Flow) with respect to base condition for different climate change scenarios. A distinct pattern can be seen from the figure. The base flow has increased substantially in the dry season for all the scenarios. Nearly 200% increase in base flow can be seen in the Figure for the warmest scenario while 40% increase in base flow occurs in the driest scenario in the dry season. This peak in base flow in the months of February and March is followed by a sharp decline in the month of April, May and June before reaching a steady state from July onwards. The base flow for the climate change scenarios starts to increase again after the month October. This sharp increase followed by a sharp decline in base flow in the dry season indicated that there is a water scarcity in those months and base flow increase tries to compensate for the lack of surface runoff.

The changes in Evapotranspiration has also been prepared for different climate change conditions which is shown in **Figure 4.18**. It can be seen from the Figure that the overall

evapotranspiration has increased for the Teesta river basin due to Climate Change scenarios. The highest increase in evapotranspiration occurs in the warmest scenario which is due to the highest increase in temperature in this scenario. The evapotranspiration has increased by nearly 50% in the month of January but overall shows increase of about 15% for the warmest scenario. However the lowest increase in evapotranspiration occurs during the driest scenario which can be explained as the lack of water supply into the system. The evapotranspiration has increased by around 8% from the base condition even during the coolest scenario.

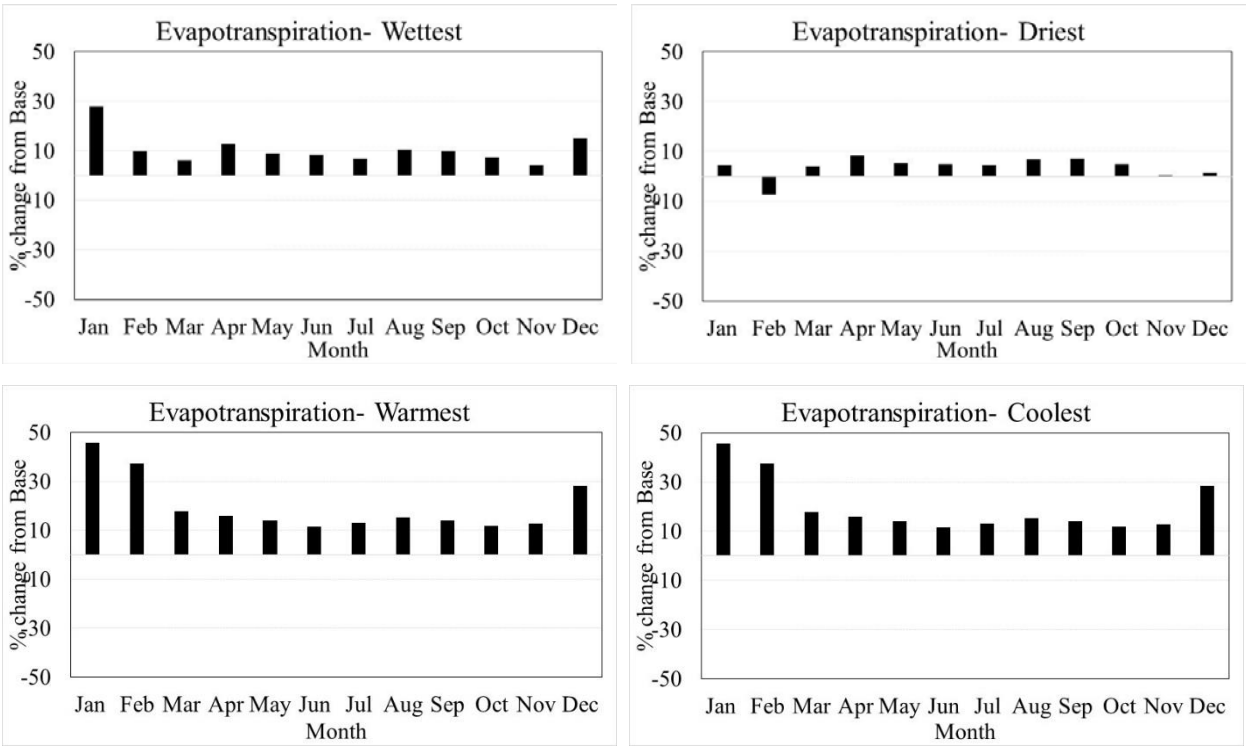

Figure 4.18: % Changes in Evapotranspiration for different Climate Change Scenarios

Figure 4.19 has been prepared to show the changes in water yield due to Climate change scenarios. Only the coolest scenario shows a continuous increase in water yield all throughout the year. The other scenarios shows a decrease in water yield in the dry season and an increase in water yield in the monsoon. The highest increase of water yield in the monsoon can be observed in the wettest scenario when the water yield increases by 52%. That means huge increase of water volume into the system during the monsoon which may cause flooding. However in the dry seasons, around a 25% percent decrease in water yield can be observed for wettest, driest as well as warmest scenarios. For the driest scenario, the water yield for February, March, April and May are considerably lower than the base condition. This implies that water scarcity may be observed during these months.

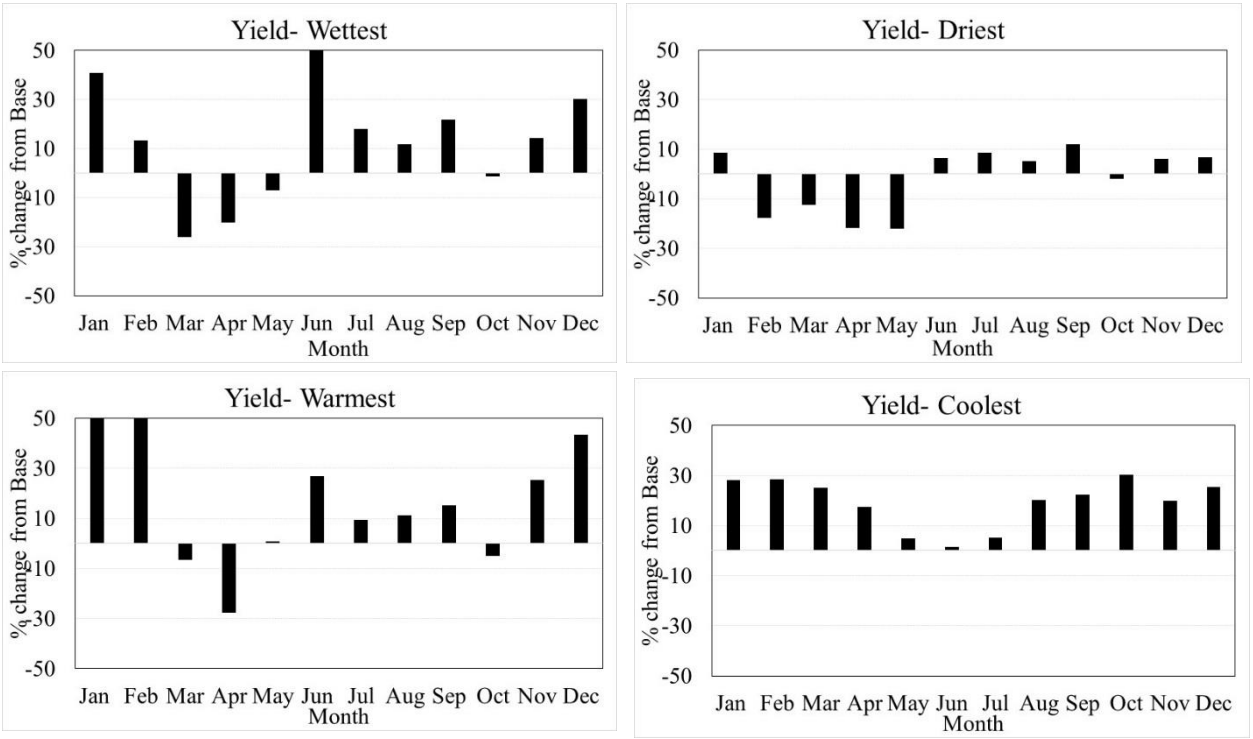

Figure 4.19: % Changes in Water Yield for different Climate Change Scenarios

4.4 Flow at Dalia Point, upstream of Teesta Barrage

The flow at Dalia Point due to different Climate Change scenarios is shown in **Table 4.17**. The data set has been presented graphically in **Figure 4.20**. From the figure it can be seen that the flow at Dalia point will increase in the monsoon season for all the scenarios. For the wettest scenario, the mean monthly flow in the month of June increases by more than 50%. The peak flow also increases by 18%. But the wettest scenario also sees more than 20% reduction in flow in the month of March and April. The lowest lean season flow occurs in the driest scenario where the lean season mean monthly flow drops to 20 cumec. The driest scenario sees 15% reduction in flow in February, 13% in March and close to 25% in the months of April and May. Hence in the driest scenario the water availability during the lean season will substantially decrease. The warmest scenario more or less follows the same pattern as the wettest and the driest scenarios, reduction in flow during the lean season while the flow increases in the monsoon. The hardest hit is the month of April in the warmest scenario when the mean monthly discharge decreases by more than 25%. The coolest scenario shows a different kind of trend comparing to the other scenarios. The flow at Dalia point shows an increasing trend throughout the year for the coolest scenario.

But from the general trend, it can be said that due to climate change the Dalia point will experience a more severe shortage of water during the lean season even without the future upstream control structures. Percent Change in Mean Monthly Flow at Dalia due to different Climate Change Scenarios is shown in **Figure 4.21**.

Table 4.17: Mean Monthly Flow at Dalia due to different Climate Change Scenarios

Month	Base	Coolest	Warmest	Wettest	Driest
Jan	37.51	49.03	58.96	54.72	41.62
Feb	24.17	32.11	60.91	29.42	20.61
Mar	66.66	84.07	67.33	51.96	58.47
Apr	250.60	295.86	185.62	198.64	194.40
May	475.98	497.96	475.61	436.01	364.97
Jun	1025.22	1037.11	1302.46	1582.08	1086.55
Jul	1575.40	1652.13	1720.20	1862.40	1712.20
Aug	1442.69	1742.40	1606.67	1620.27	1522.13
Sep	1046.33	1287.01	1211.61	1281.18	1177.17
Oct	571.31	752.28	540.12	561.86	558.22
Nov	210.45	254.96	271.47	244.05	226.15
Dec	100.40	126.97	146.35	131.77	108.07

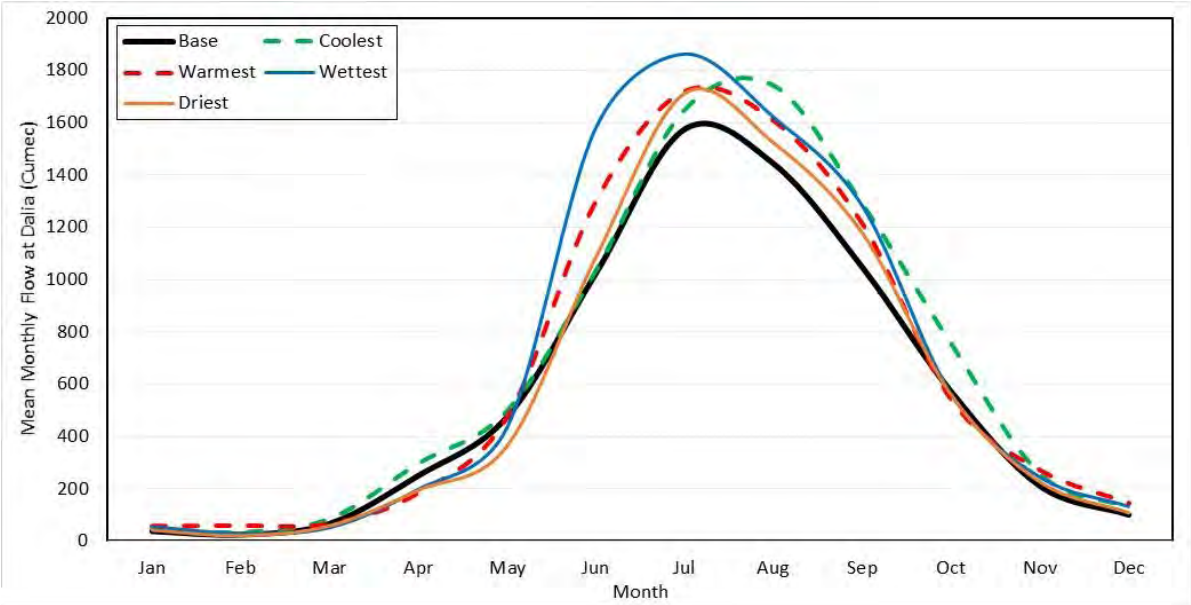

Figure 4.20: Mean Monthly Flow at Dalia due to different Climate Change Scenarios

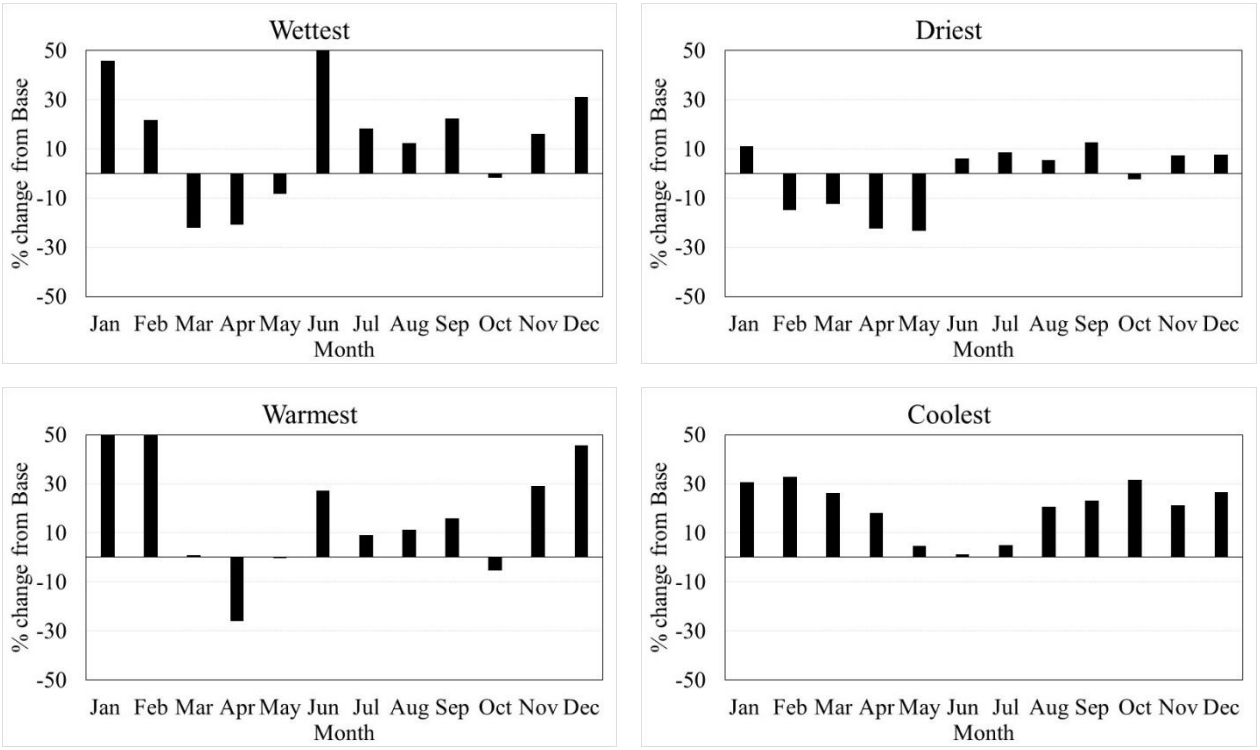

Figure 4.21: % Change in Mean Monthly Flow at Dalia due to different Climate Change Scenarios

4.5 Flow Diversion Scenarios

As mentioned above in Article 3.4, three different structures have been considered to simulate different upstream developments in the Teesta River basin. The detail result of those scenarios are discussed below:

4.5.1 Diversion at Gozoldoba

The model has been simulated for six different flow diversion scenarios each considering a portion of upstream flow diverted through Gozoldoba side canal to simulate the changes in water availability for the Bangladesh portion of Teesta River due to upstream developments. The changes in Mean Monthly flow at Dalia point for different flow diversion scenarios is show in **Table 4.18**.

Table 4.18: Mean Monthly flow of the Teesta River at Dalia due to different flow diversion scenarios

Month	Mean Monthly Flow at Dalia (Cumec)							Remarks
	Base (1995-2013)	% flow diversion through Gozoldoba						
		10%	20%	30%	40%	50%	60%	
Jan	37.51	34.06	30.65	27.22	23.80	20.61	17.96	Diversion
Feb	24.17	21.65	19.47	17.53	15.72	14.10	12.75	
Mar	66.66	60.22	54.97	50.66	47.02	43.94	41.38	
Apr	250.60	224.84	202.33	182.79	165.88	151.43	138.80	
May	475.98	476.01	476.03	476.02	476.00	476.03	476.02	No Diversion
Jun	1025.22	1025.22	1025.22	1025.22	1025.22	1025.22	1025.22	
Jul	1575.40	1575.40	1575.40	1575.40	1575.40	1575.40	1575.40	
Aug	1442.69	1442.69	1442.69	1442.69	1442.69	1442.69	1442.69	
Sep	1046.33	1046.33	1046.33	1046.33	1046.33	1046.33	1046.33	
Oct	571.31	518.16	464.91	411.88	362.65	321.35	287.59	Diversion
Nov	210.45	191.34	172.29	153.20	134.00	114.79	95.72	
Dec	100.40	91.32	82.19	73.07	64.01	55.01	46.42	

It can be seen from **Table 4.18** that with increasing rate of diversion the mean monthly flow at Dalia point decreases. And since the flow diversion activates only during Lean Season (October – April) the monsoon flow for all the diversion scenarios remains same. The mean flow decreases at its lowest in the month of February and with 60% flow diversion the mean flow reduces to 12.75 cumec for 60% diversion. The situation no very bright in the month of January as well where for 60% flow diversion the mean monthly discharge decreases to 17.96 cumec only. This amount of water diversion is bound to make a serious impact on the Teesta river basin on the Bangladesh side. The lowest water availability is present during the month of January, February and March. The mean monthly discharge of these months is plotted in **Figure 4.22**. The temporal variation of the lean season flow can be visually observed in the figure of different diversion scenarios.

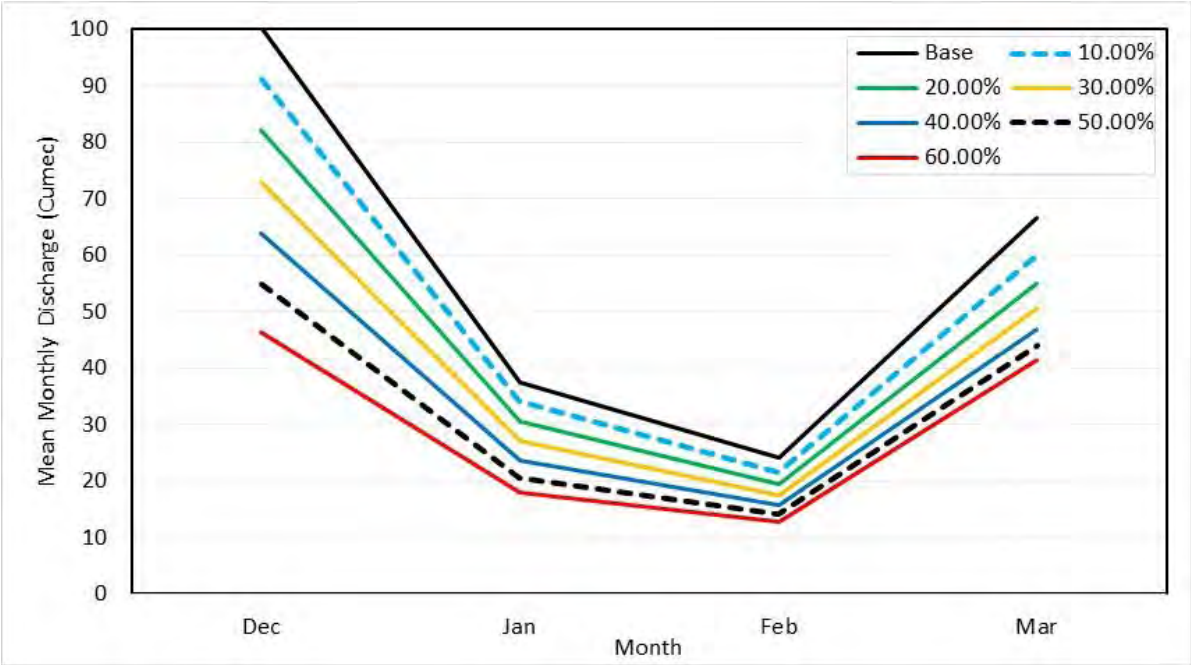

Figure 4.22: Lean Season Flow at Dalia point for different flow diversion scenarios

The reduction of discharge at Dalia point due to different flow diversion scenarios is presented in percent reduction compared to the base condition in **Table 4.19.** From the Table it can be seen that only during 10% flow diversion, the flow at Dalia reduces by 10%, in the other scenarios the flow decreases lesser than the amount diverted through Gozoldoba. The significance of baseflow can be understood from this data. In the lean period, the highest amount of reduction compared to base flow occurs during the month of January when for 60% flow diversion which amounts to 52.12% in flow reduction. The maximum reduction of flow at Dalia point due to different flow diversion scenarios is shown in **Table 4.20**.

Table 4.19: Percent reduction of flow at Dalia due to different flow diversion scenario at Gozoldoba

Month	% reduction of flow at Dalia compared to Base						Remarks
	10%	20%	30%	40%	50%	60%	
Jan	-9.19	-18.29	-27.43	-36.55	-45.06	-52.12	Flow Diversion
Feb	-10.44	-19.46	-27.48	-34.97	-41.67	-47.25	
Mar	-9.67	-17.54	-24.00	-29.47	-34.08	-37.93	
Apr	-10.28	-19.26	-27.06	-33.81	-39.57	-44.61	
May	0.01	0.01	0.01	0.00	0.01	0.01	No Diversion
Jun	0.00	0.00	0.00	0.00	0.00	0.00	

Month	% reduction of flow at Dalia compared to Base						Remarks
	10%	20%	30%	40%	50%	60%	
Jul	0.00	0.00	0.00	0.00	0.00	0.00	
Aug	0.00	0.00	0.00	0.00	0.00	0.00	
Sep	0.00	0.00	0.00	0.00	0.00	0.00	
Oct	-9.30	-18.62	-27.91	-36.52	-43.75	-49.66	Flow Diversion
Nov	-9.08	-18.14	-27.20	-36.33	-45.46	-54.52	
Dec	-9.04	-18.14	-27.22	-36.25	-45.21	-53.76	

Table 4.20: Maximum Percent reduction of flow at Dalia due to different flow diversion scenario.

% Flow Diversion through Gozoldoba	Max Reduction in Flow at Dalia (%)
10	-10.44
20	-19.46
30	-27.91
40	-36.55
50	-45.46
60	-54.52

From **Table 4.20**, Simple linear Regression Analysis was carried out to find the % reduction of flow at Dalia point. The following equation has been derived from the regression analysis,

$$Q_d = -(0.0004 \times Q_g^2 + 0.8518 \times Q_g + 2.026) \quad (4.2)$$

Here, Q_d is the maximum percent flow reduction at Dalia and Q_g is the percent flow diversion at Gozoldoba. For example, if all the water at Gozoldoba were to be diverted, $Q_g = 100$, and from equation 5.1, $Q_d = -91.21\%$. So, up to 91.21% flow reduction from base condition may occur at the Dalia point due to 100% flow diversion through Gozoldoba. The flow reduction at Dalia due to different flow extraction scenarios at Gozoldoba has been presented graphically in **Figure 4.23**.

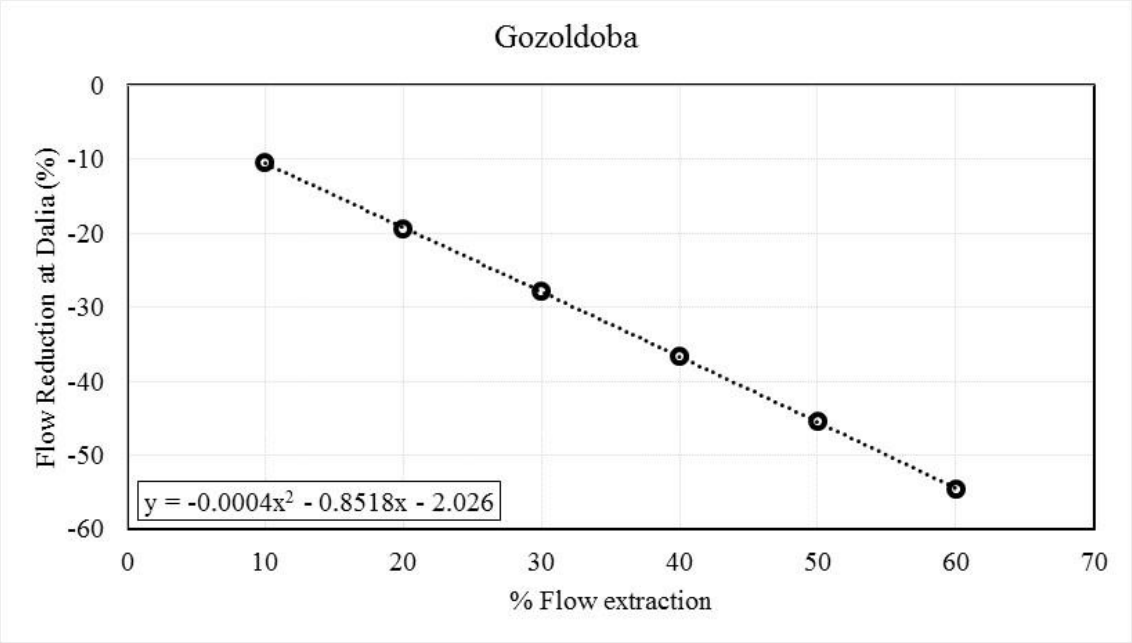

Figure 4.23: Flow reduction at Dalia due to different flow extraction scenarios at Gozoldoba

4.5.2 Storage at Teesta III

Being a hydroelectric project, the Teesta III was simulated by extracting different portion of flow from main channel during the monsoon which was kept as storage and releasing the stored amount during the lean season. The mean monthly flow at the Teesta III structure location for base and 15% flow storage is shown in **Figure 4.24.** It can be seen from the figure that due to the hydroelectric structure, the flow has decreased during the monsoon and increased during the dry season.

The reduction of discharge at Dalia point due to different flow storage scenarios is presented in percent reduction compared to the base condition in **Table 4.21**. The hydrograph comparison for Base and 15% storage at Dalia point is shown in **Figure 4.25**. Unlike the previous diversion scenario, the discharge during the lean season has increased due the presence of the Teesta III hydroelectric power plant. The flow may increase as much as 29% for 5% of flow storage during monsoon. The storage reduces the amount of discharge during monsoon. For 30% of flow extraction during monsoon, reduces the flow by nearly 7% at Dalia point. The maximum amount of flow reduction due to different flow storage scenarios at Teesta III is shown in **Table 4.22**.

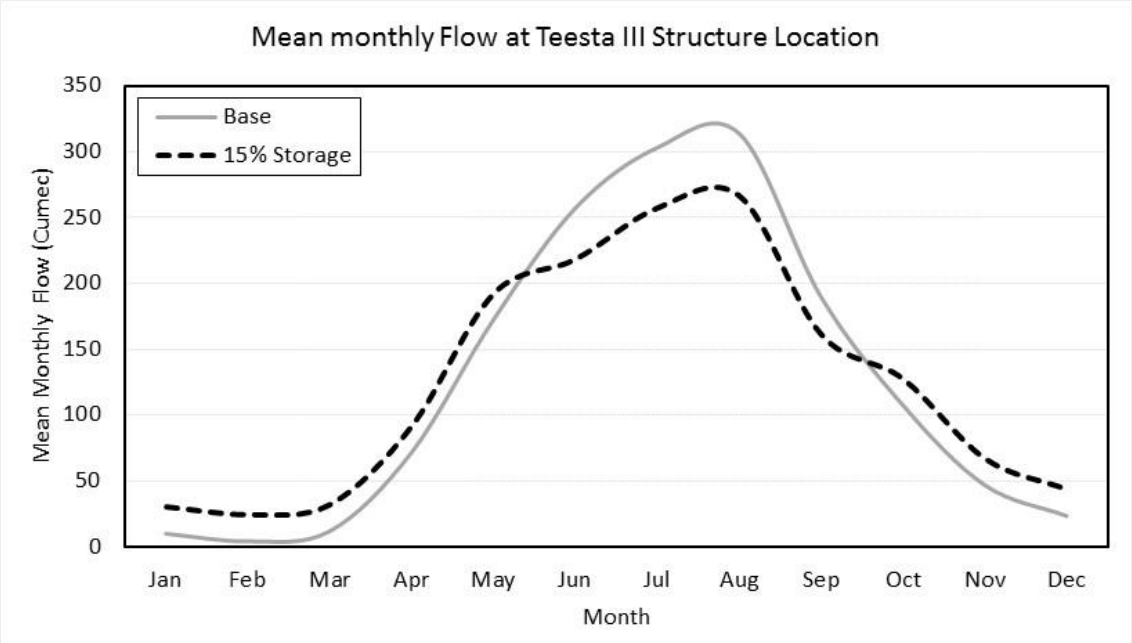

Figure 4.24: Mean Monthly flow at Teesta III Structure location with base and 15% storage scenario

Table 4.21: Percent reduction of flow at Dalia due to different flow storage scenario at Teesta III

Month	% reduction of flow at Dalia compared to Base						Remarks
	5%	10%	15%	20%	25%	30%	
Jan	17.37	34.79	52.28	69.76	87.19	104.60	Flow Release
Feb	28.77	57.57	86.33	115.13	144.00	172.82	
Mar	10.83	21.66	32.45	43.23	53.98	64.78	
Apr	2.87	5.74	8.61	11.48	14.35	17.22	
May	1.51	3.02	4.54	6.04	7.56	9.07	
Jun	-1.18	-2.36	-3.52	-4.75	-5.86	-6.98	Storage
Jul	-1.11	-2.23	-3.35	-4.45	-5.55	-6.56	
Aug	-1.12	-2.27	-3.41	-4.53	-5.69	-6.83	
Sep	-1.05	-2.10	-3.14	-4.19	-5.23	-6.27	
Oct	1.25	2.49	3.74	4.98	6.24	7.48	Flow Release
Nov	3.32	6.62	9.92	13.23	16.53	19.84	
Dec	6.77	13.54	20.32	27.09	33.89	40.68	

Table 4.22: Maximum Percent reduction of flow at Dalia during monsoon due to different flow storage scenario.

% Flow storage during monsoon at Teesta III	Max Reduction in Flow at Dalia (%)
05	-1.18
10	-2.36
15	-3.52
20	-4.75
25	-5.86
30	-6.98

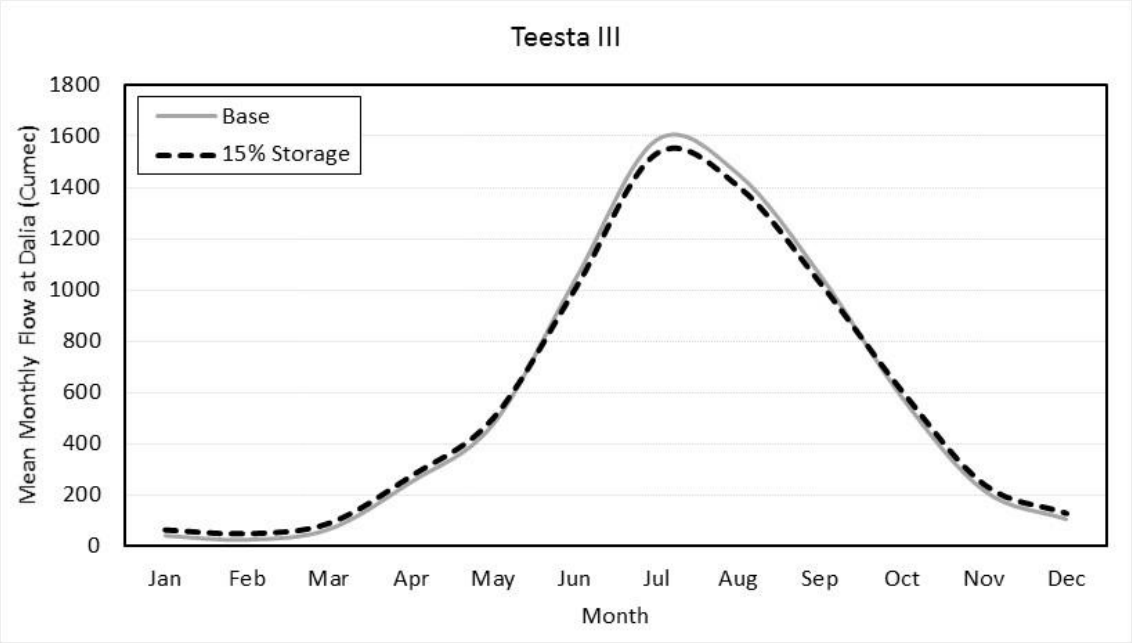

Figure 4.25: Comparison of mean monthly flow at Dalia point between base and 15% storage scenario

Based on the data of **Table 4.22**, a simple regression analysis was carried out to find the maximum % reduction of flow at Dalia point during monsoon due to the effect of Teesta III structure. The following equation was developed from the regression analysis:

$$Q_d = 0.0003 \times Q_t^2 - 0.2448 \times Q_t + 0.0434 \quad (4.3)$$

Here, Q_d is the maximum percent flow reduction at Dalia and Q_t is the percent flow extraction at Teesta III. For example, for an 80% flow storage at Teesta, $Q_t = 80$, and from equation 4.3, $Q_d = -17.62\%$. So, up to 17.62% flow reduction from base condition may occur at the Dalia point due to 80% flow storage at Teesta III. The flow reduction at Dalia due to different flow storage scenarios at Teesta III has been presented graphically in **Figure 4.26**.

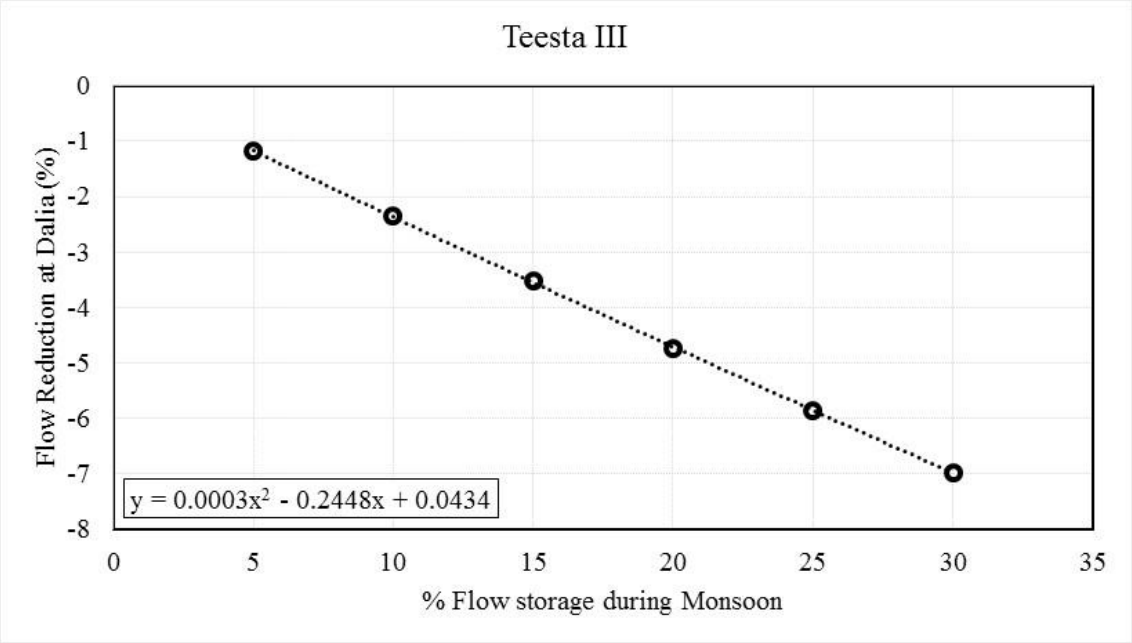

Figure 4.26: Flow reduction at Dalia due to different flow storage scenarios at Teesta III

Similar regression analysis was carried out for the increase of flow during the dry season due to the Teesta III structure. The increase of flow due the structure during the month of March is shown in **Table 4.23**.

Table 4.23: Percent increase of flow at Dalia during March due to different flow storage scenario.

% Flow storage during monsoon at Teesta III	Increase in flow during March at Dalia (%)
05	10.83
10	21.66
15	32.45
20	43.22
25	53.98
30	64.78

Based on the data of **Table 4.23**, a simple regression analysis was carried out to find the maximum % reduction of flow at Dalia point during monsoon due to the effect of Teesta III structure. The following equation was developed from the regression analysis:

$$Q_d = -0.0002 \times Q_t^2 + 2.1641 \times Q_t + 0.0241 \quad (4.4)$$

Here, Q_d is the maximum percent flow reduction at Dalia and Q_t is the percent flow extraction at Teesta III. For example, for a 2% flow storage at Teesta, $Q_t = 2$, and from equation 4.4, $Q_d = 4.35\%$. So, up to 4.35% flow increase from base condition may occur at the Dalia point due to 2% monsoon flow storage at Teesta III. The flow increase at

Dalia due to different flow storage scenarios at Teesta III has been presented graphically in **Figure 4.27**.

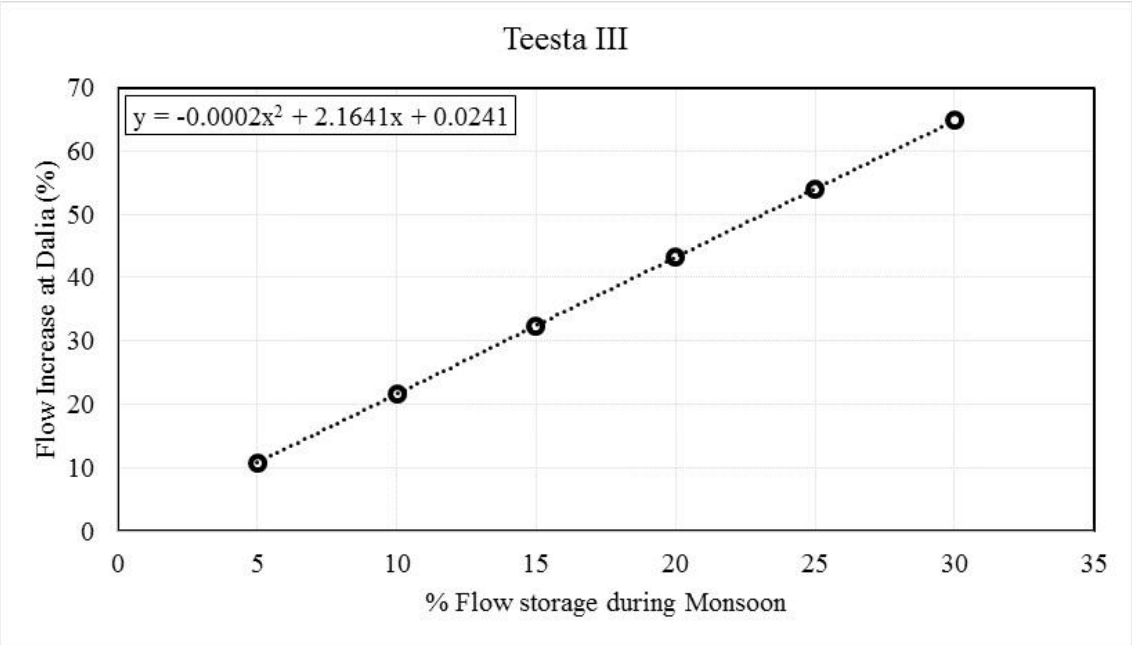

Figure 4.27: Flow increase at Dalia due to different flow storage scenarios at Teesta III

4.5.3 Storage at Rammam III

The under construction Rammam III Hydroelectric power plant was simulated following the same process of Teesta III. Rammam is one of many tributaries of the Teesta River and different extraction rate at this tributary, brings different response at the Dalia point. But similar to the Teesta III, the flow in the lean season at Dalia point has increased while the flow at monsoon has decreased due the presence of Rammam III project. The mean monthly flow at the Rammam III structure location for base and 15% flow storage is shown in **Figure 4.28**

The Percent reduction of flow during different months at Dalia due to different flow storage scenario at Rammam III is shown in tabular format in **Table 4.24**. And the hydrograph comparison for Base and 15% storage at Dalia point is shown in **Figure 4.29**. While the maximum amount of flow reduction due to different flow storage scenarios at Rammam III is shown in **Table 4.25**.

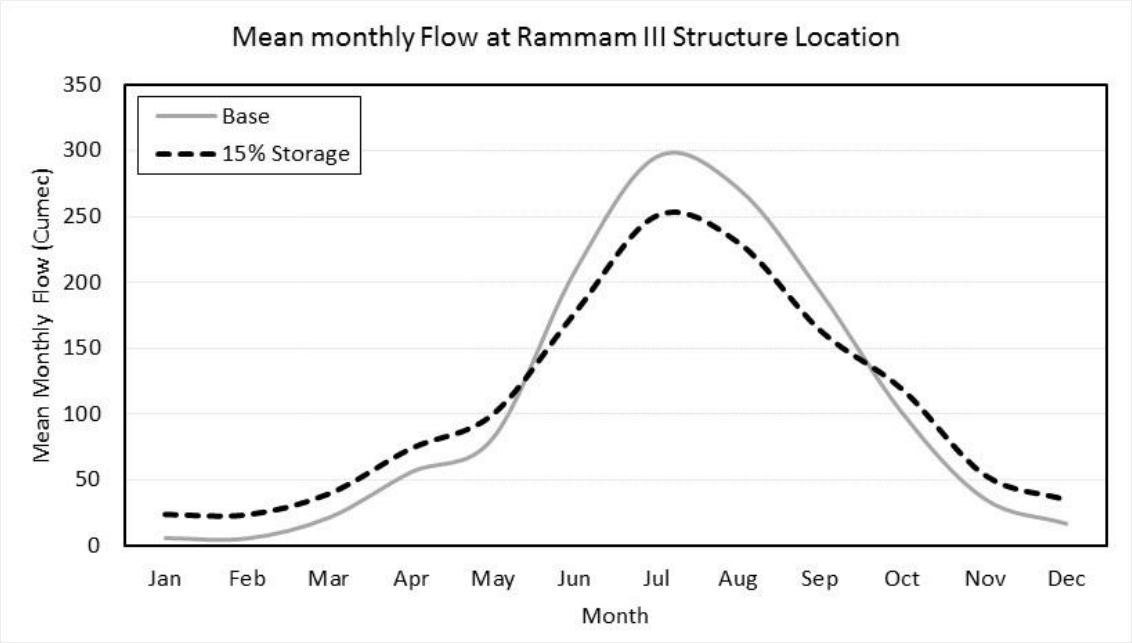

Figure 4.28: Mean Monthly flow at Rammam III Structure location with base and 15% storage scenario

Table 4.24: Percent reduction of flow at Dalia due to different flow storage scenario at Rammam III

Month	% reduction of flow at Dalia compared to Base						Remarks
	5%	10%	15%	20%	25%	30%	
Jan	16.27	32.60	48.97	65.34	81.67	98.00	Flow Release
Feb	26.91	53.86	80.82	107.79	134.83	161.83	
Mar	10.16	20.29	30.42	40.50	50.58	60.68	
Apr	2.69	5.38	8.06	10.76	13.44	16.13	
May	1.41	2.83	4.25	5.66	7.08	8.49	
Jun	-1.04	-2.08	-3.09	-4.04	-4.90	-5.72	Storage
Jul	-1.05	-2.08	-3.12	-4.15	-5.15	-6.07	
Aug	-1.06	-2.10	-3.16	-4.22	-5.27	-6.31	
Sep	-1.06	-2.13	-3.18	-4.25	-5.31	-6.36	
Oct	1.17	2.34	3.50	4.67	5.84	7.01	Flow Release
Nov	3.10	6.20	9.30	12.40	15.49	18.58	
Dec	6.36	12.70	19.04	25.40	31.73	38.09	

Table 4.25: Maximum Percent reduction of flow at Dalia due to different flow storage scenario.

% Flow storage during monsoon at Rammam III	Max Reduction in Flow at Dalia (%)
05	-1.06
10	-2.13
15	-3.18
20	-4.25
25	-5.31
30	-6.36

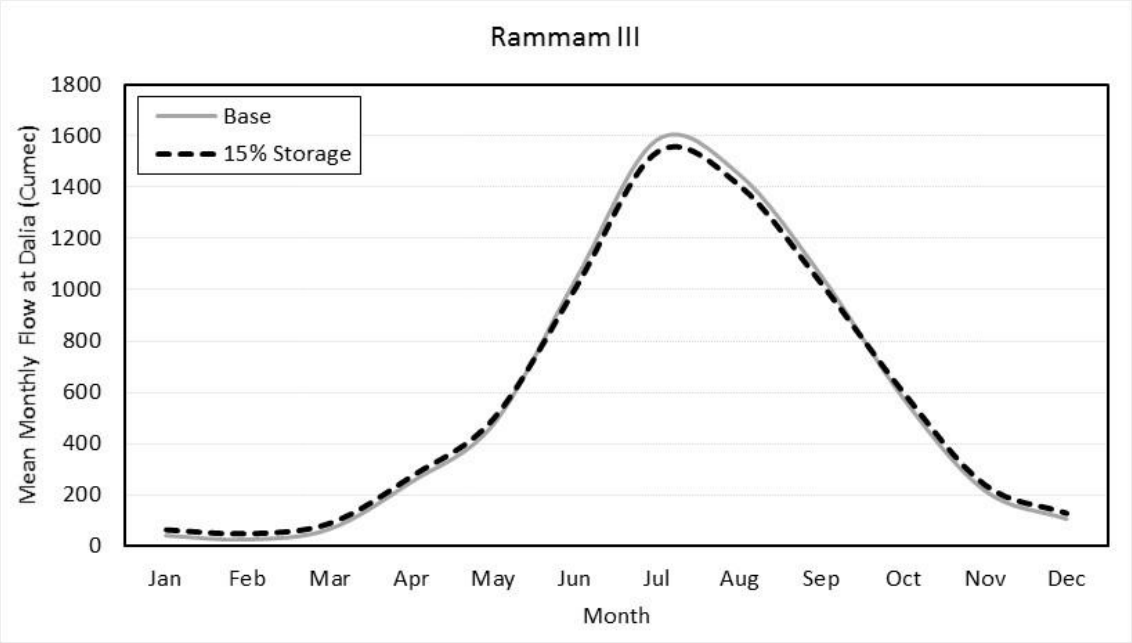

Figure 4.29: Comparison of mean monthly flow at Dalia point between base and 15% storage scenario

Based on the data of **Table 4.25**, a simple regression analysis was carried out to find the maximum % reduction of flow at Dalia point due to the effect of Rammam III structure. The following equation was developed from the regression analysis:

$$Q_d = 0.000004 \times Q_r^2 - 0.2136 \times Q_r + 0.006 \quad (4.5)$$

Here, Q_d is the maximum percent flow reduction at Dalia and Q_r is the percent flow extraction at Teesta III. For example, for an 80% flow extraction at Teesta, $Q_r = 80$, and from equation 4.5, $Q_d = -17.05\%$. So, up to 17.05% flow reduction from base condition may occur at the Dalia point due to 80% flow extraction at Teesta III. The flow reduction at Dalia due to different flow extraction scenarios at Rammam III has been presented graphically in **Figure 4.30**.

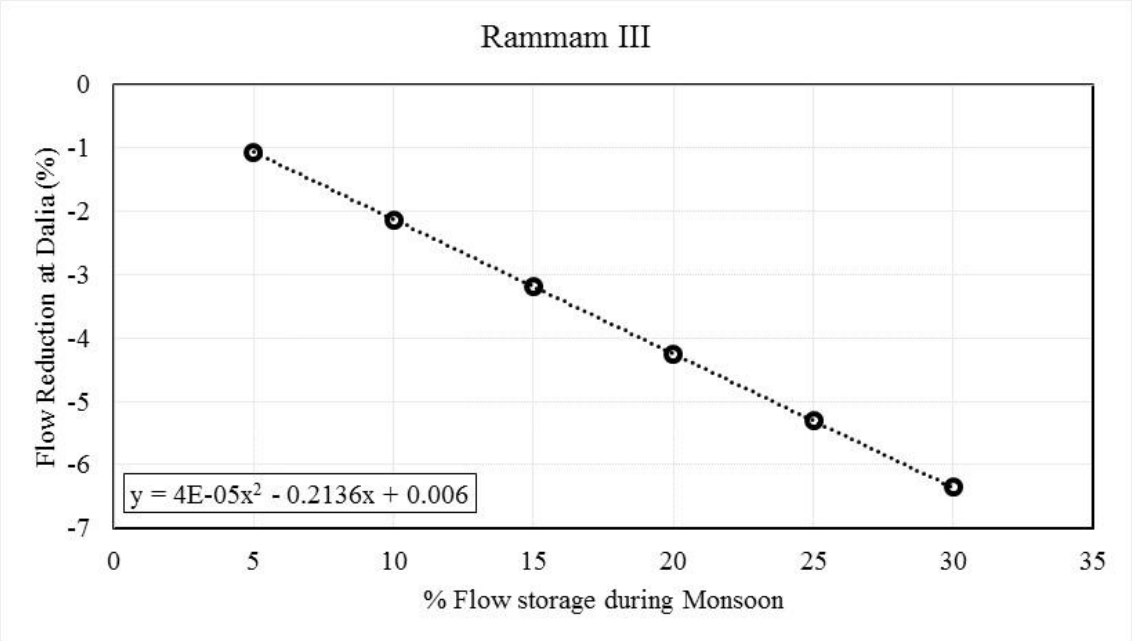

Figure 4.30: Flow reduction at Dalia due to different flow extraction scenarios at Rammam III

Similar regression analysis was carried out for the increase of flow during the dry season due to the Rammam III structure. The increase of flow due the structure during the month of March is shown in **Table 4.26**.

Table 4.26: Percent increase of flow at Dalia during March due to different flow storage scenario.

% Flow storage during monsoon at Rammam III	Increase in flow during March at Dalia (%)
05	10.16
10	20.29
15	30.42
20	40.50
25	50.58
30	60.68

Based on the data of **Table 4.31**, a simple regression analysis was carried out to find the maximum % reduction of flow at Dalia point during monsoon due to the effect of Rammam III structure. The following equation was developed from the regression analysis:

$$Q_d = -0.0003 \times Q_r^2 + 2.0294 \times Q_r + 0.0252 \quad (4.6)$$

Here, Q_d is the maximum percent flow reduction at Dalia and Q_r is the percent flow extraction at Rammam III. For example, for a 2% flow storage at Rammam, $Q_r = 2$, and

from equation 4.6, Q_d = 4.08%. So, up to 4.08% flow increase from base condition may occur at the Dalia point due to 2% monsoon flow storage at Rammam III. The flow increase at Dalia due to different flow storage scenarios at Rammam III has been presented graphically in **Figure 4.27**.

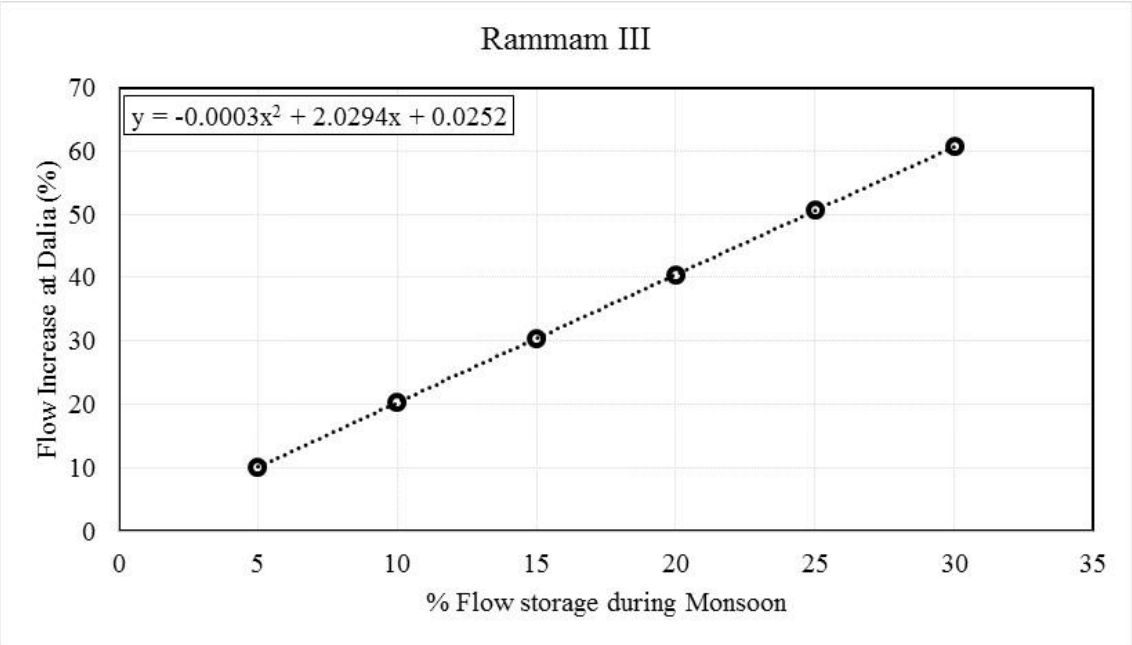

Figure 4.31: Flow increase at Dalia due to different flow storage scenarios at Rammam III

CHAPTER FIVE
CONCLUSION AND RECOMMENDATIONS

5.1 Conclusion

Potential change in the water balance due to climate change and upstream development in the Teesta River Basin has been assessed using SWAT hydrological model. The upstream development scenarios were prepared by diverting the stream flow at three different points and analyzing the impact of in further downstream. While the climate change scenarios were based on the projection of couple of GCM models (HAD GEM2 ES and CSIRO MK 3.6.0) for all the RCP scenarios of IPCC AR-5, during the 2050s and 2080s.

From the secondary data analysis, it is clear that the water availability in the Teesta River basin is on the decline. The annual maximum flow as well as the annual mean flow at Dalia point shows a decreasing trend over the past twenty eight years. The minimum flow analysis shows very low water availability during the dry season, with minimum flow dropping below 10 cumec almost every year. But the minimum water level shows a decreasing trend which indicates reduction in water availability. The increasing trend of maximum water level indicates more vulnerability to intense flood. But increase in maximum water level with the reduction in annual maximum flow points to siltation of the Teesta River basin.

The downscaled GCM model data of temperature and precipitation for all the RCPs were analyzed at different points in and around the Teesta to find the driest, wettest, warmest and coolest scenario of the Teesta basin in 2080s, which were found to be HAD GEM2 ES RCP 2.6, HAD GEM2 ES RCP 4.5, HAD GEM2 ES RCP 8.5 and CSIRO MK 3.6.0 RCP 2.6 respectively. For the wettest scenario the precipitation had increased by 11.71% while it decreased by 1.76% for the driest scenario. The increase in temperature for the coolest and the warmest scenario is found to be 2.24^{o}C and 5.34^{o}C. These scenarios were used as the input data for SWAT model to assess the changes in water balance due to climate change.

And before inputting the climate change scenarios, the hydrological model was calibrated and validated between the periods of 1998 to 2013. The 1998-2013 model result served

as the base model output to be compared against climate change model results. Comparing the water balance of the climate change model with the base model, it was clearly evident that the monsoon season will become more wetter and the dry season become more drier due to climate change for all the climate change scenarios. The monsoon may see as much as 80% increase in surface runoff (wettest scenario) while the dry season might see a 70% decrease in surface runoff (driest scenario). The base flow is expected to decrease in the month of April, May and June while increase in temperature means the evapotranspiration is expected to increase all throughout the year. The outputs of water yield shows it might increase by more than 50% in the monsoon season and reduce by 30% for the dry seasons.

The flow comparison at the Dalia point for different climate change scenarios shows similar kind of trend to that of the water balance comparison. While for the wettest scenario the mean monthly flow may increase by more than 50%, for the driest scenario the mean monthly flow in the lean season may decrease by around 20%. The general trend emerging from the flow analysis is that the Dalia point will experience a more severe shortage of water during the lean season even without the upstream development.

The impact of upstream control structures by analyzing different flow diversion scenarios shows that for a diversion of 60% of flow through Gozoldoba, dry season flow at Dalia may reduce up to 54.5%. A regression analysis was carried out to develop an equation to find the percent flow reduction at Dalia point due to different flow diversion scenarios at Gozoldoba. The equation can be used to assess the impact on Bangladesh side of the Teesta River flow due of upstream development of the basin. For 100% flow diversion at Gozoldoba, the equation predicted 91.21% decrease of flow at Dalia point.

While being storage type of structures, the Teesta III and Rammam III structures have different type of impact on the water availability. Both of the structures decreases the monsoon flow of the Teesta river when the storage actives, but increases the lean season flow of the river by releasing the stored flow during the lean season.

5.2 Recommendations for Future Studies

The RCP scenarios of two different GCM models were used during the climate change scenario development in this study. More GCM model outputs can be used to minimize the uncertainties.

All the model scenarios were simulated based on a single set of Land Use data which corresponds to the Land use pattern at the beginning of the 21st century. The land use pattern is bound to change by the end of the century and future projected land use pattern could be incorporated in this model.

The upstream development scenario was developed by extracting a portion of flow from the main channel at different structure locations, due to lack available data of the structures in the upstream reaches of the Teesta River Basin. With the availability of proper data, the model can be updated to better estimate its impact.

REFERENCE

Abbott, M.B., Bathurst, J.C., Cunge, J.A., Connell, P.E. and Rasmussen, J. 1986. 'An introduction to the European Hydrological System — Systeme Hydrologique Europeen, "SHE", 1: History and philosophy of a physically-based, distributed modelling system'. *Journal of Hydrology*, 87 (1–2), 45-59.

Afroz, R. and Rahman, A. 2013. 'Transboundary River Water for Ganges and Teesta Rivers in Bangladesh: An Assessment'. *Global Science and Technology Journal*, 1(1), 100-111.

Alam, S. 2015. '*Impact of Climate Change on Future flow of Brahmaputra River Basin Using SWAT Model'*. M.Sc. thesis, Department of Water Resources Engineering, Bangladesh University of Engineering and Technology.

Alam, S., Ali, M. M. and lslam, Z. 2015. 'Modelling Climate Change Impact on Hydrology of Brahmaputra River Basin Using The Soil Water Assessment Tool (SWAT)'. *International conference on Climate Change in relation to Water and Environment*. Gazipur: DUET, 37-44.

Ahmed, I. 2012. 'Teesta Tipaimukh and River Linking: Danger to Bangladesh India Relations'. *Economic and Political Weekly*, 47(16), 51-53.

Arnold, J. G. and Allen, P. M. 1996. 'Estimating hydrologic budgets for three Illinois watersheds'. *Journal of Hydrology*, 176 (1-4), 57–77.

Arnold, J.G and Williams, J.R. 1995. 'SWRRB- A watershed scale model for soil and water resources management'. *Computer models of watershed hydrology*, 847-908

Bangladesh Bureau of Statistics. 2012. '*Census of Population 2011'*. Dhaka: Bangladesh Bureau of Statistics.

Bates, B.C., Kundzewicz, Z.W., Wu, S. and Palutikof, J.P., 2008, '*Climate Change and Water*'. Geneva, Switzerland: Intergovernmental Panel on Climate Change (IPCC).

Beven, K. 1989. 'Changing ideas in hydrology –The case of physically based models'. *Journal of Hydrology*, 105 (1-2), 157-172.

Beven, K.J. and Kirkby, M.J. 1979. 'A Physically Based, Variable Contributing Area Model of Basin Hydrology. Un modèle à base physique de zone d'appel variable de l'hydrologie du bassin versant'. *Hydrological Sciences Bulletin*, 24(1), 43-69.

Bharati, L., Gurung, P. and Jayakody, P. 2012. 'Hydrologic Characterization of the Koshi Basin and the Impact of Climate Change'. *Hydro Nepal: Journal of Water, Energy and Environment*, 2012 (Special issue), 23 – 29.

Bouraoui, F., Grizzetti, B., Granlund, K., Rekolainen, S. and Bidoglio, G. 2004. 'Impact of climate change on the water cycle and nutrient losses in a finnish catchment'. *Climatic Change*, 66 (1-2), 109 –126.

Centre for Inter Disciplinary Studies of Mountain and Hill Development (CISMHE). 2006. '*Carrying Capacity Study of Teesta Basin in Sikkim'*. Delhi, India: University of Delhi.

Chakrabarty, A., Mandal, S. 2015. 'Flash Flood risk assessment for upper Teesta river basin: using hydrological modelling system (HEC-HMS) software'. *Modelling Earth Systems and Environment*, 2(2), 1-10

Chellaney, B. 2011. '*Water Asia's New Battleground'*. Washington D.C.: Georgetown University Press.

Chow, V.T., Maidment, D.R., and Mays, L.W., 1988. '*Applied Hydrology*'. New York: McGraw-Hill.

Clark D.B. and Gedney, N. 2008. 'Representing the effects of subgrid variability of soil moisture on runoff generation in a Land surface model'. *Journal of Geophysical Research Atmospheres*, 113(D10), 239-270.

Clarke, L., Edmonds, J., Jacoby, H., Pitcher, H., Reilly, J., Richels, R. 2007. '*Scenarios of Greenhouse Gas Emissions and Atmospheric Concentrations: Sub-report 2.1A of Synthesis and Assessment Product 2.1 by the U.S. Climate Change Science Program and the Subcommittee on Global Change Research'*. Washington D.C., USA: Department of Energy, Office of Biological & Environmental Research.

Cohen, S. and Kulkarni, T. 2001. '*Water Management & Climate Change in the Okanagan Basin'*. Vancouver: Environment Canada & University of British Columbia

Collins, W.J., Bellouin, N., Doutriaux-Boucher, M., Gedney, N., Hinton, T., Jones, C. D., Liddicoat, S., Martin, G., O'Connor, F., Rae, J., Senior, C., Totterdell, I., Woodward, S., Reichler, T. and Kim, J. 2011. 'Development and evaluation of an Earth-System model – HadGEM2'. *Geoscientific Model Development*, 4(2011), 1051-1075.

Condon, E, Hillman, P., King J. 2009. '*Resource Disputes in South Asia: Water Scarcity and the Potential for Interstate Conflict*'. Madison, Wisconsin: Robert M. La Follette School of Public Affairs, University of Wisconsin–Madison.

Covey, C., AchutaRao, K.M., Cubasch, U., Jones, P., Lambert, S.J., Mann, M.E., Phillips, T.J., and Taylor, K.E. 2003. 'An overview of results from the Coupled Model Intercomparison Project'. *Global Planet. Change*, 37(2003), 103–133.

Dahal, V., Shakya, N.M. and Bhattara. R. 2016. Estimating the Impact of Climate Change on Water Availability in Bagmati Basin, Nepal. *Environmental Processes*, 3(1), 1-17.

Dai, A., and K. E. Trenberth. 2002. 'Estimates of freshwater discharge from continents: Latitudinal and seasonal variations'. *Journal of Hydrometeorology*, 3, 660-687

Dai, A., T. Qian, K. E. Trenberth, and J. D Milliman. 2009. 'Changes in continental freshwater discharge from 1948-2004'. *Journal of Climate*, 22(10), 2773-2791

Davies, A. S. 2004. 'Urban water management vs. Climate change, impacts on cold region wastewater inflows'. *Climatic Change*, 64(1-2), 103–126.

Earle, A., Cascão, A.E, Hansson, S., Jägerskog, A., Swain, A. and Öjendal, J. 2015. 'Transboundary Water Management and the Climate Change Debate'. New York: Taylor & Francis.

ESCAP, 2010, '*Protecting Development Gains: Reducing disaster vulnerability and building resilience in Asia and the Pacific*'. Bangkok, Thailand: Economic and Social Commission for Asia and the Pacific (ESCAP)

Fowler, H.J. and Ekström, M. 2009. Multi-model ensemble estimates of climate change impacts on UK seasonal precipitation extremes. International Journal of Climatology, 29(3), 385–416.

Fujino, J., Nair, R., Kainuma, M., Masui, T., Matsuoka, Y. 2006. 'Multi-gas mitigation analysis on stabilization scenarios using AIM global model. Multigas Mitigation and Climate Policy'. *The Energy Journal*, 3 (Special Issue), 343-354.

Ganju, A.K., Mathur, N.K. and Rai, N.N. 2012. 'Distributed Hydrological Model for Design Flood Review of Projects in Teesta Basin'. Paper presented at the India Water Week 2012 – Water, Energy and Food Security: Call for Solutions, New Delhi, 10-14 April 2012.

Gedney, N. and Cox, P. M. 2003. 'The sensitivity of global climate model simulations to the representation of soil moisture heterogeneity'. *Journal of Hydrometeorology*. 4 (6), 1265–1275.

Giang, P.Q., Toshiki, K., Sakata, M., Kunikane S. and Vinh, T.Q. 2014. 'Modelling Climate Change Impacts on the Seasonality of Water Resources in the Upper Ca River Watershed in Southeast Asia'. *The Scientific World Journal*, 2014, 1-14.

Giorgi, F. 1990. 'Simulation of Regional Climate Using a Limited Area Model Nested in a General Circulation Model'. *Journal of Climate*, 3, 941–963.

Gordon, H.B. and co-authors. 2010. '*The CSIRO Mk3.5 Climate Model*'. The Centre for Australian Weather and Climate Research (CAWCR), Bureau of Meteorology, Canberra.

Gosain, A.K., Mani, A. and Dwivedi, C. 2009. 'Hydrological modelling literature review', *Advances in Fluid Mechanics*, 339, 63-70

Granier, C., Bessagnet, B., Bond, T., D'Angiola, A., van der Gon, H.D., Frost, G.J., Heil, A., Kaiser, J.W., Kinne, S., Klimont, Z., Kloster, S., Lamarque, J.-F, Liousse, C., Masui, T., Meleux, F., Mieville, A., Ohara, T., Raut, J.-C., Riahi, K., Schultz, M.G., Smith, S.J., Thompson, A., van Aardenne, J., van der Werf, G.R. and van Vuuren, D.P. 2011. 'Evolution of anthropogenic and biomass burning emissions of air pollutants at global and regional scales during the 1980–2010 period'. *Climatic Change*, 109(1-2), 163-190.

Grayson, R.B., More, I.D., and McMahon, T.A. 1992. 'Physically based hydrological modelling'. *Water Resource Research*, 28(10), 2639-2658.

Green, W.H. and G.A. Ampt. 1911. 'Studies on soil physics'. *Journal of Agricultural Sciences*. 4(1), 11-24.

Guo, S., Wang, J., Xiong, L., Ying, A., and Li, D. 2002. 'A macro-scale and semi-distributed monthly water balance model to predict climate change impacts in China'. *Journal of Hydrology*, 268 (1-4), 1–15.

Gurung, P., Bharati, L. and Karki, S. 2013. 'Application of the SWAT Model to assess climate change impacts on water balances and crop yields in the West Seti River Basin'. Paper presented at the *2013 International SWAT Conference*, Toulouse, France, July 17-19, 2013.

Haque, A.E., Aich, D., Subhani, R., Bari, E.& Diyan, M.A.A. 2014. '*Tale of a Tamed River: The value of Ecosystem Services of Teesta River – An estimate of value of provisional services in agriculture and fisheries*'. Dhaka: IUCN and Asian Center for Development

Hijioka, Y., Matsuoka, Y., Nishimoto, H., Masui, M. and Kainuma, M. 2008. 'Global GHG emissions scenarios under GHG concentration stabilization targets'. *Journal of Global Environmental Engineering*, 13, 97-108.

Hijmans, R. J., Cameron, S. E., Parra, J. L., Jones, P. G. and Jarvis, A. 2005. 'Very high resolution interpolated climate surfaces for global land areas'. *International Journal of Climatology*, 25 (2005), 1965–1978.

Hurtt, G.C., Chini, L.P. and Frolking, S. 2011. 'Harmonization of land-use scenarios for the period 1500–2100: 600 years of global gridded annual land-use transitions, wood harvest, and resulting secondary lands'. *Climatic Change*, 109(1), 117-161.

Institute of Water Modelling (IWM). 2014a. '*Surface Water Assessment and Impact of Climate Change*'. Technical Report, Institute of Water Modelling, Dhaka.

Institute of Water Modelling (IWM). 2014b. '*Physical Assessment of the Brahmaputra River*'. Technical Report, Institute of Water Modelling, Dhaka.

Immerzeel, W. W., van Beek, L.P.H., and Bierkens. M.F.P. 2010. 'Climate Change Will Affect the Asian Water Towers'. *Science*, 328(5984), 1382–1385.

IPCC. 2001. '*Climate Change: The Scientific Basis. Contribution of Working Group I to the IPCC Third Assessment Report'*. Cambridge University Press, Cambridge, United Kingdom: IPCC.

IPCC. 2013. '*Climate Change: The Physical Science Basis. Contribution of Working Group I to the Fourth Assessment Report of the Intergovernmental Panel on Climate Change'*. Cambridge University Press, Cambridge, United Kingdom: IPCC.

Islam, Z. 2011. '*A Review on Climate Change Modeling for Hydrological Impact Studies*'. Technical Report, Department of Civil and Environmental Engineering University of Alberta.

Jaitley, A. 2009. 'South Asian perspectives on climate change and water policy'. In D. Michel & A. Pandya (Eds.), *Troubled waters: Climate change, hydropolitics, and transboundary resources*, Washington, DC: Stimson Institute.

Jiang, T., Chen, Y.D., Xu, C.-Y., Chen, X., Chen, X., and Singh, V.P. 2007. 'Comparison of hydrological impacts of climate change simulated by six hydrological models in the Dongjiang Basin, South China'. *Journal of Hydrology*, 336(3-4), 316–333

Karlssona, I.B., Sonnenborg, T.O., Refsgaard, J.C., Trolle, D., Børgesen, C.D., Olesen, J.E., Jeppesen, E., Jensen. K.H. 2016. 'Combined effects of climate models, hydrological model structures and land use scenarios on hydrological impacts of climate change'. *Journal of Hydrology*, Volume 535, 301-317

Khalid, A.R.M. 2013. 'Water negotiations in the Ganges-Brahmaputra-Meghna Basin- "multilateral" is the way forward'. Paper presented at *the International Conference on Water Resources of South Asia – Conflict to Cooperation (IC WRSA CC)*, Dhaka, Bangladesh, January 04–05, 2013.

Krasovskaia, I. and Gottschalk, L. 1992. 'Stability of River Flow Regimes'. *Nordic Hydrology*, 23(3), 137-154

Knox, J.C. 1993. ‘Large increases in flood magnitude in response to modest changes in climate’. *Nature*, 361, 430 - 432.

Kumar, R., Sharma, K.D. and Singh. R.D. 2005. ‘Water Resources of India’. *Current Science*, 89(5), 794-811.

Lamarque, J.-F., J.R. McConnell, D.T. Shindell, J.J. Orlando, and G.S. Tyndall. 2011. ‘Understanding the drivers for the 20th century change of hydrogen peroxide in Antarctic ice-cores’. *Geophysical Research Letters*, 38, L04810.

Masui, T., Matsumoto, K., Hijioka, Y., Kinoshita, T., Nozawa, T., Ishiwatari, S., Kato, E., Shukla, P.R., Yamagata, Y. and Kainuma, M. 2011. ‘An emission pathway for stabilization at 6 Wm−2 radiative forcing’. *Climatic Change*, 109, 59-76.

Meinshausen, M., Smith, S.J., Calvin, K., Daniel, S., Kainuma, M. L. T., Lamarque, J-F., Matsumoto, K., Montzka, S. A., Raper, S. C. B., Riahi, K., Thomson, A., Velders, G. J. M. and van Vuuren, D.P. P. ‘The RCP greenhouse gas concentrations and their extensions from 1765 to 2300’. *Climatic Change,* 109, 213-241.

Mengistu, D.T. and Sorteberg, A. 2012. ‘Sensitivity of SWAT Simulated Streamflow to Climatic Changes within the Eastern Nile River Basin’. *Hydrology and Earth System Sciences*, 16, 391-407.

Ministry of Environment and Forests (MoEF), Government of India. 2010. ‘*Climate Change and India: A 4X4 Assessment- A Sectoral and Regional Analysis for 2030s’*. Ministry of Environment and Forests (MoEF), New Delhi.

Mitra, S. and Mishra, A. 2014. ‘Hydrologic response to Climate Change in the Baitarni Basin’. *Journal of Indian Water Resources Society*, 34(1), 24-33.

Mondal, S.H. and Islam, S. 2017. ‘Chronological trends in maximum and minimum water flows of the Teesta River, Bangladesh, and its implications’. *Jàmbá: Journal of Disaster Risk Studies*, 9(1), 373-384.

Moss, R.H., Nakicenovic N. and O'Neill B.C. 2008. ‘*Towards New Scenarios for Analysis of Emissions, Climate Change, Impacts, and Response Strategies*’. Technical Summary, Intergovernmental Panel on Climate Change, Geneva.

Moss, R.H., Edmonds, J.A., Hibbard, K.A., Manning, M.R., Rose, S.K., van Vuuren, D.P., Carter, T.R., Emori, S., Kainuma, M., Kram, T., Meehl, G.A., Mitchell, J.F.B., Nakicenovic, N., Riahi, K., Smith, S.J., Stouffer, R.J., Thomson, A.M., Weyant J.P. and Wilbanks, T.J. 2010. ‘The next generation of scenarios for climate change research and assessment’. *Nature*, 463, 747-756.

Myhre, G., Highwood, E.J., Shine, K.P., Stordal, F. 1998. 'New estimates of radiative forcing due to well mixed greenhouse gases'. *Geophysical Research Letters*, 25(14), 2715-2718.

Nash, L. and Gleick, P. 1990. 'Sensitivity of stream flow in the Colorado basin to climatic changes'. *Journal of Hydrology*, 125(3-4), 221-241

National Council for Applied Economic Research. 2008. '*Economic Impact of Interlinking of Rivers Program*'. Technical Report. National Council for Applied Economic Research, New Delhi.

Nemec, J. and Schaake, J. 1982. 'Sensitivity of water resources system to climate variation'. *Hydrological Sciences Journal*, 27(3), 327–343.

Oki, T. and Y.C. Sud, 1998. 'Design of Total Runoff Integrating Pathways (TRIP)—A Global River Channel Network'. *Earth Interactions*, 2, 1–37.

Orlowsky, B., Bothe, O., Fraedrich, K., Gerstengarbe, F.W., and Zhu, X. 2010. 'Future Climates From Bias-Bootstraed Weather Analogs, An Alication to The Yangtze River Basin'. *Journal of Climate*, 23, 3509-3524.

Palutikof, J.P. 1987. '*The Influence of Climate Change and Climatic Variability on the Hydrologic Regime and Water Resources in England and Wales*'. Wallingford, Oxfordshire, U.K.: International Association of Hydrological Sciences.

Parsai, G. 2012. 'Water Ministry Mulls Review'. In: *The Hindu*, Available at: http://www.thehindu.com/news/national/water-ministry-mulls-review-of-court-order-on-linking-of-rivers/article3259040.ece. [Accessed on: 28 February 2018]

Prasai, S. and Mandakini D.S. 2013. '*Political economy Analysis of the Teesta River Basin'*. New Delhi: The Asia Foundation.

Pradhan, R., Pradhan, M.P., Ghose, M.K., Agarwal, V.S. and Agarwal. S. 2010. 'Estimation of Rainfall Runoff using Remote Sensing and GIS in and around Singtam, East Sikkim'. *International Journal of Geomatics and Geosciences*, 1(3), 466-476.

Refsgaard, J.C., and Abbott, M.B. 1996. 'The role of distributed hydrological modelling in water resources management'. *Water Science and Technology Library*, 22, 1-16.

Riahi, K. Gruebler, A. and Nakicenovic N. 2007. 'Scenarios of long-term socio-economic and environmental development under climate stabilization'. *Technological Forecasting and Social Change*, 74(7), 887-935.

Riahi K., Rao, S., Krey, V., Cho, C., Chirkov, V., Fischer, G., Kindermann, G., Nakicenovic, N. and Rafaj. P. 2011. 'RCP 8.5—A scenario of comparatively high greenhouse gas emissions'. *Climatic Change*. 109(2011), 33-57.

Rotstayn, L.D., Collier, M.A., Dix, M.R., Feng, Y., Gordon, H.B., O'Farrell, S.P., Smith, I.N. and J.I. Syktus. 2010. 'Improved Simulation of Australian Climate and ENSO-related rainfall variability in a global climate model with interactive aerosol treatment'. *International Journal of Climatology*. 30, 1067-1088.

Rotstayn, L.D., Collier, M.A., Mitchell, R.M., Qin, Y., S.K. Campbell and S. M. Dravitzki. 2011. 'Simulated enhancement of ENSO-related rainfall variability due to Australian dust'. *Atmospheric Chemistry and Physics Discussions*, 11(1), 1595-1639.

Schaake, J. C. and Liu, C. 1989. 'Development and alications of simple water balance models to understand the relationship between climate and water resources'. *New Directions for Surface Water Modelling*, Proceedings of the Baltimore Symposium, May 1989, 343–352.

Shackley, S., Young, P., Parkinson, S. and Wynne, B. 1998. 'Uncertainty, Complexity and Concepts of Good Science in Climate Change Modelling, Are GCMs the Best Tools?' *Climatic Change*, 38 (2), 159-205.

Sloan, P.G. and I.D. Moore. 1984. 'Modeling subsurface stream flow on steeply sloping forested watersheds'. *Water Resources Research*. 20(12), 1815-1822.

Sloan, P.G., I.D. Moore, G.B. Coltharp, and J.D. Eigel. 1983. '*Modeling surface and subsurface stormflow on steeply-sloping forested watersheds*'. Research Report, Water Resources Research Institute, University of Kentucky.

Smedema, L.K. and Rycroft, D.W. 1983. 'Land drainage: planning and design of agricultural drainage systems'. New York: Cornell University Press.

Smith, S.J. and Wigley, T.M.L. 2006. 'Multi-Gas Forcing Stabilization with the MiniCAM'. *The Energy Journal*, 27 (Special Issue), 373-391

Sorooshian, S. and Gupta, K. 1995. '*Model calibration, in Computer Models of Watershed Hydrology*'. Colorado: Water Resources Publications.

Stackhouse, P.W., Whitlock, C.W., DiPasquale, R.C., Brown II, D.E., and Chandler, W.S. 2002. 'Meeting Energy-Sector Needs with NASA Climate Datasets'. *Earth Observation Magazine*, 11, 6-10.

Strategic Foresight Group. 2013. '*Rivers of Peace*'. Mumbai: Strategic Foresight Group.

Tabor K and Williams JW. 2010. 'Globally downscaled climate projections for assessing the conservation impacts of climate change'. *Ecological Applications*, 20(2), 554-65.

Thomson A., Calvin, K., Smith, S., Kyle, P., Volke, V., Patel, P., Delgado-Arias, S., Bond-Lamberty, B., Wise, M., Clarke, L. and Edmonds J. 2011. 'RCP4.5: a pathway for stabilization of radiative forcing by 2100'. *Climatic Change*, 109, 77-94.

Van Vuuren D.P., Den Elzen M.G.J., Lucas P.L., Eickhout B., Strengers B.J., Van Ruijven B., Wonink S. and Van Houdt R. 2007. 'Stabilizing greenhouse gas concentrations at low levels: an assessment of reduction strategies and costs'. *Climatic Change*, 81(2), 119-159.

van Vuuren, D.P. Edmonds, J., Kainuma, M., Riahi, K., Thomson, A., Hibbard, K., Hurtt, G.C., Kram, T., Krey, V., Lamarque, J.F., Masui, T., Meinshausen, M., Nakicenovic, N., Smith, S.J. and Rose S.K. 2008. '*Work Plan for Data Exchange Between the Integrated Assessment and Climate Modeling Community in Support of Phase-0 of Scenario Analysis for Climate Change Assessment (Representative Community Pathways)*'.Available at: https://cmip.llnl.gov/cmip5/docs/RCP_handshake.pdf. [Accessed on: 28 February 2018]

van Vuuren D.P., Edmonds, J.A., Kainuma, M., Riahi, K., Thomson, A.M., Hibbard, K., Hurtt, G.C., Kram, T., Krey, V., Lamarque, J.F., Masui, T., Meinshausen, M., Nakicenovic, N., Smith, S.J. and Rose, S. 2011. 'The representative concentration pathways: an overview'. *Climatic Change*, 109. 5-31.

Weiland, S., van Beek, F. C., L. P. H., Weerts, A. H. and Bierkens, M. F. P. 2012. 'Extracting information from an ensemble of GCMs to reliably assess future global runoff change'. *Journal of Hydrology*. 412-413, 66 – 75.

Whetton, P.H., Fowler, A.M., Haylock, M.R. and Pittock, A.B. 1993. 'Implications of climate change due to the enhanced greenhouse effect on floods and droughts in Australia'. *Climatic Change*, 25(3-4), 289-317.

Wilby, R. L., Troni, J., Biot, Y., Tedd, L., Hewitson, B. C., Smithe, D. M. and Suttonf, R. T. 2009. 'A review of climate risk information for adaptation and development planning'. *International Journal of Climatology*, 29, 1193–1215.

Williams, J.R., 1969. '*Flood routing with variable travel time or variable storage coefficients*'. St. Joseph, Michigan: American Society of Agricultural and Biological Engineers.

Williams, J.R. and R.W. Hann. 1973. 'HYMO, a problem-oriented computer language for building hydrologic models'. *Water Resource Research*, 8(1), 79-85.

Wise, M.A., Calvin, K.V., Thomson, A.M., Clarke, L.E., Bond-Lamberty, B., Sands, R.D., Smith, S.J., Janetos, A.C. and Edmonds, J.A. 2009. 'Implications of Limiting CO_2 Concentrations for Land Use and Energy'. *Science*, 324(5931), 1183-1186.

World Bank. 2008. '*Climate Change Impacts in Drought and Flood Affected Areas: Case Studies in India'.* Washington, DC: World Bank

Xu, C. and Halldin, S. 1997. 'The Effect of Climate Change on River Flow and Snow Cover in the NOPEX Area Simulated by a Simple Water Balance Model'. *Nordic Hydrology*, 28 (4-5), 273-282.

Xu, C. 2000. 'Modelling the Effects of Climate Change on Water Resources in Central Sweden'. *Water Resources Management*, 14(3), 177-189

Yan, D., Werners, S.E., Ludwig, F. and Huang, H.Q. 2015. 'Hydrological response to climate change: The Pearl River, China under different RCP scenarios'. *Journal of Hydrology: Regional Studies*, 4(B), 228-245.

Yao, H., Scott, L., Guay, C. and Dillon, P. 2009. 'Hydrological impacts of climate change predicted for an inland lake catchment in Ontario by using monthly water balance analyses'. Hydrological processes, 23, 2368–2382.

Zorita, E. and von Storch, H. 1999. 'The Analog Method as a Simple Statistical Downscaling Technique, Comparison with more Complicated Methods'. *Journal of Climate*, 12, 2474–2489.

Zuo, D., Xu, Z., Yao, W., Jin, S., Xiao, P. and Ran, D. 2016. 'Assessing the effects of changes in land use and climate on runoff and sediment yields from a watershed in the Loess Plateau of China'. *Science of The Total Environment*, 544, 238-250.